EXHIBIT D
REDACTED

CONTAINS CONFIDENTIAL ATTORNEY EYES ONLY INFORMATION SUBJECT TO PROTECTIVE ORDER

UNITED STATES DISTRICT COURT
WESTERN DISTRICT OF PENNSYLVANIA

LAMBETH MAGNETIC STRUCTURES, LLC, Plaintiff, v. SEGATE TECHNOLOGY (US) HOLDINGS, INC. and SEAGATE TECHNOLOGY LLC, Defendants.	Civil Action No. 2:16-cv-00538-CB Judge Cathy Bissoon **CONTAINS CONFIDENTIAL ATTORNEY EYES ONLY INFORMATION SUBJECT TO PROTECTIVE ORDER**

PLAINTIFF LAMBETH MAGNETIC STRUCTURES, LLC'S
INITIAL EXPERT REPORT OF DR. WILLLIAM ALAN THOMAS CLARK

CONTAINS CONFIDENTIAL ATTORNEY EYES ONLY
INFORMATION SUBJECT TO PROTECTIVE ORDER

TABLE OF CONTENTS

A. Introduction 1
1. Professional Background and Qualifications 1
B. Subject Matter and Scope of Opinions/Assignment 4
C. Claim Construction of the '988 Patent 4
D. Materials Reviewed 5
E. Technology Background and Investigative Techniques 5
1. Crystallography 5
a) The structure of crystalline materials 5
b) Directions and planes – Miller indices 8
(1) Planes 8
(2) Directions 10
c) Orientation relationships and variants 11
2. Transmission Electron Microscopy (TEM) 15
a) Basic principles 15
b) Diffraction 16
c) Diffraction patterns 20
d) Microbeam diffraction 23
e) Bright and dark field imaging in the TEM 24
f) Dark field image analysis 26
g) High resolution imaging 29
h) Scanning transmission electron microscopy (STEM) 29
i) Epitaxy, growth directions, and Fast Fourier Transforms (FFTs) 30
3. Energy Dispersive X-Ray Spectrometry (EDS) 33
F. Results of Investigation of Seagate Hard Disk Drive Products 36
1. Analysis of [redacted] Products 37
a) S0GPPC 37
(1) EDS analysis 37
(2) TEM high resolution images of cross-sections 42
(3) FFT on TEM high resolution images of cross-sections 48
(4) TEM—microbeam diffraction on plan view samples 58
(5) Dark field image analysis 65

CONTAINS CONFIDENTIAL ATTORNEY EYES ONLY INFORMATION SUBJECT TO PROTECTIVE ORDER

b) S2MMMC 72
(1) EDS analysis 72
(2) TEM high resolution images of cross-sections 77
(3) FFT on TEM high resolution images of cross-sections 83
(4) TEM—microbeam diffraction on plan view samples 91
(5) Dark field image analysis 97
2. Analysis of [redacted] Products 105
a) SBRD8K 105
(1) EDS analysis 105
(2) TEM high resolution images of cross-sections 108
(3) FFT on TEM high resolution images of cross-sections 114
(4) TEM—microbeam diffraction on plan view samples 122
(5) Dark field image analysis 127
G. Reservation of Rights 134

CONTAINS CONFIDENTIAL ATTORNEY EYES ONLY
INFORMATION SUBJECT TO PROTECTIVE ORDER

A. Introduction

1. I, Dr. William Clark, resident at 5696 Morlich Square, Dublin, OH, 43017, have been retained by counsel for Lambeth Magnetic Structures, LLC ("LMS") to provide my opinions regarding the below.

2. In reaching the conclusions herein, I have considered the documents and materials identified in Appendix A below. My opinions are further based on my education, training, research and related publications, knowledge, and personal and professional experience in the relevant art.

3. I am prepared to testify to the matters set out in this report at trial. To support or summarize my opinions, any testimony I give may include appropriate visual aids, some or all of the data or other documents and information cited herein or identified in Appendix A below, and additional data or other information identified in discovery.

4. I may modify or supplement my opinions and/or the basis for my opinions based on the nature and content of the documentation, data, proof, and other evidence or testimony that Seagate Technology (US) Holdings, Inc. and Seagate Technology LLC (collectively, "Seagate") or its experts may present or based on any additional discovery or other information provided to me or found by me in this matter.

5. I am being compensated for my time at my standard consulting rate of $250 per hour in conjunction with my work on this report. I am also being reimbursed for expenses that I incur. My compensation is not dependent on the results of my study, the substance of my testimony, or the outcome of this litigation.

1. Professional Background and Qualifications

6. I am presently employed as a Professor Emeritus in the Department of Materials Science and Engineering at Ohio State University.

CONTAINS CONFIDENTIAL ATTORNEY EYES ONLY
INFORMATION SUBJECT TO PROTECTIVE ORDER

7. My general expertise is in the field of materials science, metallurgy, electron microscopy and characterization of materials. My specific expertise is in analyzing interfaces, grain boundaries, and epitaxial boundaries of metallic materials. I have made pioneering contributions to the fields of metallurgy and crystallography, specifically the crystallography of slip transmission across interfaces of metallic materials.

8. I received a B.Sc. degree with honors from the University of Liverpool School of Physics with Materials Science in 1972. I received a D. Phil. degree from the University of Oxford Department of Metallurgy and Science of Materials in 1976. My doctoral research area was the study of interfaces in metallic materials using electron microscopy and diffraction. From 1976 to 1978, I completed a postdoctoral research fellowship at the University of Oxford researching the structure of nickel-chromium alloys. From 1978 to 1979, I worked as a research associate at Michigan Technological University characterizing interfaces in copper-zinc alloys.

9. In 1979, I went to work as an Assistant Professor at the Department of Metallurgical Engineering at Ohio State University. I was promoted to tenured Associate Professor in 1983 and to Professor in 1989. In 1988, the Department of Metallurgical Engineering at Ohio State University became the Department of Materials Science and Engineering. Throughout my career of over 40 years I have used electron microscopy techniques including diffraction, energy dispersive spectrometry, and Fast Fourier transforms to analyze the crystal structure and texture of materials. In 2014, I retired from my position as a full-time Professor and became a Professor Emeritus, after which I have continued to do research, teach, and advise graduate students.

10. I have supervised at least 40 to 50 graduate students who received Ph.D. or M.S. degrees in Materials Science. From 1979 to 2014 I maintained an active graduate and

undergraduate teaching program in materials characterization, electron microscopy, crystallography, and crystal structure. From 1992 to 1993 I was the Vice Chairman of the Department of Materials Science and Engineering at Ohio State University. From 1995 to 2005, I served as Associate Dean of the Graduate School at Ohio State University. I also served on and chaired several committees for the Department of Materials Science and Engineering and for Ohio State University from 1985 to 2014.

11. I have published over 100 articles in peer-reviewed journals in the field of metallic materials with a focus on the characterization of crystal structures using electron microscopy. I have given more than 100 conference presentations since 1976, including at the Materials Research Society ("MRS"), the Electrochemical Society, the International Congress for Electron Microscopy, and the Electron Microscopy Society of America ("EMSA"), which is now known as the Microscopy Society of America.

12. I have been a Fellow of the American Society for Metals ("ASM International") since 1995. I am a member of the Minerals, Metals, and Materials Society ("TMS") for which I served as Director from 1993 to 1996. I received a leadership award from TMS in 1999. I am also a member of the Institute of Materials among other professional groups. I have reviewed articles for numerous peer-reviewed journals such as Philosophical Magazine, Acton Materialia, Scripta Materialia, and Metallurgical Transactions. I served on the Board of Review for Metallurgical Transactions from 1984 to 1989. I have been the editor of three conference proceedings and co-chair of five symposiums for TMS, MRS and EMSA.

13. A copy of my curriculum vitae (CV), which contains information pertaining to my education, experience, scholarship, awards, professional activities, and list of publications are attached as Appendix B.

CONTAINS CONFIDENTIAL ATTORNEY EYES ONLY INFORMATION SUBJECT TO PROTECTIVE ORDER

B. Subject Matter and Scope of Opinions/Assignment

14. I have been retained by Radulescu LLP on behalf of LMS in the above-captioned matter. I have been asked to determine: the composition of certain material layers; the crystal structure and texture for certain FeCo and NiFe layers; whether the NiFe layers directed the growth of the FeCo layers deposited directly on top of the respective NiFe layers; the presence of crystallographic orientational variants; whether there is an unequal amount of variants in a six-variant system in the lower FeCo layer of the write pole; and the fractional distribution of the different orientations of the crystallites in the lower FeCo layer.

C. Claim Construction of the '988 Patent

15. It is my understanding that the Court issued its Claim Construction Order in this matter on October 18, 2017. Memorandum Order (Dkt. No. 78). I have used the claim constructions for the construed term in the '988 Patent, as set forth in the Memorandum Order, to formulate my opinions in this Report.

16. Specifically, I understand that the Court construed eight terms from the claims of the '988 patent as reflected in the table below. I understand that the Court resolved disputes between the parties to arrive at the constructions for "atomic template," "[layer] providing a (111) textured hexagonal atomic template," "uniaxial," "symmetry broken structure," "uniaxial symmetry broken structure," and "variant(s)/orientational variant(s)." I understand that the parties agreed on and the Court subsequently ordered the constructions for "bcc-d" and "fcc-d."

Term	Construction
"atomic template"	An atomic pattern upon which material is grown and which is used to direct the growth of an overlying layer
"[Layer] providing a (111) textured hexagonal	Layer that is predominately (111) hexagonal

CONTAINS CONFIDENTIAL ATTORNEY EYES ONLY INFORMATION SUBJECT TO PROTECTIVE ORDER

Term	Construction
atomic template"	and that provides an atomic template
"Uniaxial"	Having an anisotropy energy density function with only a single maximum and a single minimum as the magnetization angle is rotated by 180 degrees from a physical axis
"Symmetry broken structure"	A structure consisting of unequal volumes or unequal amounts of the bcc-d variants of a six variant system
"Uniaxial symmetry broken structure"	A structure that is uniaxial as a result of the structure being symmetry broken
"Variant/orientational variant" "Variants/orientational variants"	One of a set of possible crystal orientations Two or more of a set of possible crystal orientations
"bcc-d"	Either a body centered cubic or a body centered cubic derivative crystal structure
"fcc-d"	Either a face centered cubic or a face centered cubic derivative crystal structure

See Memorandum Order at 7-8.

D. Materials Reviewed

17. A complete list of the materials that I reviewed in forming my opinions set forth in this Report is attached as Appendix A.

E. Technology Background and Investigative Techniques

18. Various technologies and investigative techniques within my expertise were employed in my analysis below. A brief background of these technologies and techniques follows.

1. Crystallography

a) The structure of crystalline materials

19. Solid materials can be classified by the way in which atoms, ions, or molecules arrange with respect to one another. A crystalline material is one in which the atoms form a repeating or periodic array over large atomic distances. Many of the properties of these materials depend on this crystalline structure.

CONTAINS CONFIDENTIAL ATTORNEY EYES ONLY
INFORMATION SUBJECT TO PROTECTIVE ORDER

20. One simple way to visualize and describe crystalline structures is to consider atoms as hard spheres and stack them together. One example is shown in the Figure 1 below.

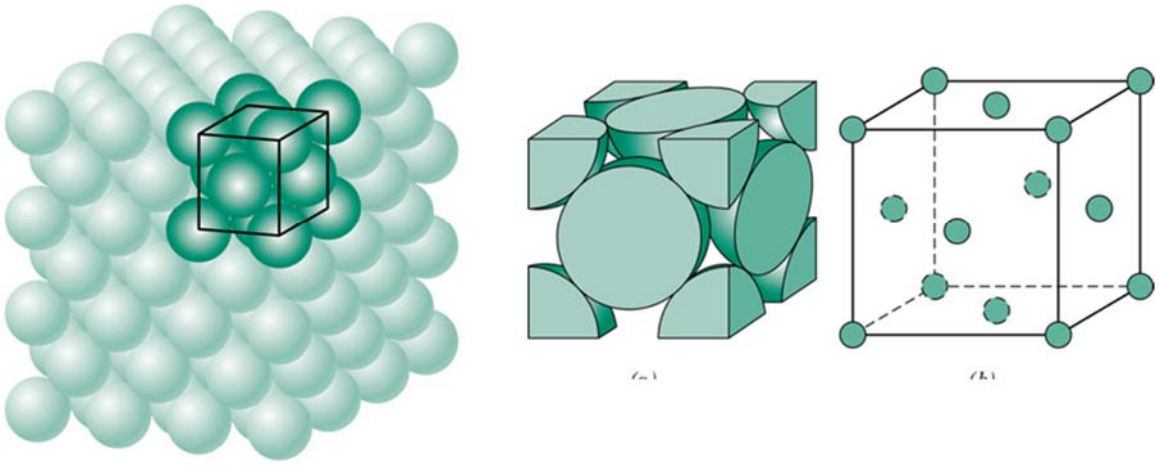

Figure 1: *Materials Science and Engineering,* W.D. Callister and D.G. Rethwisch, 9th ed., Wiley, Hoboken NJ, (2014), fig. 3.1, p. 53

21. Figure 1 depicts atoms stacked together as closely as possible, resulting in a structure we referred to as face centered cubic, or FCC for short.[1] The left-hand figure shows the three-dimensional arrangement of an FCC structure over many atoms, but the entire three-dimensional structure can be described by the small unit cell shown in a darker green, and simply repeating that unit cell to make up the full crystal. This is analogous to describing a wall by specifying a single brick and repeating that to make the entire structure. This building unit, known as the unit cell, is shown in the figure in the center in hard sphere form, and on the right as a simple exploded cell. This face centered cubic structure is found in many metallic materials, such as gold, silver, aluminum, and nickel, for example.

[1] I understand that the Court has construed "fcc-d" to mean "either a face centered cubic or a face centered cubic derivative crystal structure."

22. If, on the other hand, the atoms are stacked in a fashion that is still cubic but not as densely packed as FCC, another crystal form known as body centered cubic, or BCC,[2] results. This is shown in Figure 2 below together with hard sphere and open versions of its unit cell. This structure is also common in metallic materials, although less so than FCC. It is, however, the basis for metals such as iron, molybdenum, and tungsten, for example.

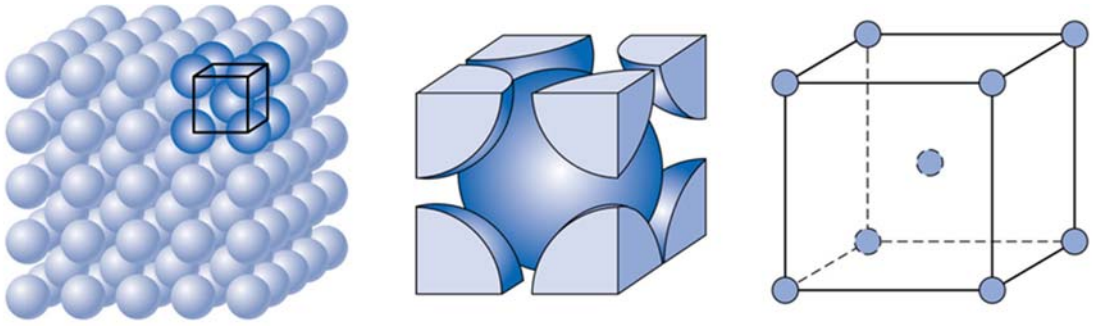

Figure 2: *Materials Science and Engineering,* W.D. Callister and D.G. Rethwisch, 9th ed., Wiley, Hoboken NJ, (2014), fig. 3.2, p. 56

23. A third, but less common, crystal structure is shown in Figure 3 below, in which the close packed layers are stacked in a different order from those in the FCC structure, as depicted on the right-hand side of Figure 3. This produces a crystal that no longer has the symmetry of a cube, as FCC and BCC do, but is instead hexagonal. The stacked example and its unit cell are shown in Figure 3 below. Materials that have the hexagonal form include titanium, ruthenium, and magnesium.

[2] I understand that the Court has construed "bcc-d" to mean "either a body centered cubic or a body centered cubic derivative crystal structure."

CONTAINS CONFIDENTIAL ATTORNEY EYES ONLY INFORMATION SUBJECT TO PROTECTIVE ORDER

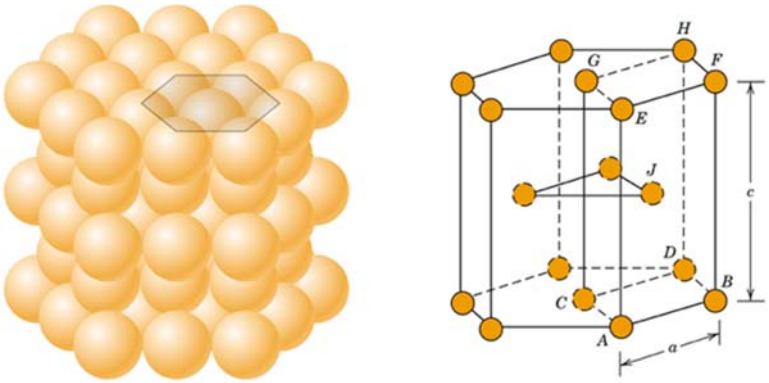

Figure 3: *Materials Science and Engineering,* W.D. Callister and D.G. Rethwisch, 9th ed., Wiley, Hoboken NJ, (2014), fig. 3.4, p. 57

24. Crystalline materials are formed by the repetition of small repeating building blocks – the unit cell. It is this feature that enables descriptions of crystalline material structure and behavior in simple terms.

b) **Directions and planes – Miller indices**

25. It is often convenient to specify a particular crystallographic plane of atoms, or a specific direction, within crystalline materials. For instance, planes are used to refer to interfaces in materials, and to external surfaces. The notational system that specifies these planes or directions is known as Miller indices.

(1) Planes

26. Miller indices for planes are obtained as follows. First, a coordinate system with its three axes *x*, *y*, and *z* situated at the cell corners and coinciding with the edges of the unit cell is specified. This is simple for FCC and BCC because the unit cell itself is a cube, and so these axes are mutually perpendicular to one another (see Figure 4 below). A plane of interest in the crystallographic material is then identified. For instance, in Figure 4 below, two planes, a red plane and a green plane, are depicted. That plane is assigned a series of numbers—its Miller indices—that uniquely identify it.

CONTAINS CONFIDENTIAL ATTORNEY EYES ONLY
INFORMATION SUBJECT TO PROTECTIVE ORDER

27. First, the fractional intersection of the plane along each of the three unit cell axes, *x*, *y*, and *z* is determined and designated as A, B, and C, respectively. Next, the reciprocals of A, B, and C are determined and multiplied by the common factor that converts them into the set of smallest integers *h*, *k*, and *l*. These integers *h*, *k*, and *l* are then enclosed in round brackets to identify the Miller indices of the plane, (*hkl*).

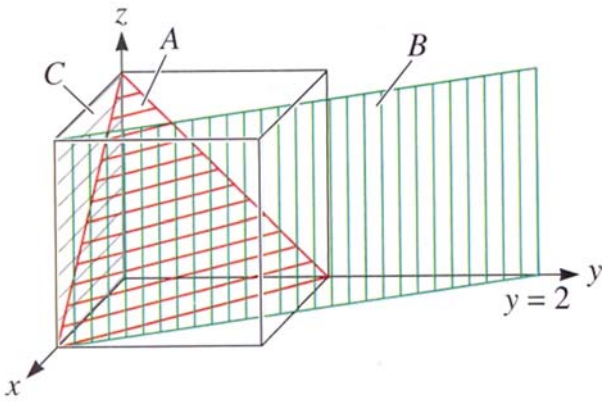

Figure 4: *The Science and Engineering of Materials*, D.R. Askeland and W.J. Wright, 7th ed., Cengage, Boston, (2016). Fig. 3-16, p. 70

28. In the example above, the red plane A intercepts *x* at 1, *y* at 1, and *z* at 1, so the reciprocals are simply 1, 1, and 1; there are no fractions to clear, so the plane has indices (111). The green plane crosses the *y* axis at 2, but never incepts the *z* axis, so $x = 1$, $y = 2$, and $z = \infty$. The reciprocals are then 1, ½, and 0, and clearing the fractions gives 2, 1, and 0. The plane is therefore (210).

29. Miller indices can also refer to "families" of planes that have the same three *h, k, l* indices but in differing orders, and allow all positive and negative combinations of indices, by enclosing them in curly brackets, {*hkl*}. Importantly, any plane of the {*hkl*} family is identical in terms of its atomic arrangement to any other plane of the same family, even though its specific indices may differ. For example, the six faces of a cubic unit cell, whether FCC or BCC, have

CONTAINS CONFIDENTIAL ATTORNEY EYES ONLY
INFORMATION SUBJECT TO PROTECTIVE ORDER

indices (100), (010), and (001), and their three negatives $(\bar{1}00)$, $(0\bar{1}0)$ and $(00\bar{1})$. All these planes are identical in structure and so can be referred to collectively as the {100} family.

(2) Directions

30. Using the same coordinate system as above, a particular direction in a crystal is determined using the coordinates of two points that lie on the direction, and then subtracting the coordinates of the starting point from those at the tip. (This procedure is greatly simplified if the starting point is the origin of the unit cell.) Once fractions are cleared, and the result reduced to the lowest possible integers, *p*, *q*, and *r*, the resulting numbers are enclosed in square brackets, [*pqr*]. As was the case with planes, families of directions of the form *pqr* may be indicated by enclosing these in angled brackets, <*pqr*>.

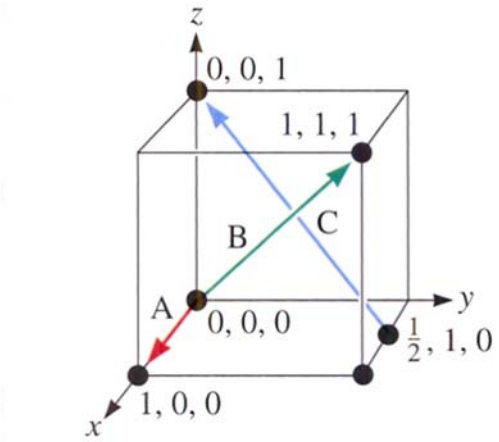

Figure 5: *The Science and Engineering of Materials*, D.R. Askeland and W.J. Wright, 7th ed., Cengage, Boston, (2016). Fig. 3-13, p. 68

31. For example, in Figure 5 above, the direction *A* ends at the point 1, 0, 0, so its Miller indices are [100]. The direction *B* is similarly indexed as [111]. Direction *C* has end points 0, 0, 1 and ½, 1, 0, so subtracting one from the other gives -½, -1, 1, which when multiplied by 2 gives $[\bar{1}\bar{2}2]$.

CONTAINS CONFIDENTIAL ATTORNEY EYES ONLY
INFORMATION SUBJECT TO PROTECTIVE ORDER

32. For hexagonal crystals, a special set of indices called Miller-Bravais indices is used. This is a four-index system, with axes a_1, a_2, a_3, and c, where the axis a_3 is redundant. The reason for this complexity is that in the three-index system described above, because of the hexagonal symmetry of the crystal, planes and directions belonging to the same family of indices no longer have identical atomic arrangements. The Miller-Bravais indexing restores their equivalence. Figure 6 below illustrates the indexing of planes in the HCP system using a four-axis coordinate system. Following the same procedure as for cubic crystals, the indices of the planes *A* and *B* are determined as (0001) and $(11\bar{2}1)$ respectively. The directions *C* and *D* are $[\bar{2}113]$ and $[\bar{1}100]$.

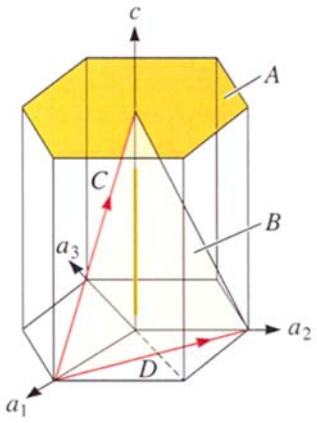

Figure 6: *The Science and Engineering of Materials*, D.R. Askeland and W.J. Wright, 7th ed., Cengage, Boston, (2016). Fig. 3-19, p. 73

c) **Orientation relationships and variants**

33. When one material is deposited onto another, especially when they have different crystal structures, the deposited material will try to minimize the interfacial energy between it and the material upon which it is grown, or the "atomic template."[3] One way in which this direction of the growth of the deposited material layer is achieved is that directions <*pqr*> in the

[3] I understand that the Court has construed "atomic template" to mean "an atomic pattern upon which material is grown and which is used to direct the growth of an overlying layer."

CONTAINS CONFIDENTIAL ATTORNEY EYES ONLY
INFORMATION SUBJECT TO PROTECTIVE ORDER

atomic template and the deposited material are matched, such that they are roughly similar and so "fit" well together. In the case of FCC and BCC materials, a number of orientation relationships that satisfy this requirement may be found. Two examples are the Kurdjumov-Sachs and Nishiyama-Wasserman orientations. Both share the same basis in which a {111} FCC plane is parallel to a {110} BCC plane. A schematic diagram of these two orientations is shown in Figure 7 below.

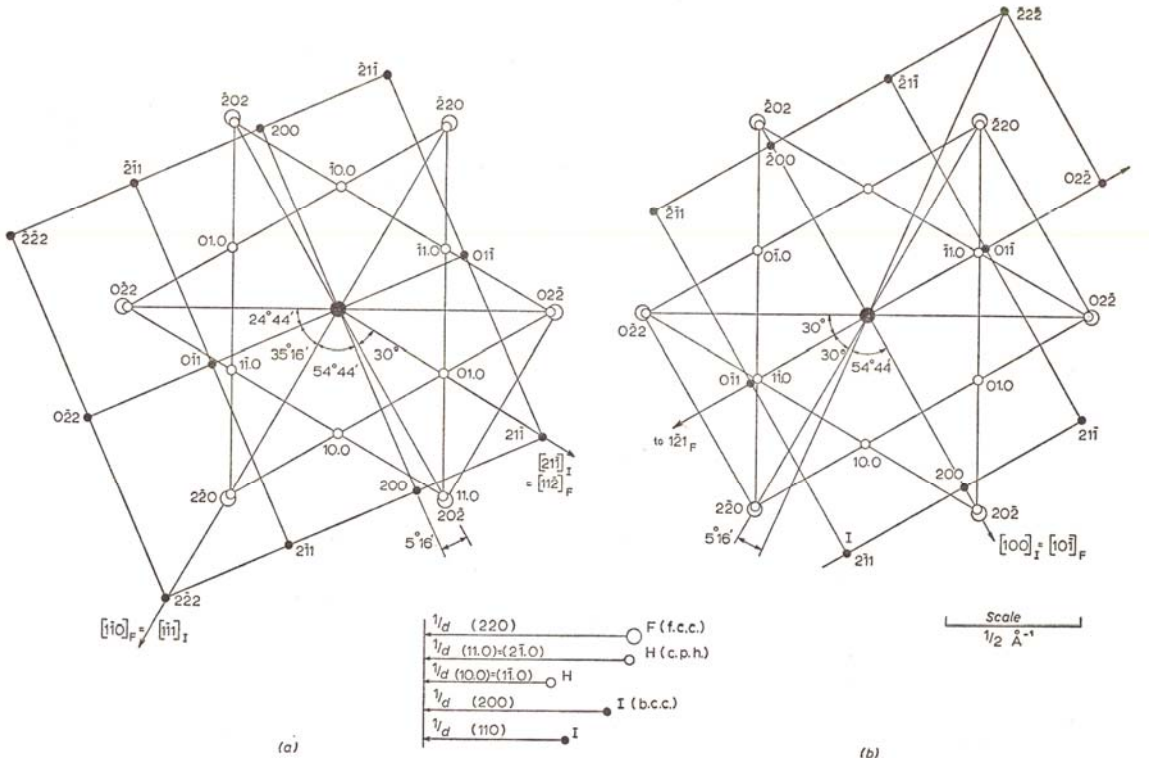

Figure 7: Kurdjumov-Sachs (a) and Nishiyama–Wasserman (b) orientation relations, viewed looking down on their common $(111)_{FCC}||(011)_{BCC}$ plane. The open circles belong to the FCC crystal, while the filled ones are the BCC one. *Interpretation of Electron Diffraction Patterns,* K.W. Andrews, D.J. Dyaon, and S.R. Keown, Plenum, New York, (1967), fig. 50, p. 170

34. The Kurdjumov-Sachs orientation is on the left, and Nishiyama-Wasserman on the right. The diagram has the common $(111)_{FCC}||(011)_{BCC}$ direction pointing out of the page, and the open circles belong to the FCC lattice while the filled black ones are from the BCC lattice.

CONTAINS CONFIDENTIAL ATTORNEY EYES ONLY
INFORMATION SUBJECT TO PROTECTIVE ORDER

35. These relationships occur mainly because the {111} plane in FCC is the closest packed plane in that structure, and the atomic arrangement on the {110} BCC plane matches it closely. The symmetry of these cubic crystals leads to a number of alternative descriptions of these orientation relationships, known as variants.[4] In the case of the Kurdjumov-Sachs orientation relationship, this symmetry leads to 24 variants. For Nishiyama-Wasserman, the number of variants reduces to 12. However, for any given {111} FCC plane, this reduces to six physically distinct variants for Kurdjumov-Sachs, and three for Nishiyama-Wasserman. The six possible variants for Kurdjumov-Sachs in thin film materials are illustrated in Figure 8 below.

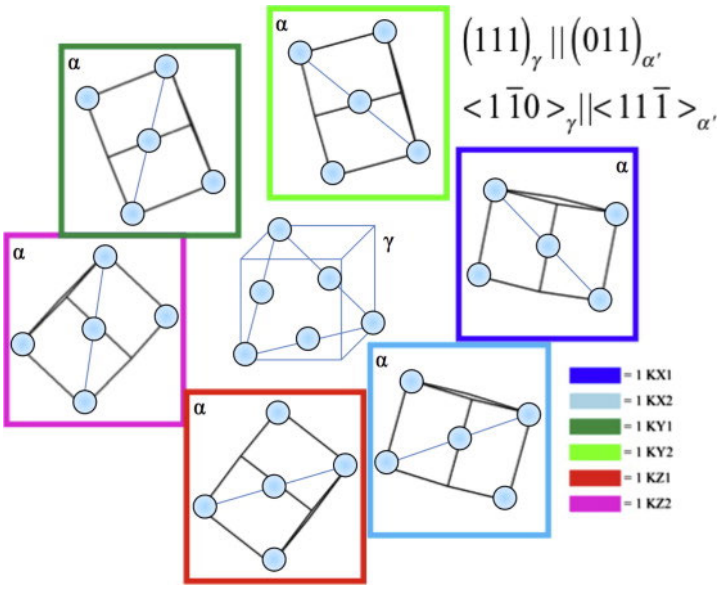

Figure 8: The six variants of $\{110\}_{BCC}$ (α) on $\{111\}_{FCC}$ (γ) in the Kurdjumov-Sachs relationship. "*The microstructure of dislocated martensitic steel: Theory*", L. Qi, A.G. Khachaturyan, and J.W. Morris, Jr., Acta Materialia, **76**, (2014), fig. 2, p. 24

36. There are two equivalent <111> directions that are the diagonals of the rectangular $(011)_{BCC}$ (α) planes, shown as the diagonal lines in Figure 8. There are three equivalent <110> directions marked in the triangular $(111)_{FCC}$ (γ) plane. Therefore there are six

[4] I understand that the Court has construed "variant/orientational variant" to mean "one of a set of possible crystal orientations" and "variants/orientational variants" to mean "two or more of a set of possible crystal orientations."

CONTAINS CONFIDENTIAL ATTORNEY EYES ONLY
INFORMATION SUBJECT TO PROTECTIVE ORDER

distinct ways of arranging the outer $(011)_{BCC}$ plane so that one of its $<111>_{BCC}$ directions aligns parallel to one of the three $<110>_{FCC}$ directions in the $(111)_{FCC}$ plane. These are the six possible variants of the Kurdjumov-Sachs orientation relationship for thin film materials.

37. In some cases, the template for the Kurdjumov-Sachs orientation relationship for thin film materials is not $\{111\}_{FCC}$ (as is the case with, for example, the NiFe atomic templates discussed in Sections F.1 and F.2 below), but is instead, yet equivalently for the purposes of this Report, $\{0001\}_{HCP}$ (close packed hexagonal) (as is the case with, for example, Ru atomic templates).[5,6] Since the atomic arrangement of $\{0001\}_{HCP}$ is exactly the same as that of $\{111\}_{FCC}$, the same epitaxial orientations are found, but in this case are referred to as the Burgers orientation. Just as with Kurdjumov-Sachs, there are 6 possible variants of the Burgers orientation on any given $\{0001\}_{HCP}$ plane, and these are shown in Figure 9 below. In this case, the $(110)_{BCC}$ planes are shown superimposed on the hexagonal $(0001)_{HCP}$ planes, rather than being set alongside it.

[5] I understand that the Court has construed "[layer] providing a (111) textured hexagonal atomic template" to mean "layer that is predominately (111) hexagonal and that provides an atomic template."

[6] In the HCP arrangement, the {0001} plane is equivalent to the {0002} plane because the HCP unit cell is two layers high and the {0002} plane has the same atomic arrangement as the {0001} plane, just in the layer below the {0001} plane. Additionally, the atomic arrangement of the $\{111\}_{FCC}$ plane is exactly the same as the $\{0002\}_{HCP}$ plane, where both are the closest packed possible arrangements.

CONTAINS CONFIDENTIAL ATTORNEY EYES ONLY
INFORMATION SUBJECT TO PROTECTIVE ORDER

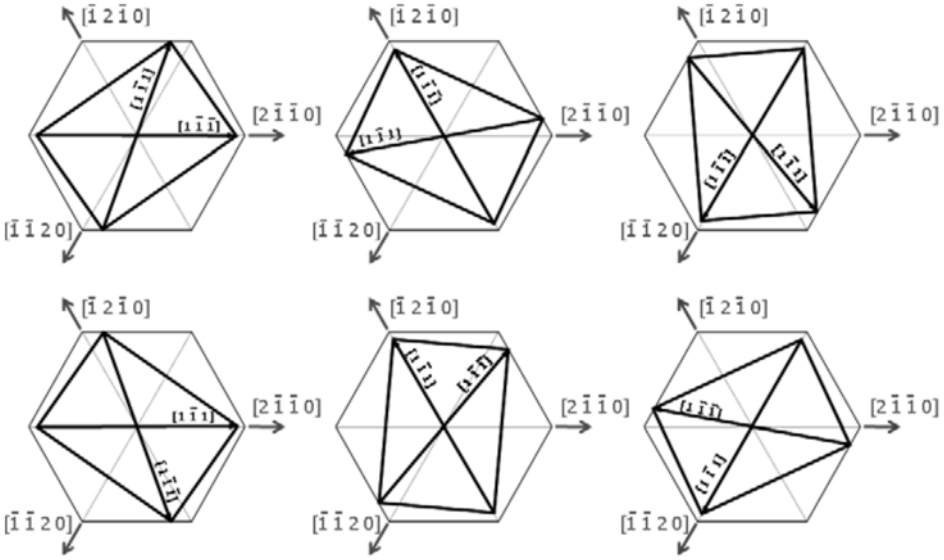

Figure 9: The six variants of $\{110\}_{BCC}$ on $\{0001\}_{HCP}$ in the Burgers orientation relationship. "Evaluation of misorientation angle-axis set between variants during transformation of bcc to hcp phase obeying Burgers orientation relation", T.Karthikeyan, S.Saroja and M.Vijayalakshmi, Scripta Materialia, **55**, (2006), fig. 2, p. 773.

2. **Transmission Electron Microscopy (TEM)**

a) **Basic principles**

38. The transmission electron microscope (TEM) is analogous to the more common light microscope, which is composed of a light source (a), a transparent specimen (b) (usually mounted on a glass slide), and an imaging system that ends at the eyepiece (c) through which the observer views the specimen. The smallest image detail that can be resolved in this (or any) microscope is limited by the wavelength λ of the illumination (*see Electron Microscopy of Thin Crystals,* P.B. Hirsch, A. Howie, R.B. Nicholson, D.W. Pashley, and M.J. Whelan, Butterworths, London, (1965) at p. 9), which for the optical microscope is visible light, where λ is about 400 – 800 nm. TEMs, on the other hand, can resolve much finer detail. TEMs contain the same components as the light microscope, but upside down, with the illumination source (a)

CONTAINS CONFIDENTIAL ATTORNEY EYES ONLY
INFORMATION SUBJECT TO PROTECTIVE ORDER

at the top, the sample (b) in the middle, and the imaging system (a camera, rather than the human eye) at (c) at the bottom.

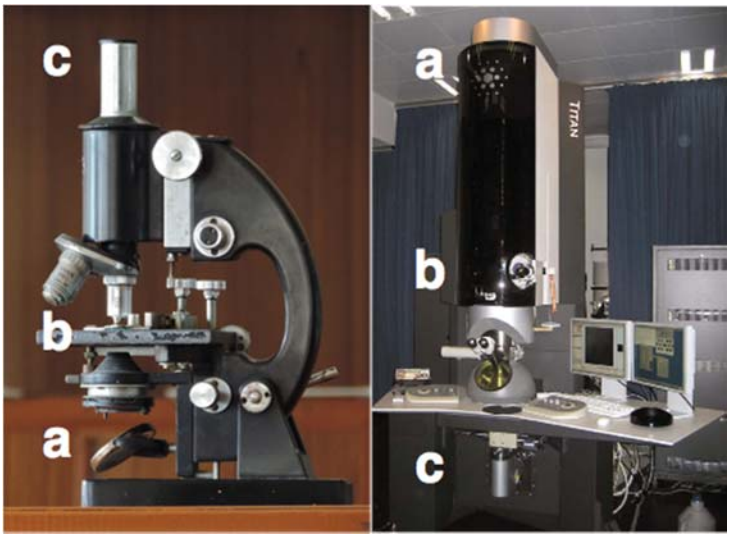

Figure 10: Right hand figure from *Transmission Electron Microscopy*, D.B. Williams and C.B. Carter, Springer, (2009), fig. 1.9, p. 13.

39. The illumination in the TEM is not light, but electrons produced from a filament, and it is this difference that gives the improvement in resolution over the light microscope. Much like light, these electrons have an associated "wavelength" and are treated like light is in the optical microscope. The wavelength of the electron in the TEM is much smaller than that of visible light, as little as 0.00196pm in the TEM shown above. While instrumental limitations of the TEM mean that we do not achieve this theoretical resolution, a TEM such as the FEI Titan 80-300 S-Twin (shown above) can resolve structures with features in the 0.07 nm range, i.e., smaller than the spaces between atoms in many materials.

b) **Diffraction**

40. The TEM offers more than just imaging of the structure of materials. As in any optical imaging system, the TEM forms not just a final image, but in the back focal plane of the imaging lens, there is a diffraction pattern. Diffraction is the process that occurs when a wave encounters an obstacle, such as a crystalline specimen. The incident illumination is

CONTAINS CONFIDENTIAL ATTORNEY EYES ONLY
INFORMATION SUBJECT TO PROTECTIVE ORDER

scattered in such a way that its angular spacing in the diffraction pattern is inversely proportional to the dimensions of the object causing the diffraction. As a result, it reveals valuable information about the symmetry and structure of a crystalline specimen. It is easier to view these diffraction patterns in the TEM than in an optical microscope, since the focal length of the lenses used in the TEM can be varied in a way that glass lenses cannot. Specific uses for diffraction patterns are discussed further in Section E.2.c. below.

41. Figure 11 below shows the paths light takes in an optical system, but the electrons in a TEM follow similar paths and work on similar principles. In Figure 11, for example, the light paths (rays) emerging from two different points on the specimen, illuminated from above, are traced, and at each point we follow one ray leaving the specimen scattered directly down the page, and two others inclined at some angle to either side of the first. There are many more rays scattered at each point of the specimen, but just three are shown here for two different points on the specimen to illustrate.

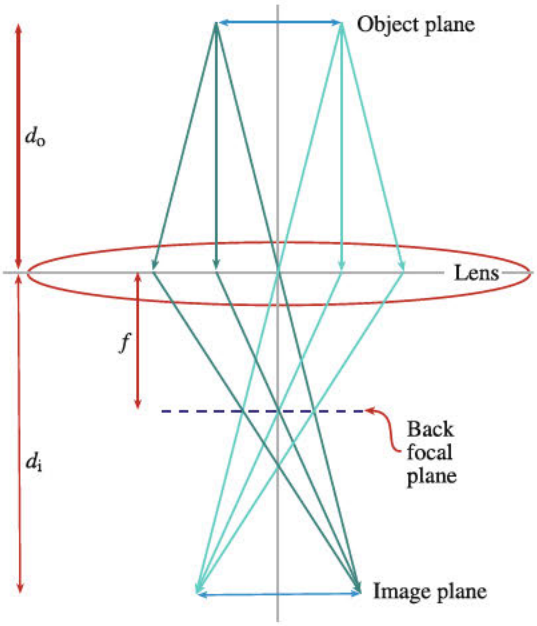

Figure 11: *Transmission Electron Microscopy,* D.B. Williams and C.B. Carter, Springer, (2009), fig. 6.3, p. 94

CONTAINS CONFIDENTIAL ATTORNEY EYES ONLY
INFORMATION SUBJECT TO PROTECTIVE ORDER

42. The rays travel through the objective lens, called the "Lens" in Figure 11, through the back focal plane of the lens, and then onto the image plane where an image of the specimen can be observed. There are two important features to note here.

43. First, all the rays that leave the sample travelling in the *same direction*, regardless of where on the sample they originate, pass though the *same spot* in the back focal plane. Accordingly, three such spots can be seen in the back focal plane in the figure above – one for the forward scattered beams, and one for each of those at an angle to the forward scattered direction. These "spots" form the basis for the Fraunhofer *diffraction pattern*, which is used extensively in imaging the sample, and in determining its crystal structure, as discussed further in Section E.2.d below.

44. Second, all the rays that leave the sample from the *same point*, regardless of the direction in which they are travelling, meet at the *same point* in the first image plane, and so form an *image* of the sample.

45. TEMs can take advantage of these features because of the nature of electromagnetic lenses. Because electrons carry a charge, they can be deflected by a magnetic field. The "electron lens" consists of a coil through which a current passes. In doing so, a magnetic field is created inside the lens that will deflect, i.e. focus, the electrons, producing a lens whose focal length can be varied by changing the current through the coil. This change of focal length cannot be done in a microscope with glass lenses, but TEMs allow this simple way of imaging not only the sample but also its diffraction pattern. Figure 12 below shows a TEM set for imaging the diffraction pattern, on the left, and the sample on the right.

46. The diagrams show the formation of a diffraction pattern in the back focal plane at (a) in both diagrams and the formation of the first image at (b) in both. Below the objective

CONTAINS CONFIDENTIAL ATTORNEY EYES ONLY
INFORMATION SUBJECT TO PROTECTIVE ORDER

lens, there is an intermediate lens and a projector lens. By weakening the current in the intermediate lens, and so increasing its focal length, we can change the image observed from the first image plane at (b) up to the diffraction pattern at (a). This is simply accomplished by a single switch in the microscope. In the left-hand diagram we can follow the ray path of the red dot, representing a spot in the diffraction pattern, through the intermediate image plane and on to the final image place, showing that it is the diffraction pattern that appears at the final image plane.

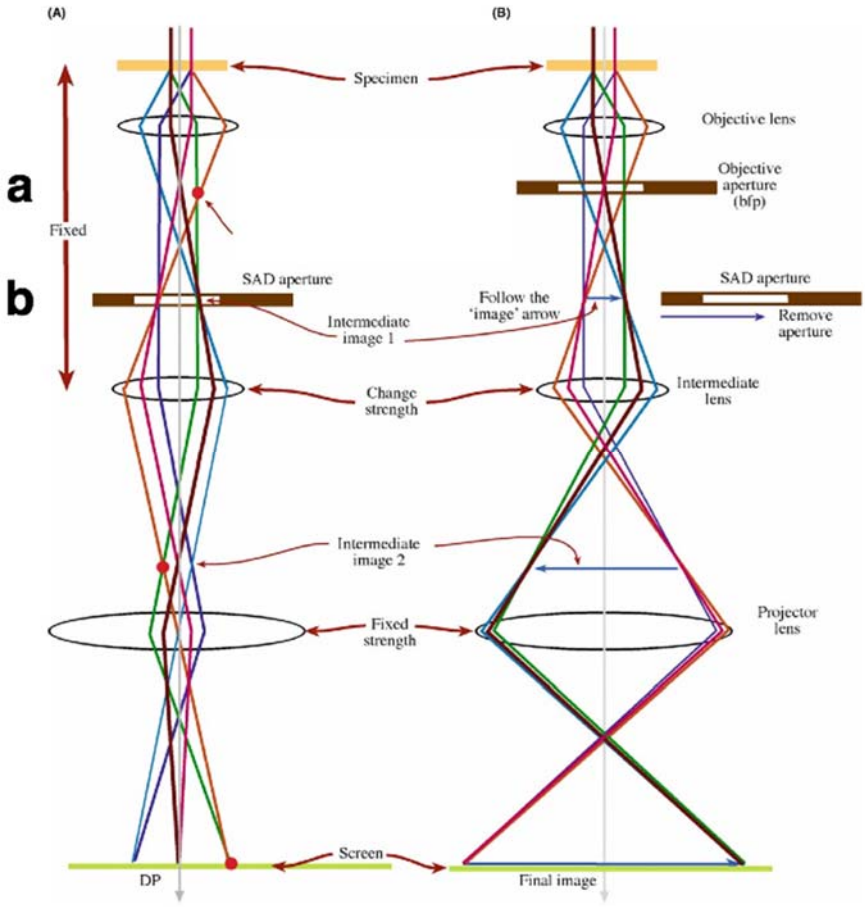

Figure 12: Ray diagrams showing a TEM set up to examine the diffraction pattern (left) and the image of the specimen (right). *Transmission Electron Microscopy*, D.B. Williams and C.B. Carter, Springer, (2009), fig. 9.12, p. 153

CONTAINS CONFIDENTIAL ATTORNEY EYES ONLY INFORMATION SUBJECT TO PROTECTIVE ORDER

c) **Diffraction patterns**

47. A typical diffraction pattern as observed in the TEM is shown in Figure 13 below. This figure shows a bright center spot, corresponding to the direction in which the forward scattered electrons will arrive in the image, surrounded by an array of other spots lying on a well-defined rectangular grid. In fact, this diffraction pattern is just a two-dimensional section through a three dimensional array of points, one for every family of planes in the crystal. This three-dimensional array is known as the reciprocal lattice, and is characteristic of the crystal that gave rise to it. The reciprocal lattice can be imagined to be cut by a sphere of radius 1/(electron wavelength), known as the Ewald sphere[7], and only those spots that actually touch the sphere will show bright in a diffraction pattern.

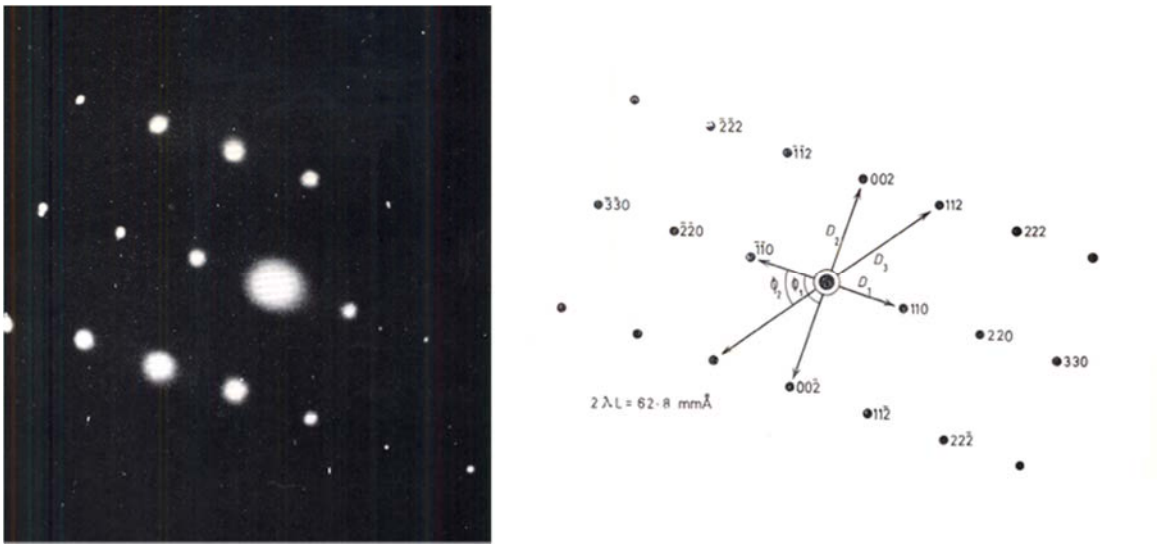

Figure 13: Diffraction pattern from BBC α-iron (left), and its indexed solution (right). *Interpretation of Electron Diffraction Patterns,* K.W. Andrews, D.J. Dyson, and S.R. Keown, Plenum, New York, (1967), plate 9, p. 224

48. Each spot represents diffraction from a single family of planes in the specimen. When a family of planes is inclined to the incident electron beam by a particular small angle (see

[7] See e.g. *Transmission Electron Microscopy,* D.B. Williams and C.B. Carter, Springer, (2009), p.214 et seq.

CONTAINS CONFIDENTIAL ATTORNEY EYES ONLY
INFORMATION SUBJECT TO PROTECTIVE ORDER

angle 2θ in Figure 14 below), known as the Bragg angle, strong diffraction will occur, and the electrons will be diffracted and change direction. The angle involved is small, typically on the order of a degree or less, and the diffracted electrons will pass through a single spot in the back focal plane of the objective lens, i.e. in the diffraction pattern.

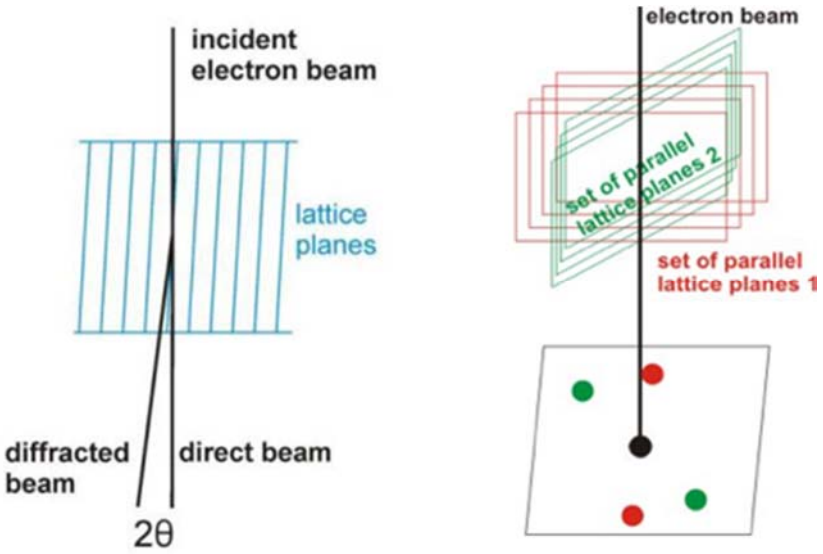

Figure 14: Illustration of the mechanism of Bragg scattering in the TEM (left), and the formation of a diffraction pattern (right). "Properties of Electrons, their Interactions with Matter and Applications in Electron Microscopy", F. Krumeich, ETH Zurich, Switzerland, *available at* www.microscopy.ethz.ch, fig. 16, p. 12, and fig. 19, p. 14

49. As illustrated on the right-hand side of Figure 14 above, the spacing of the spots from the center spot is inversely proportional to the spacing of that family of planes in the actual specimen, and the angles that the spots subtend with one another through the center spot are the angles that the planes make with one another in the specimen. This information is enough to determine which family of planes each spot comes from, index them, and hence which direction points out of the page. In the case of the diffraction pattern above, this analysis reveals that we are looking down onto a $(1\bar{1}0)_{BCC}$ plane. The diffraction pattern can therefore be used to identify the crystal structure of the sample—for example, bcc, fcc, or hcp.

CONTAINS CONFIDENTIAL ATTORNEY EYES ONLY
INFORMATION SUBJECT TO PROTECTIVE ORDER

50. The TEM is also designed to allow the sample to tilt in the microscope over a wide angular range, approximately ± 45˚. As the sample is tilted, the section of the reciprocal lattice cut by the static Ewald sphere changes as the direction along which the sample is viewed is changed, so that the observed diffraction pattern changes to reflect this. Identifying how the diffraction pattern changes as the sample is tilted allows for a determination of the orientation of the specimen in the microscope at any tilt angle.

51. In some instances, such as that shown in Figure 15 below, more than one crystallite contributes to the observed pattern. These crystallites may simply be contiguous, and both captured in the pattern, or overlapping, as in the case of a layered structure. In the diffraction pattern above, a rectangular $\{110\}_{BCC}$ pattern is observed. When a second pattern from a neighboring crystal with the same symmetry, but rotated with respect to the first, is also allowed to contribute to the diffraction pattern, we see the compound pattern seen contributions of each crystal to this diffraction pattern, as is shown in the diagram below the two diffraction patterns. I use this technique in obtaining diffraction information from plan view samples, and so examining the orientation relationships between crystallites.

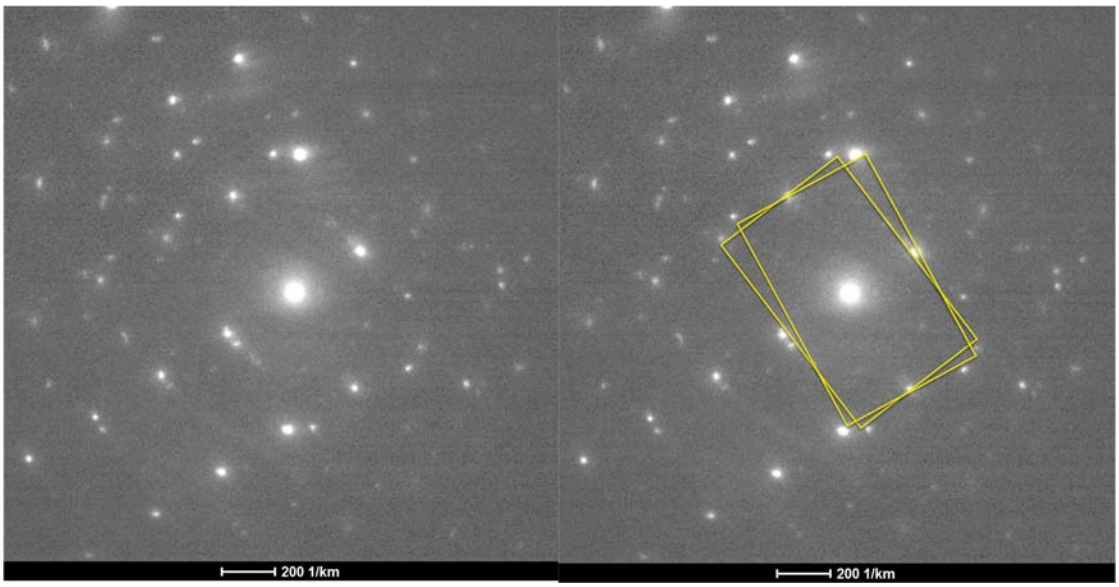

CONTAINS CONFIDENTIAL ATTORNEY EYES ONLY
INFORMATION SUBJECT TO PROTECTIVE ORDER

Figure 15: Diffraction pattern from S0GPPC, frame 721, showing patterns from two adjacent crystallites, both in the $\{011\}_{BCC}$ orientation, but rotated by ~5˚ relative to one another.

d) **Microbeam diffraction**

52. Microbeam diffraction is performed with a finely focused electron beam (considerably smaller than the diameter of the crystallites in the sample), and the TEM is adjusted to image the resulting diffraction pattern. By scanning the electron beam systematically point by point over an area of the sample, as many as 1,600 individual diffraction patterns from a single small area may be generated. An example is shown in Figure 16 below, where the area from which the patterns were obtained is marked as a red box shown on the left, and a typical pattern showing that an $\{011\}_{BCC}$ direction is parallel to the electron beam is shown on the right. These patterns can be analyzed to determine crystallite orientations, as explained earlier, and especially to investigate the relative orientations of contiguous crystallites.

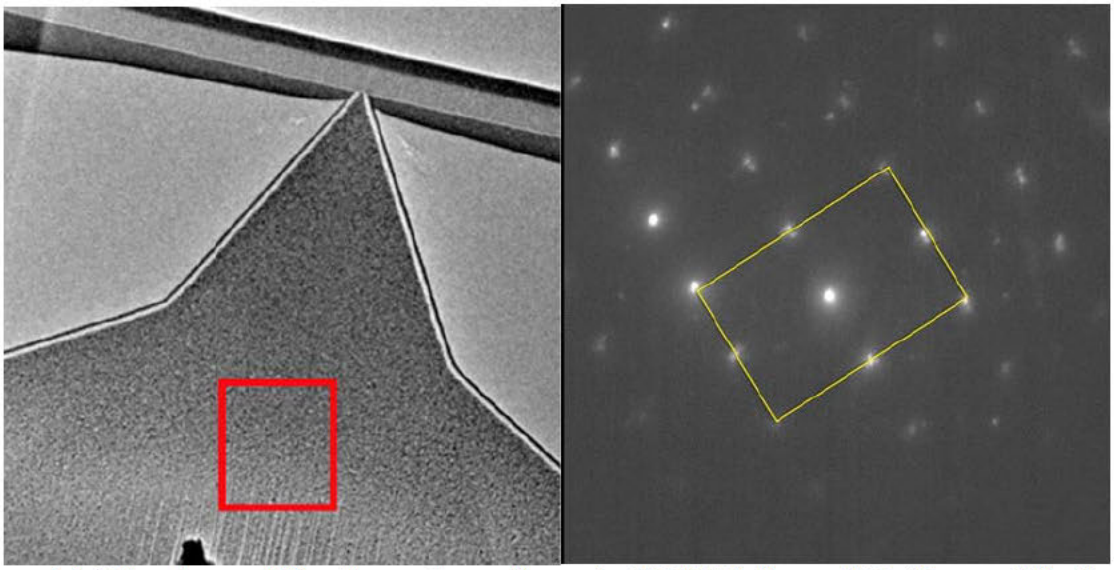

Figure 16: Microbeam diffraction pattern of sample S0GPPC, frame 722, discussed further in Section F.1.a.4 below. The red box on the left indicates the area in the sample from which the diffraction patterns were taken. A typical diffraction pattern is shown on the right, with a single $\{011\}_{BCC}$ orientational variant indicated by the yellow box.

53. When two or more crystallites are simultaneously excited by the electron beam, the resulting patterns may contain information about variants in special orientations. The pattern

CONTAINS CONFIDENTIAL ATTORNEY EYES ONLY
INFORMATION SUBJECT TO PROTECTIVE ORDER

below, for example, shows three common $\{011\}_{BCC}$ directions, rotated relative to each other by approximately 11˚ and 55˚, consistent with the special Kurdjumov-Sachs orientation. Analysis of diffraction patterns for each sample is discussed further below.

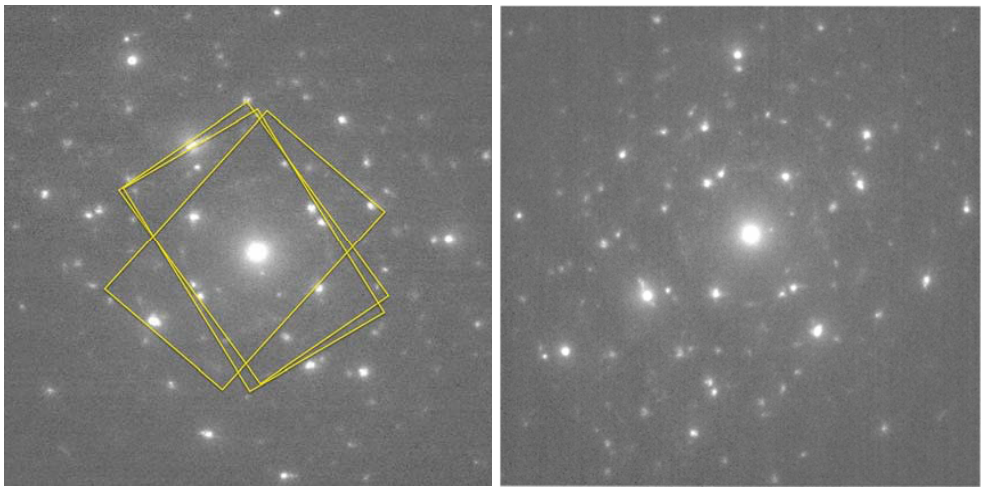

Figure 17: Diffraction pattern from sample S0GPPC, frame 1487, showing three orientational variants.

e) **Bright and dark field imaging in the TEM**

54. There are two modes of diffraction imaging in the TEM known as bright field and dark field imaging. As Figure 18 below shows, an objective aperture can be inserted into the back focal plane of the TEM, i.e. at the level of the diffraction pattern, and used to select a single diffraction spot to contribute to the final image, blocking the others. This means that the final image of the sample from the TEM contains only those electrons that passed through this aperture. Since the diffraction spot itself consists of those electrons scattered in a particular direction by one particular set of planes in the sample, it allows us to examine the contribution of only those planes to the overall image. In Figure 18(A) below, the effect of placing the aperture around the central spot in the diffraction pattern is shown. This allows those electrons which pass down the optic axis in the forward scattered direction—that is, those electrons which are *not* diffracted into other diffraction spots—to form the image. This is called the ”bright field” image

CONTAINS CONFIDENTIAL ATTORNEY EYES ONLY
INFORMATION SUBJECT TO PROTECTIVE ORDER

and is composed of all those electrons that arrive in the back focal plane in the forward scattered direction. It has a bright background, dark only where electrons have been scattered by some planes into one of the other diffraction spots.

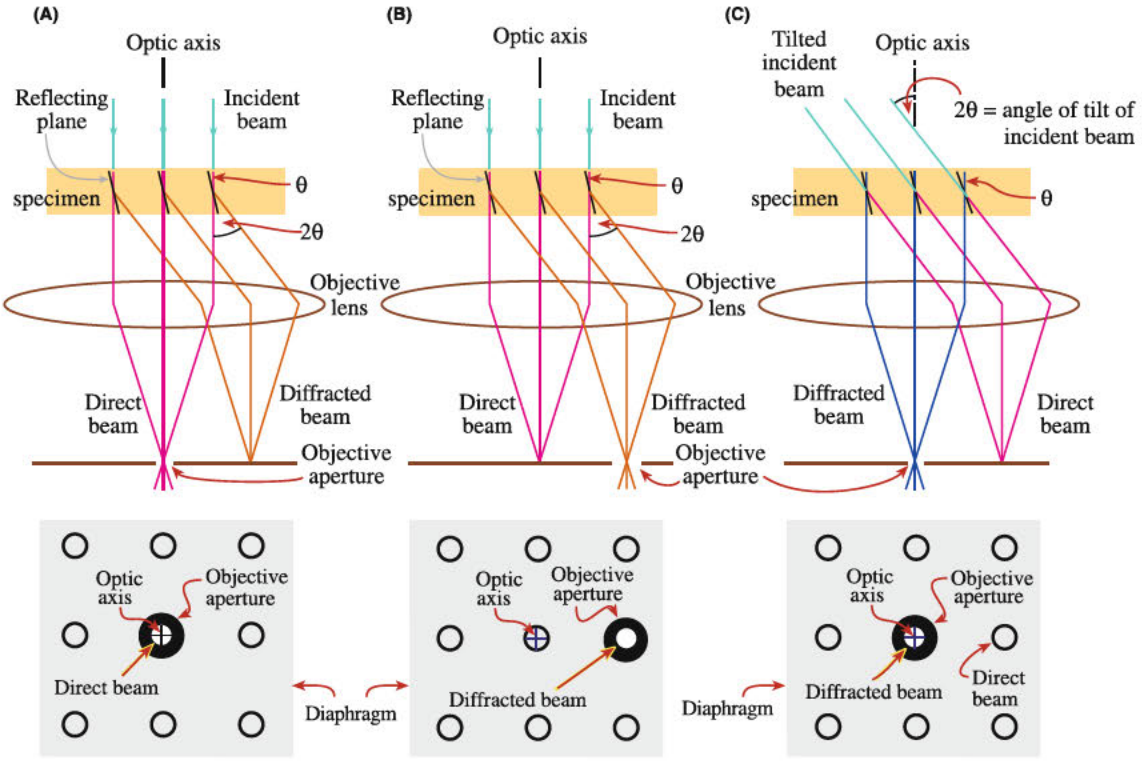

Figure 18: *Transmission Electron Microscopy,* D.B. Williams and C.B. Carter, Springer, (2009), fig. 9.14, p. 156

55. In Figure 18(B), the effect of placing this aperture around one of the diffracted spots is shown. This will allow only those electrons scattered into that spot by the particular set of planes that correspond to it to form the image. This is the "dark field" image, since the background to the image is dark everywhere except where the particular family of planes have scattered electrons. Although this image can be used, displacing the aperture off the optic axis leads to a degradation of image quality. To rectify this, the illumination is adjusted to bring the diffraction spot desired to the optic axis, and then the aperture is placed around it. This is the "centered dark field" image, and it results in an image that highlights only those regions of the

sample in which that particular family of planes is oriented with respect to the electron beam so as to diffract strongly. This allows, for example, to see directly in an image which parts of the sample satisfy this diffraction condition for a chosen set of planes. Planes that show bright have their normal aligned so as to point in the direction of the aperture placed on the diffraction pattern. As the aperture is moved around the central spot in the diffraction pattern, the number and position of the bright crystallites in the image will change, depending on their orientation in the plane.[8] This technique is used to investigate how the <200>$_{BCC}$ directions, that are the directions of easy magnetization in the FeCo layer(s), are oriented with respect the read/write head; this is discussed further in Sections F.1.a.5, F.1.b.5, and F.2.a.5 below.

f) **Dark field image analysis**

56. The basics of dark field imaging in the TEM are discussed in Section E.2.e above. A specific application of this imaging technique is utilized to determine the fraction of FeCo crystallites with their <100> directions perpendicular to the long axis of the recording head.[9] The scope of my assignment includes an analysis of the fraction of crystallites in the magnetic layer of the write pole as a function of orientation in the write pole plane. In the magnetic materials in question, the <100> directions perpendicular to the long axis of the recording head are the "easy" directions of interest, and thus, analyzed in this Report.

57. Because there are many small crystallites contained in the imaged area of the head, and these crystallites have varying orientations, the diffraction pattern does not show discrete diffraction spots, but is rather a series of concentric rings, each corresponding to one family of planes within the sample.

---

[8] *See generally Transmission Electron Microscopy,* D.B. Williams and C.B. Carter, Springer, (2009), section 9.38, p. 155.

[9] *See, e.g., Electron Microscopy of Thin Crystals,* P.B. Hirsch, A. Howie, R.B. Nicholson, D.W. Pashley, and M.J. Whelan, Butterworths, London, (1965), pp. 295-310; *Transmission Electron Microscopy,* D.B. Williams and C.B. Carter, Springer, (2009), section 9.38, pp. 155-158.

CONTAINS CONFIDENTIAL ATTORNEY EYES ONLY
INFORMATION SUBJECT TO PROTECTIVE ORDER

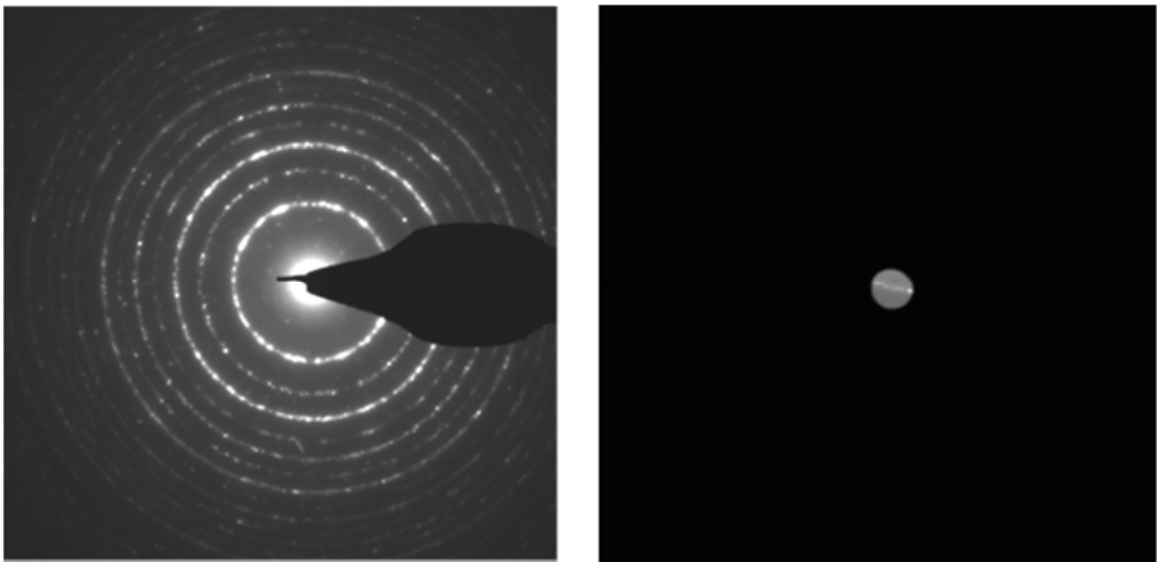

Figure 19: Diffraction pattern taken from S0GPPC, and incorporating many crystallites. On the right is an image of the objective aperture selecting the small segment of the 002 diffraction ring from which a dark field image is formed.

58. In Figure 19 above, the second ring from the center is formed by diffraction from {200} planes, and is the one of interest. Note that for the analysis conducted in Sections F.1.a.5, F.1.b.5, and F.2.a.5 below, while the orientation of the <100> directions in the magnetic write pole material is of interest, spots from $\{100\}_{BCC}$ do not appear in a diffraction pattern since they are forbidden by the structure factor. The first diffraction spot in the <100> direction that does show up is <200>, from planes that are one half the spacing of the {100} planes. The <200> and <100> directions point in the same direction in the crystal, and so can be used interchangeably when referring to directions in the specimen. This ring is not continuous but contains some brighter and some darker regions.

59. To determine which orientations of the crystallites in the sample are preferred, a segment of the {200} ring is selected with the objective aperture, as can be seen on the right-hand side of Figure 19 above. As a result, only those crystallites whose <200> directions fall within this aperture will appear bright in a dark field image. The aperture is then moved in ~10° increments around the ring, at the same time keeping the ring on the optic axis, and a dark field

CONTAINS CONFIDENTIAL ATTORNEY EYES ONLY
INFORMATION SUBJECT TO PROTECTIVE ORDER

image at each 10° setting is taken. Note that since the results are symmetric about 180˚, it is not necessary to repeat the procedure about the entire 360˚ ring. An example of two such images, taken from different parts of the {200} ring, is shown in Figure 20 below. The contrast between the number of bright crystallites in the two images is clear; the image on the left shows more bright crystallites than the one on the right. This indicates that more {200} planes are oriented to scatter into the objective aperture positioned for the left hand image, than do when it is set for the right hand one.

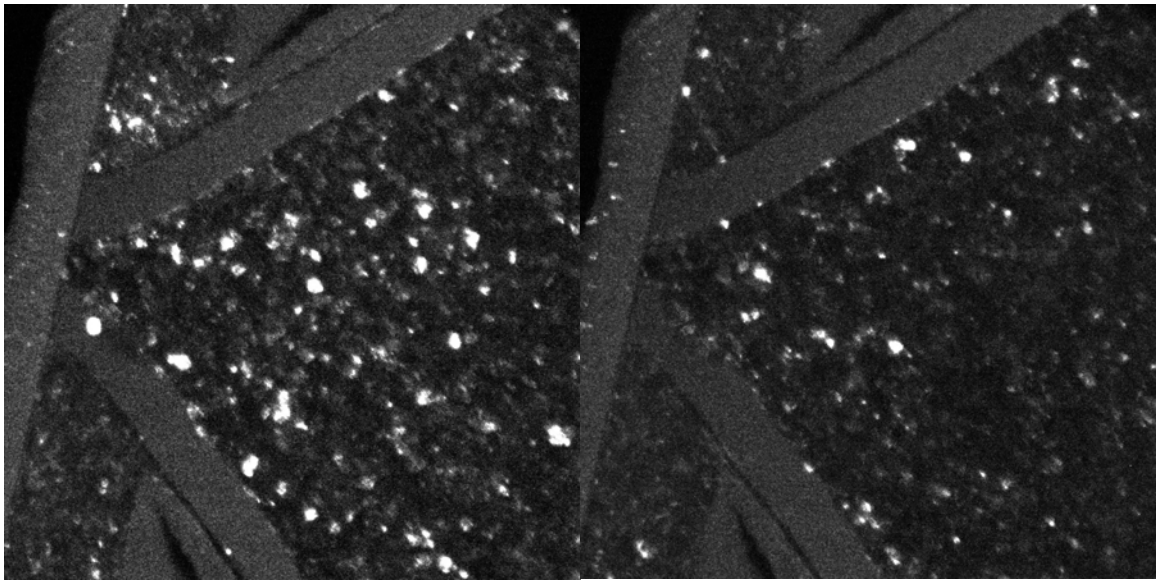

Figure 20: Dark field images taken from sample S0GPPC.

60. The area fraction of bright crystallites in each image is obtained by standard quantitative stereological procedures, using software such as ImageJ or MIPAR, and the results analyzed to determine the preferred orientations of the easy directions in the recording head. This area fraction is plotted against the angular position of the aperture as in the example of Figure 21 below, and this graph shows how the <200> directions prefer to align with respect to the read/write head. The example of Figure 21 below shows the <200> directions align preferentially at 0˚ and 180˚ with respect to the direction perpendicular to the long axis of the head, rather than simply being aligned at random in all directions.

CONTAINS CONFIDENTIAL ATTORNEY EYES ONLY
INFORMATION SUBJECT TO PROTECTIVE ORDER

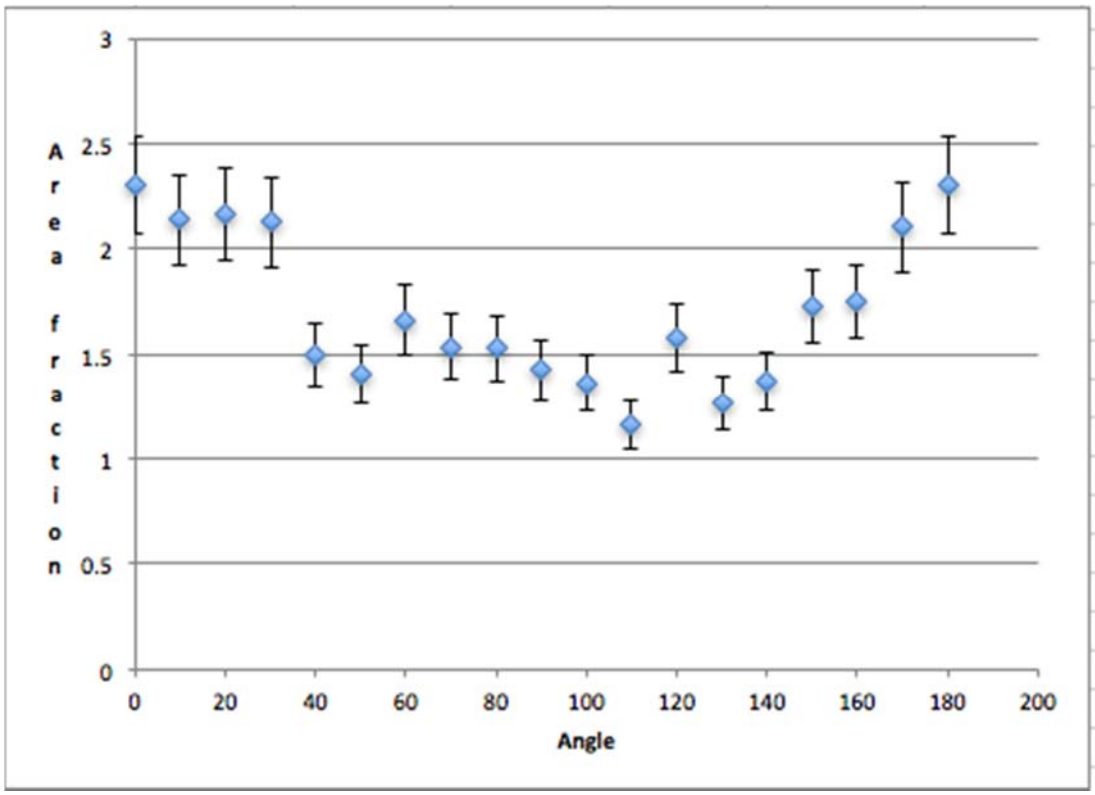

Figure 21: Graph for S0GPPC showing the area fraction of <200> oriented crystals as a function of angles around the {200} diffraction ring.

g) **High resolution imaging**

61. High-resolution TEM imaging allows for the formation of as complete an image of the crystal structure of the sample as possible. In high-resolution TEM imaging, as many diffracted beams as possible contribute to the image so that the resulting image is as faithful a representation of the structure of the sample as possible. The current generation of advanced TEMs allow for more efficient high-resolution imaging by operating the microscope in the high-resolution scanning transmission (STEM) mode.

h) **Scanning transmission electron microscopy (STEM)**

62. In the scanning transmission mode, the TEM is operated like a scanning electron microscope. Instead of a static broad beam of illumination, incident over a wide area of the sample, a very fine electron probe is formed that is then scanned point by point over the specimen surface. At each point, information from the small area of the sample currently excited

CONTAINS CONFIDENTIAL ATTORNEY EYES ONLY
INFORMATION SUBJECT TO PROTECTIVE ORDER

is collected and can be used to form an image, or perform chemical and other analyses. This imaging mode is especially efficient when the STEM is equipped with a high angle annular dark field (HAADF) detector, which is very efficient at capturing the scattered electrons in STEM. High resolution images may contain information on details as small as atomic positions, and so can provide information about the structure of the crystal lattice. An example of a typical high-resolution TEM image, taken from a cross-section of a hard drive write head, is shown below.

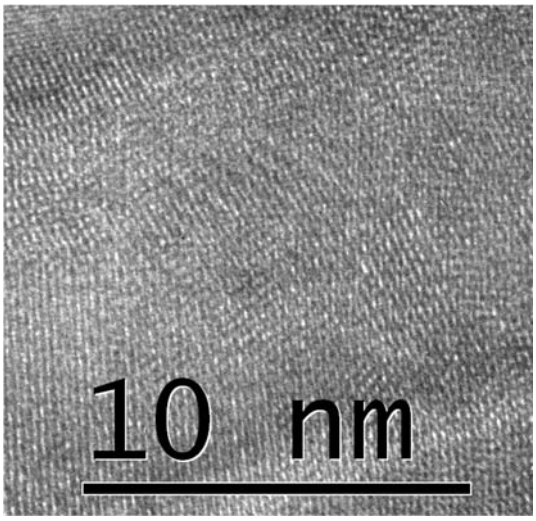

Figure 22: A section of a high-resolution TEM cross section taken from sample S0GPPC, discussed further in Section F.1.a.2 below.

63. In this image, there are patterns of fringes that correspond to spacings and orientations of planes in the crystal that lie close to the direction of the incident beam. See Sections F.1.a., F.1.b, and F.2.a below for analyses of orientations and growth directions for particular hard drive write head samples.

i) **Epitaxy, growth directions, and Fast Fourier Transforms (FFTs)**

64. The high-resolution TEM images obtained from cross-section samples provide information about the growth behavior of the FeCo relative to the template material upon which it is grown (e.g., NiFe, Ru). The fast Fourier transform (FFT) is a computational procedure that results in reconstructing the diffraction pattern from a region of a high-resolution image. By

CONTAINS CONFIDENTIAL ATTORNEY EYES ONLY
INFORMATION SUBJECT TO PROTECTIVE ORDER

comparing FFTs taken from the template layer with those taken from the FeCo layer above or below, it can be determined whether an epitaxial relationship exists between the two, and how that relationship contributes to the growth of the FeCo layers and the formation of orientational variants. As an example, consider the cross-section image below, in which there is a NiFe atomic template on the right in the area marked "B", and a FeCo layer to the left in the area marked "A".

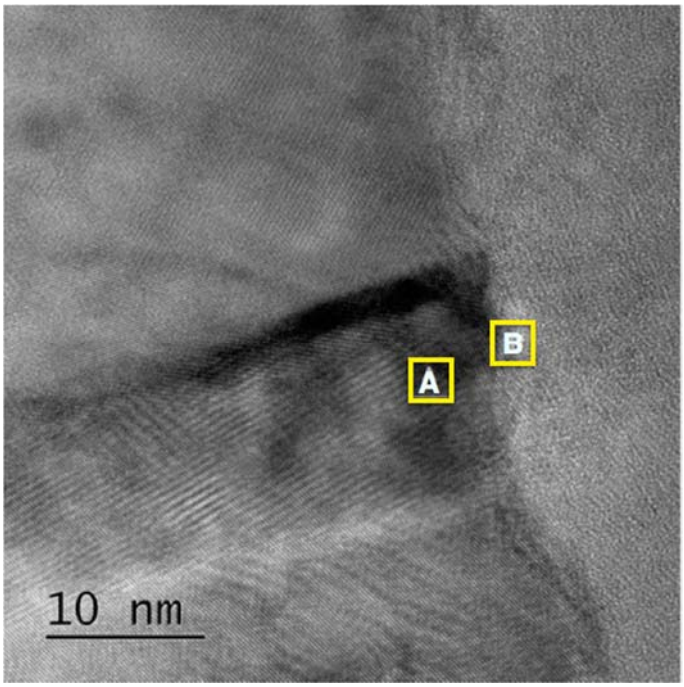

Figure 23: High-resolution cross section of a selected area of the write pole of sample S0GPPC.

65. FFTs were taken from the lower FeCo layer in sample S0GPPC from the region in the box marked "A", and from the lower NiFe layer in the region in the box marked "B". The resulting FFTs are shown in Figure 24 below.

CONTAINS CONFIDENTIAL ATTORNEY EYES ONLY
INFORMATION SUBJECT TO PROTECTIVE ORDER

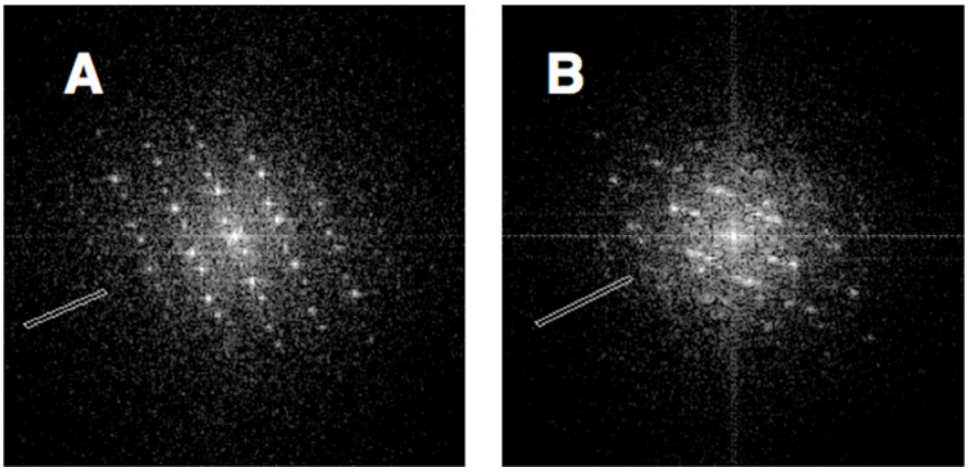

Figure 24: FFTs taken from regions A and B from Figure 23 above.

66. While the two diffraction patterns are different, as expected for a bcc layer growing on top of an FCC NiFe layer that functions as a template, they have parallel rows of diffraction spots (marked by the line in each FFT), that align normal to the interface between the NiFe layer and the FeCo layer. Comparing these diffraction patterns with standard patterns[10] indicates that this parallel direction is <110> in the BCC FeCo, and <111> in the FCC NiFe layer, indicating the presence of an epitaxial relationship. The bamboo-like structure of the crystallites in the image indicate that their growth is influenced by the template on which they nucleate and grow. In this case, the majority of FeCo crystallites exhibit columnar growth in a direction parallel to the template normal.

67. Since these FFTs are a diffraction pattern, they provide further information about the identification of the crystal structure of the various layers, and help distinguish between fcc, bcc, and hcp structures. They may also provide information about orientation relationships, such as those present in six-variant systems.[11] They also show that the lower NiFe layer, for instance,

[10] See, e.g. *Transmission Electron Microscopy,* D.B. Williams and C.B. Carter, Springer, (2009), pp. 299-301

[11] *See, e.g., Transmission Electron Microscopy,* D.B. Williams and C.B. Carter, Springer, (2009), pp. 298-303.

CONTAINS CONFIDENTIAL ATTORNEY EYES ONLY
INFORMATION SUBJECT TO PROTECTIVE ORDER

is a template to the FeCo layer growing upon it, at least because they share a predominate common direction normal to the template, and this direction is $<111>_{FCC}||<110>_{BCC}$, the orientation for epitaxial growth.

3. **Energy Dispersive X-Ray Spectrometry (EDS)**

68. When a high-energy electron beam interacts with a specimen in a TEM, it produces much more than just an image. As Figure 25 below shows, a whole range of different signals are produced simultaneously, and they each provide different, complementary information about the specimen. One of the most important signals is the characteristic x-rays, and it is their capture and analysis that forms the basis of energy dispersive x-ray spectrometry (EDS), used for identifying the elemental composition of the specimen.

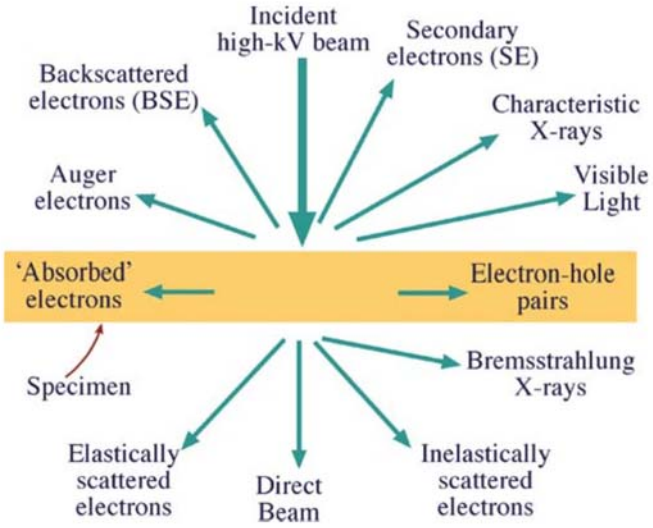

Figure 25: *Transmission Electron Microscopy,* D.B. Williams and C.B. Carter, Springer, (2009), fig. 1.3, p. 7

69. These characteristic x-rays are generated when an incident electron from the electron beam interacts with an atom in the specimen, and ionizes it by knocking out a tightly-bound inner shell electron residing in the attractive field of the nucleus of an atom in the specimen. To fill the vacancy left in the electron shell by this ionization, an outer shell electron

CONTAINS CONFIDENTIAL ATTORNEY EYES ONLY
INFORMATION SUBJECT TO PROTECTIVE ORDER

drops into the vacancy, and so reduces the energy of the ionized atom. The transition of this electron from one bound state into one of lower energy means that the atom must release the excess energy, and it usually does so in the form of an x-ray photon. The energy of this photon is exactly the difference in energy of the atom before and after the electron drops into the inner shell, and so is a function of the material and its particular ionization energy. Capturing and measuring the energy of the released x-ray photons allows for a determination of what elements are present in the specimen, and in what proportion. The captured x-rays are sorted by energy and used to form a spectrum, such as that shown in Figure 26 below, in which the number of x-ray photons of each energy are displayed. A computer program then identifies each peak in the spectrum with the element that produced it, and so calculates the overall composition of the specimen.

70. The EDS analyses described in Sections F.1.a.1, F.1.b.1, and F.2.a.1 below were performed using the Super-X EDS system in the Titan 80-300 S/TEM system. This EDS system is a high efficiency detector, with 4 Silicon Drift Detector (SDD) crystals of 30mm^2 spaced symmetrically around the sample. This detector is fitted with collimators to ensure minimum contribution of system peaks or spurious X-ray counts, and has a total active area of 120mm^2. Specifically, this analytical configuration achieves a higher peak to background ratio than can be obtained in most other EDS detectors currently available.

CONTAINS CONFIDENTIAL ATTORNEY EYES ONLY
INFORMATION SUBJECT TO PROTECTIVE ORDER

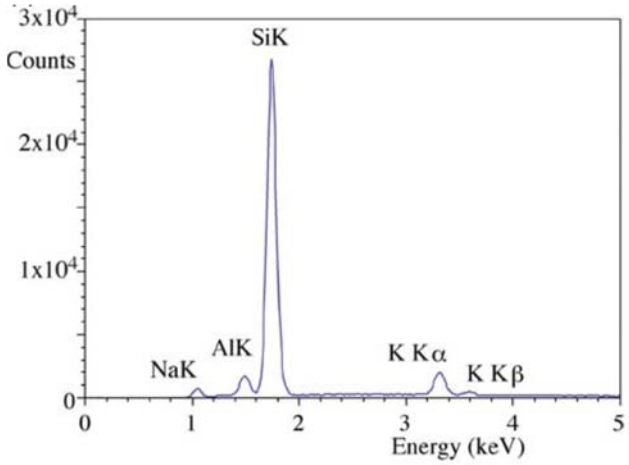

Figure 26: *Transmission Electron Microscopy,* D.B. Williams and C.B. Carter, Springer, (2009), fig. 32.2 (F), p. 583

71. If the microscope is operated in STEM mode and the x-ray spectrum is collected point-by-point as the beam scans the specimen, as was done for those samples discussed in Section F.1.a.1 below, the x-ray signals can be used to form an image that directly indicates how the various elements are distributed in the sample. This technique produces an elemental "map," as shown for example in Figure 27 below.

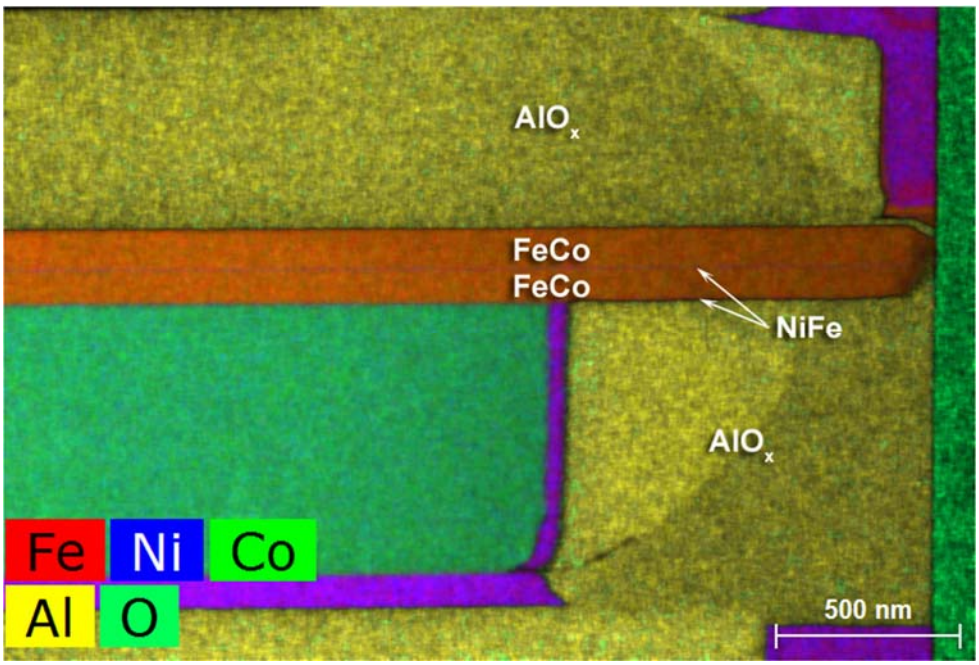

Figure 27: EDS map, taken in HAADF STEM, of a cross-section view of S0GPPC. The color legend for the various elements is shown along the bottom of the image

72. The elements present can be identified from the legend, with additional colors arising where there is significant alloying. Information from these EDS maps is valuable in understanding the layer structures and elemental distribution in the write pole material thin films I analyzed herein.

73. Further, an elemental analysis of FeCo layers was performed in Bruker ESPRIT. I note that in some instances, other spurious elements were occasionally detected in the FeCo layers. This was likely caused by a variety of factors. For instance, with respect to tantalum, because the samples were placed on copper grids, the detector might mistake this copper for tantalum in a sample in which Ta is not present. Additionally, fluorescence effects, secondary scattering, and other causes may contribute to other elements appearing in the FeCo layers. Finally, the thickness of each sample will affect the composition results, with thicker samples generally yielding more accurate data.

F. Results of Investigation of Seagate Hard Disk Drive Products

74. The Seagate Accused Products contain write heads. The analysis below concerns certain properties of materials used in these write heads.

75. Each Seagate Accused Product is referred to by a designation beginning with "S" for Seagate, followed by the last five alphanumeric characters in the serial number of the Seagate Accused Product under examination.

76. I understand that the Seagate Accused Products fall under one of three configurations of different write pole material layer structures used in the write pole. I understand that Seagate refers to these write pole material configurations as [redacted], and [redacted].[12] I further understand that [redacted] and [redacted] have write pole materials as follows:

[12] I understand that LMS was unable to obtain a sample of an [redacted] head, and I therefore do not provide an analysis of [redacted] below.

CONTAINS CONFIDENTIAL ATTORNEY EYES ONLY
INFORMATION SUBJECT TO PROTECTIVE ORDER

77. [redacted]

[redacted]

78. [redacted]

[redacted]

79. The principles behind EDS are discussed generally in Section E.3 above. EDS color maps are shown in Figures 28-32 below and indicate the concentration of elements in the area indicated by the color assigned to that element. Overviews are first shown in Figures 28-29,

CONTAINS CONFIDENTIAL ATTORNEY EYES ONLY
INFORMATION SUBJECT TO PROTECTIVE ORDER

and individual elemental mappings are shown in Figures 30-32. These mappings indicate the composition of individual layers in the write pole.

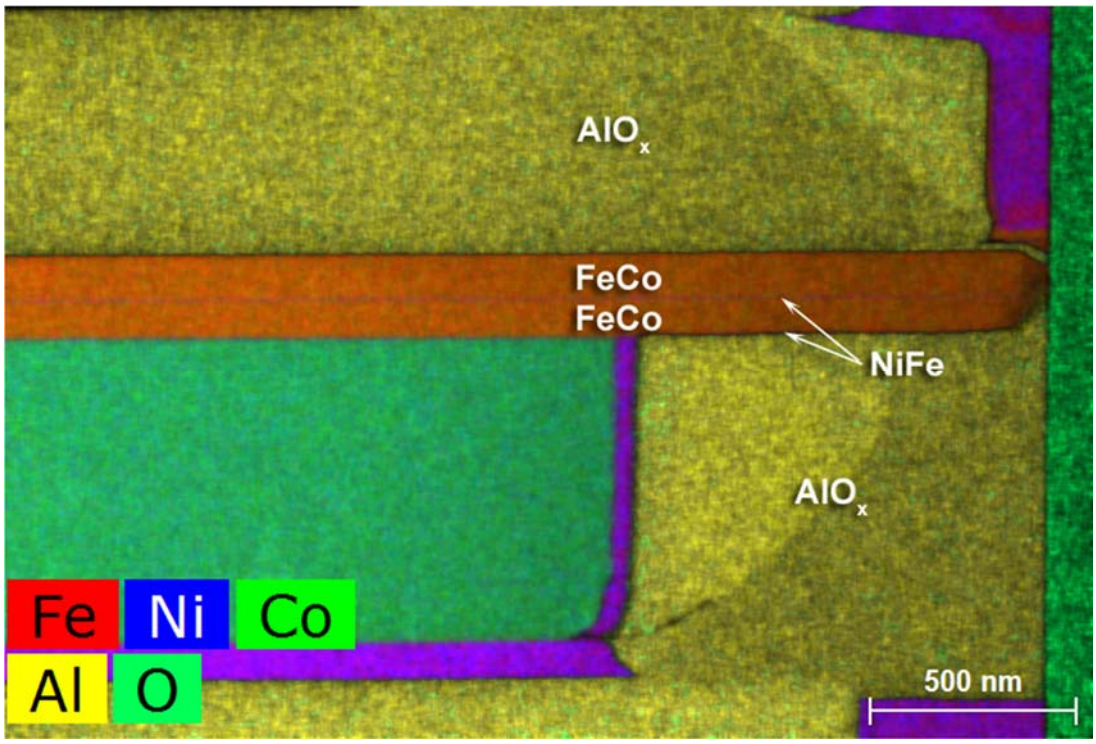

Figure 28: Overall EDS map. Note that the growth direction in the EDS maps for S0GPPC is from bottom to top.

CONTAINS CONFIDENTIAL ATTORNEY EYES ONLY
INFORMATION SUBJECT TO PROTECTIVE ORDER

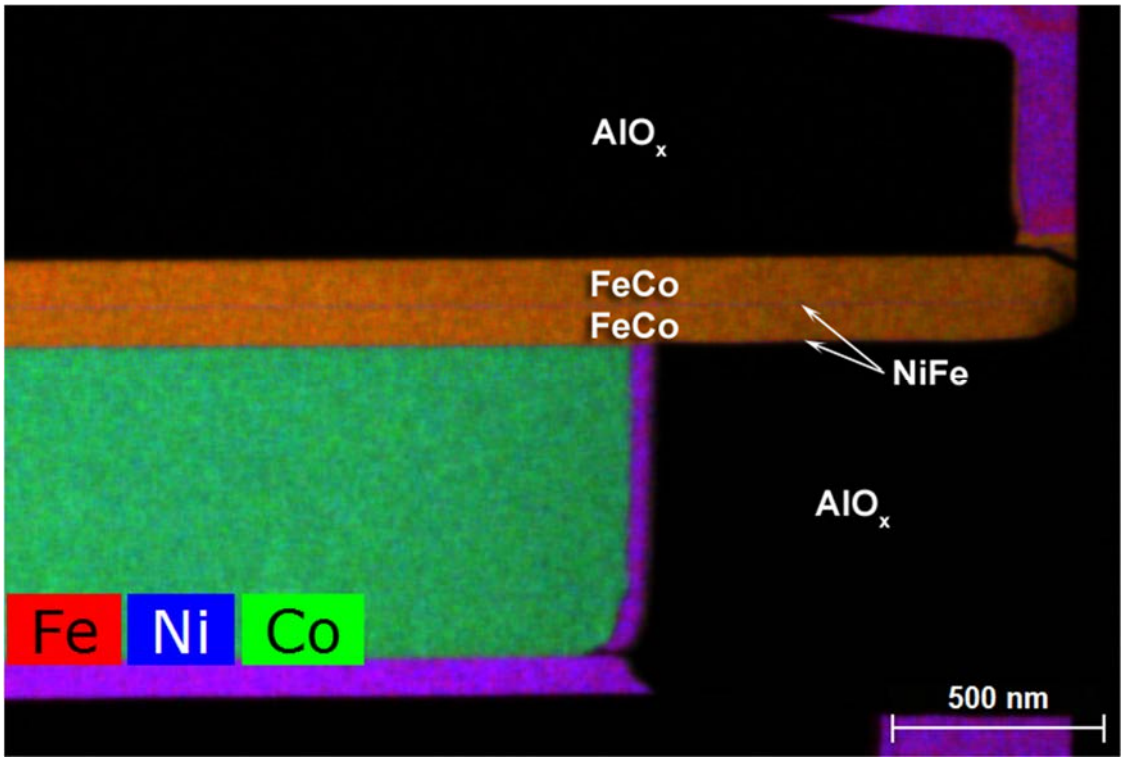

Figure 29: EDS map of Fe, Ni, and Co.

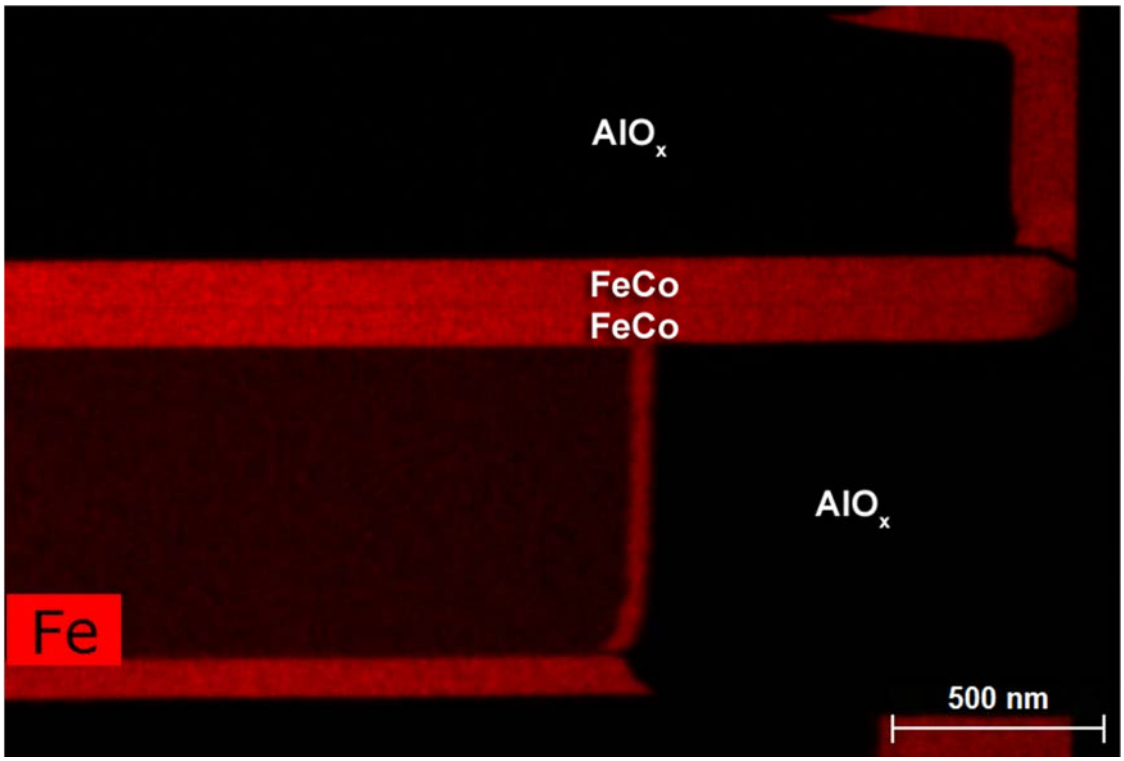

Figure 30: EDS map showing just Fe.

CONTAINS CONFIDENTIAL ATTORNEY EYES ONLY
INFORMATION SUBJECT TO PROTECTIVE ORDER

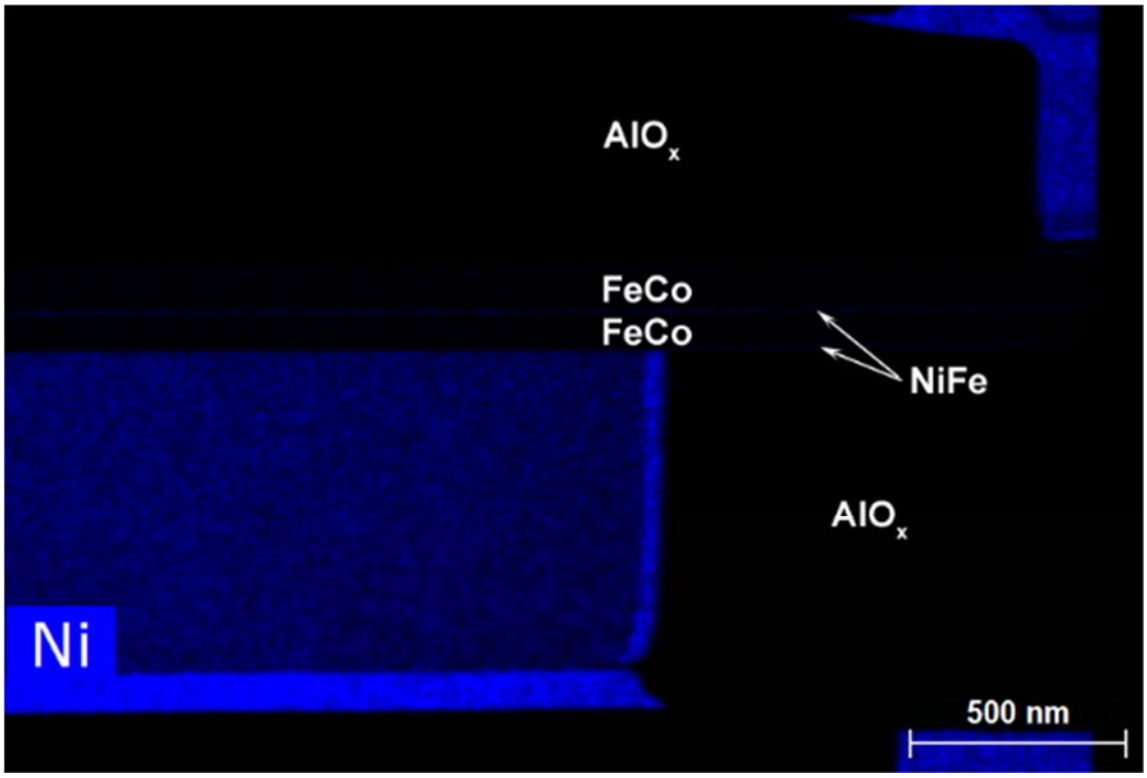

Figure 31: EDS map showing just Ni.

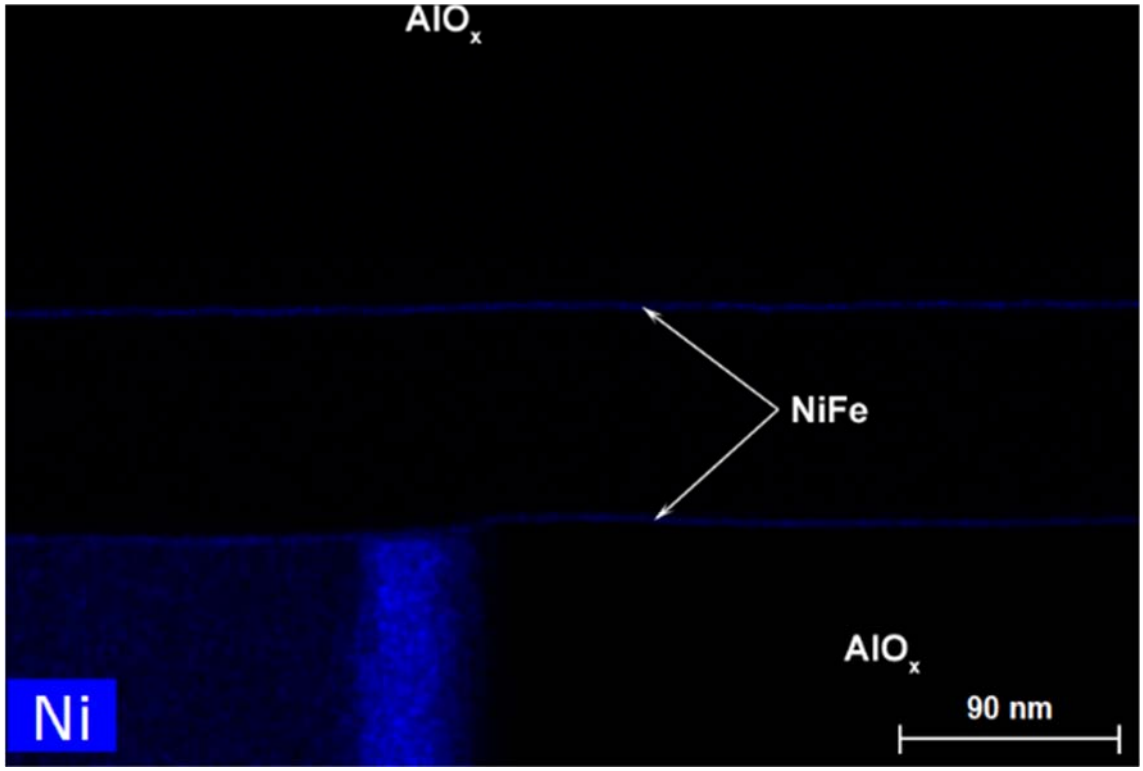

Figure 32: A higher magnification showing the Ni in the NiFe layers.

CONTAINS CONFIDENTIAL ATTORNEY EYES ONLY
INFORMATION SUBJECT TO PROTECTIVE ORDER

80. Additionally, a quantitative assessment of the composition of the FeCo layers was performed Bruker ESPRIT as shown below.

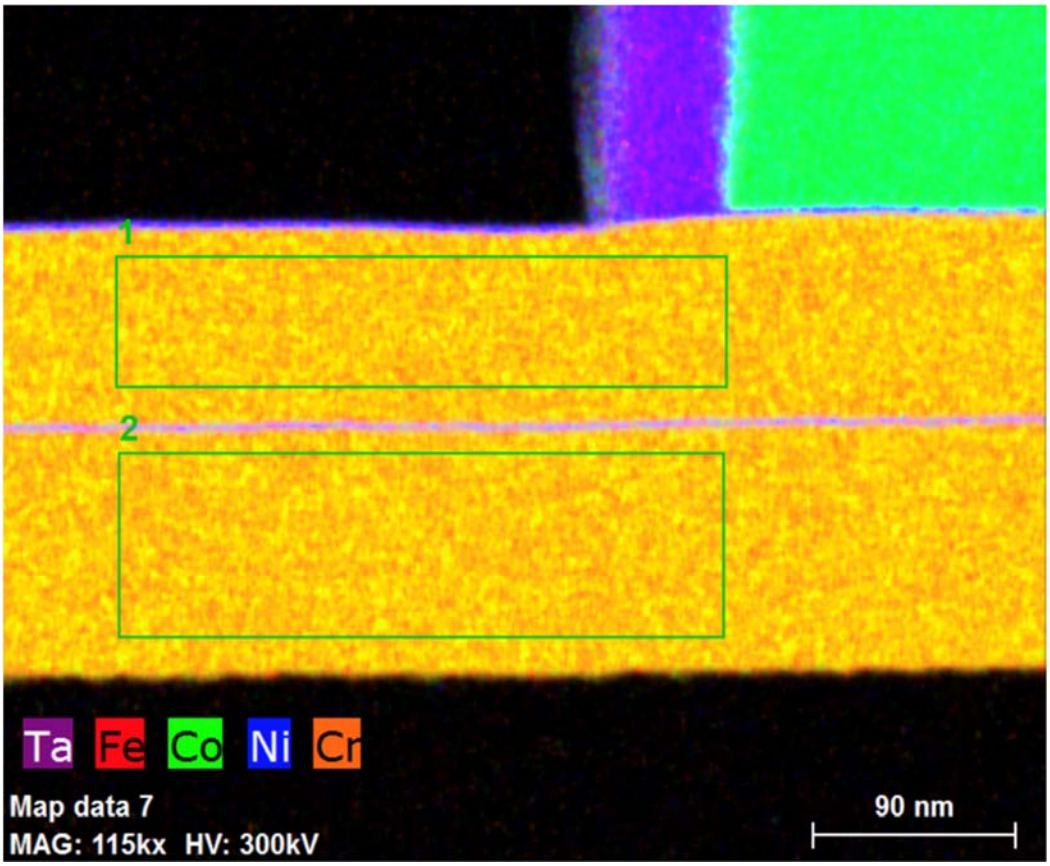

Figure 33: Quantitative assessment performed in the regions enclosed by the green rectangles. Note that this image is flipped upside down as compared to the images above.

Spectrum: 1

Element	Series	unn. C [wt.%]	norm. C [wt.%]	Atom. C [at.%]	Error (3 Sigma) [wt.%]
Iron	K-series	60.74	60.74	61.99	5.55
Cobalt	K-series	37.96	37.96	36.71	3.50
Nickel	K-series	1.01	1.01	0.98	0.17
Chromium	K-series	0.30	0.30	0.33	0.11
	Total:	100.00	100.00	100.00	

CONTAINS CONFIDENTIAL ATTORNEY EYES ONLY
INFORMATION SUBJECT TO PROTECTIVE ORDER

Spectrum: 2

Element	Series	unn. C [wt.%]	norm. C [wt.%]	Atom. C [at.%]	Error (3 Sigma) [wt.%]
Chromium	K-series	0.34	0.34	0.38	0.11
Iron	K-series	60.83	60.83	62.08	5.56
Cobalt	K-series	37.80	37.80	36.55	3.48
Nickel	K-series	1.03	1.03	1.00	0.17
	Total:	100.00	100.00	100.00	

Figure 34: Output from Bruker ESPRIT showing composition in regions enclosed by the green rectangles.

(2) TEM high resolution images of cross-sections

81. The principles behind TEM imaging are discussed generally in Section E.2 above. High resolution cross-section images were taken using the FEI Titan 80-300 S-Twin microscope ("Titan"), operating in TEM mode at 300 kV, and fitted with an automated image corrector to enhance the spatial resolution.. The high resolution cross-section images were obtained from two regions of the write pole of S0GPPC as shown in Figure 35 below – at the left-hand edge (A), where the lower NiFe layer is, and in the center (B), where the upper NiFe layer is.

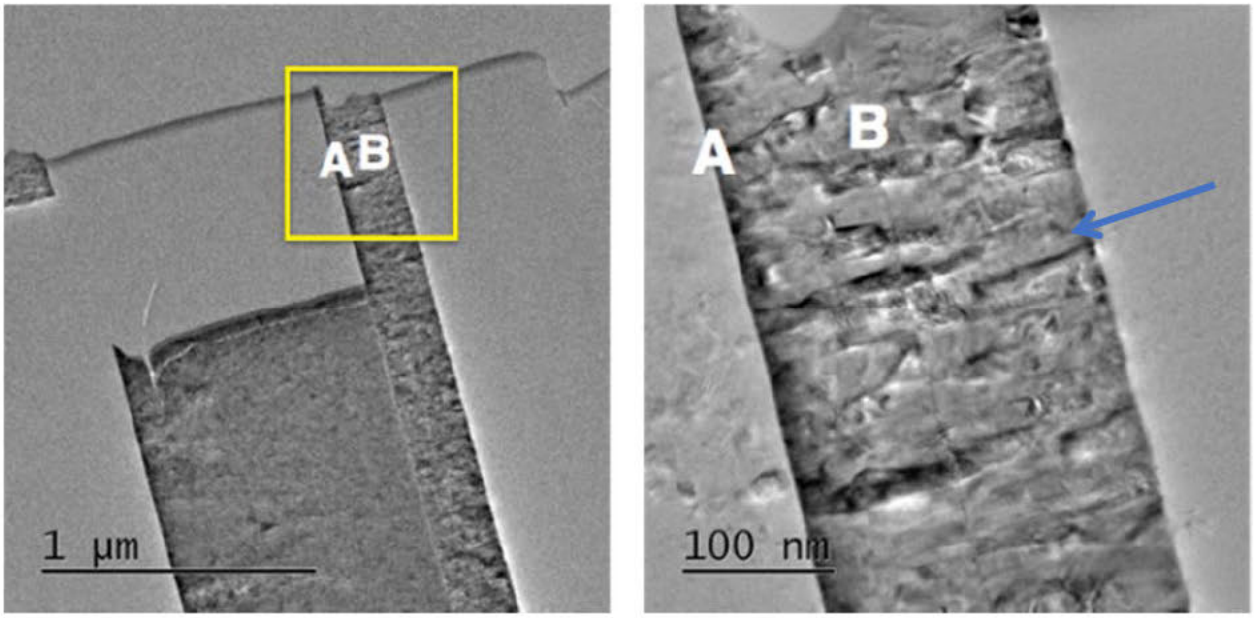

CONTAINS CONFIDENTIAL ATTORNEY EYES ONLY
INFORMATION SUBJECT TO PROTECTIVE ORDER

Figure 35: TEM overview of S0GPPC, with regions where high resolution cross-sections were taken marked A and B. Note the pronounced columnar growth seen in the right-hand image, with an approximately right-to-left growth direction.

82. The medium magnification image on the right-hand side of Figure 35 shows a grain structure that is elongated perpendicular to the lower NiFe layer normal (in the direction indicated by the blue arrow). Such a morphology is typically referred to as a "bamboo" structure, more formally defined as a grain structure in which the boundaries of the grains tend to be aligned normal to the long axis and to extend through the thickness.[13] The directional nature of this structure modifies the mechanical and electrical properties of a material significantly, by aligning the majority of the grain boundaries parallel to one another, as opposed to being homogeneously distributed. It is very commonly observed in epitaxial growth, where the orientation relationship between the template and the growth layers favors growth in one direction.

83. High resolution images were taken at several points along each interface in the regions marked A and B in Figure 35 above. Nine such images taken, five in region A and four in region B, are shown below.

[13] *Analysis of grain-boundary structure in Al–Cu interconnects*, D.P. Field, J.E. Sanchez, P.R. Besser, and D.J. Dingley, J.Appl. Phys., **82** (5), (1997), pp. 2383-2392

CONTAINS CONFIDENTIAL ATTORNEY EYES ONLY
INFORMATION SUBJECT TO PROTECTIVE ORDER

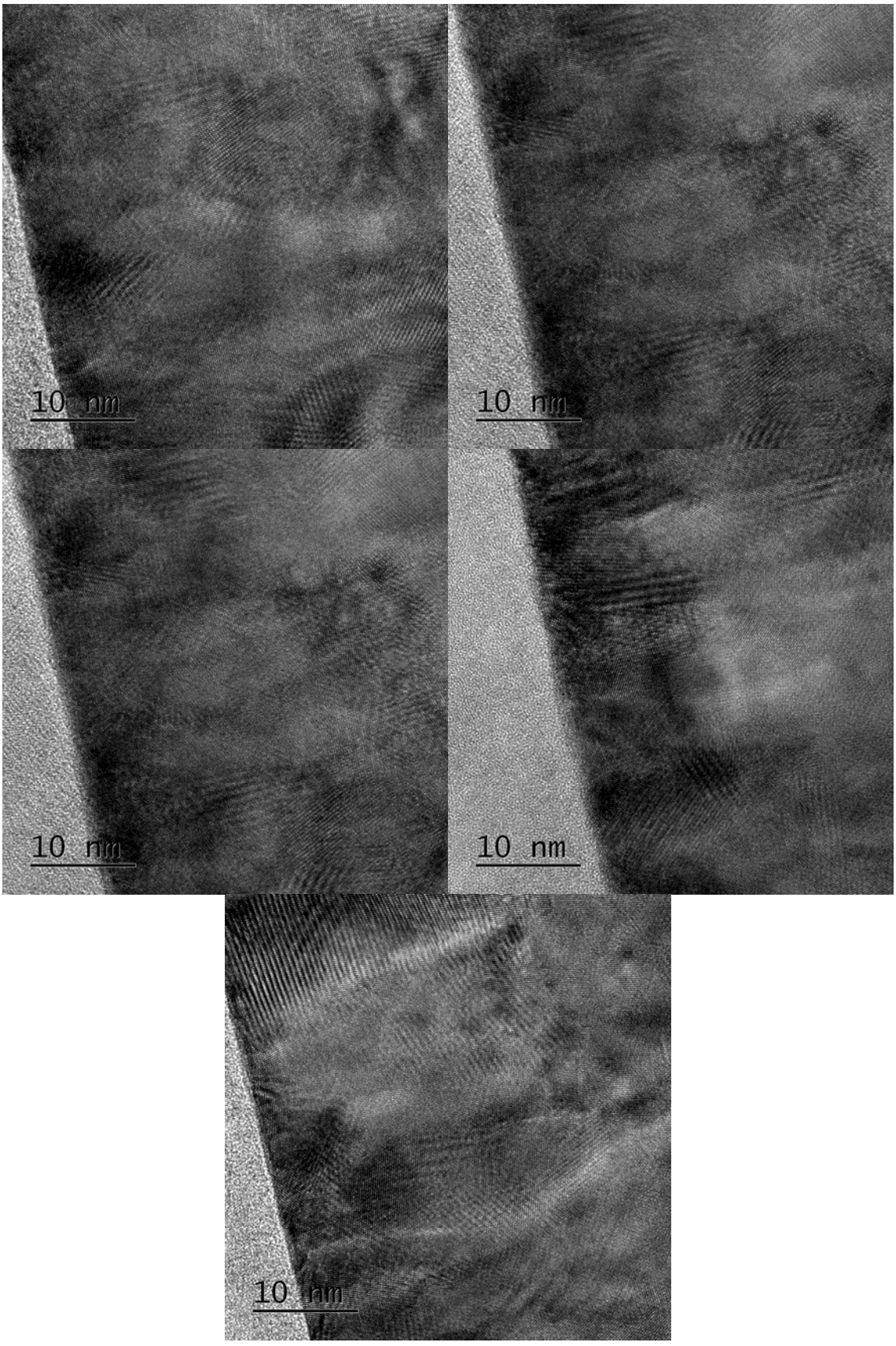

CONTAINS CONFIDENTIAL ATTORNEY EYES ONLY
INFORMATION SUBJECT TO PROTECTIVE ORDER

Figure 36: High resolution cross-section images taken at the left-hand NiFe/FeCo interface in region A

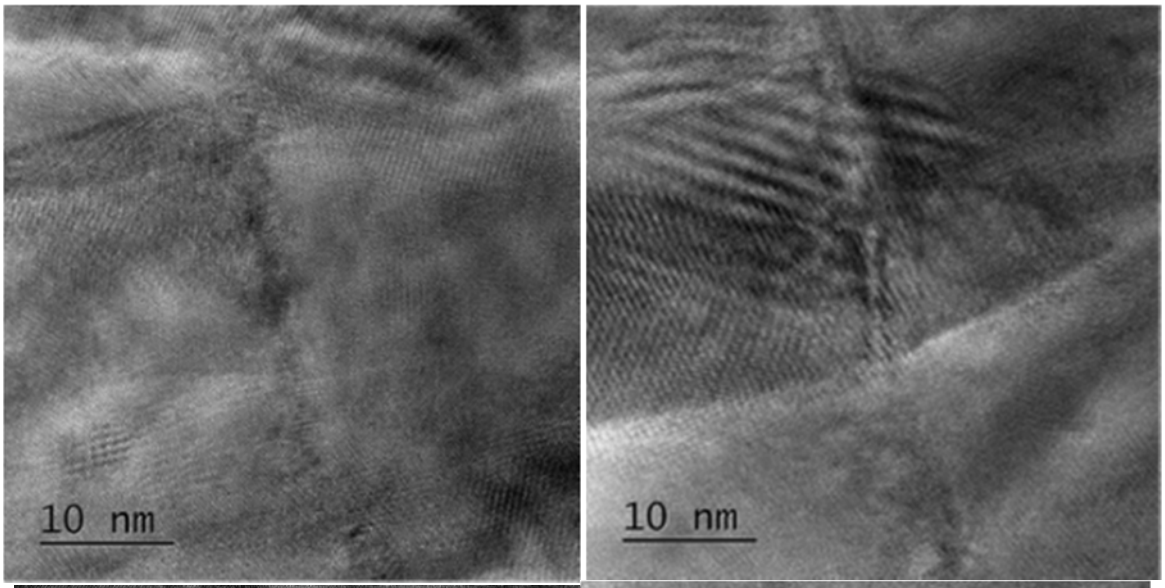

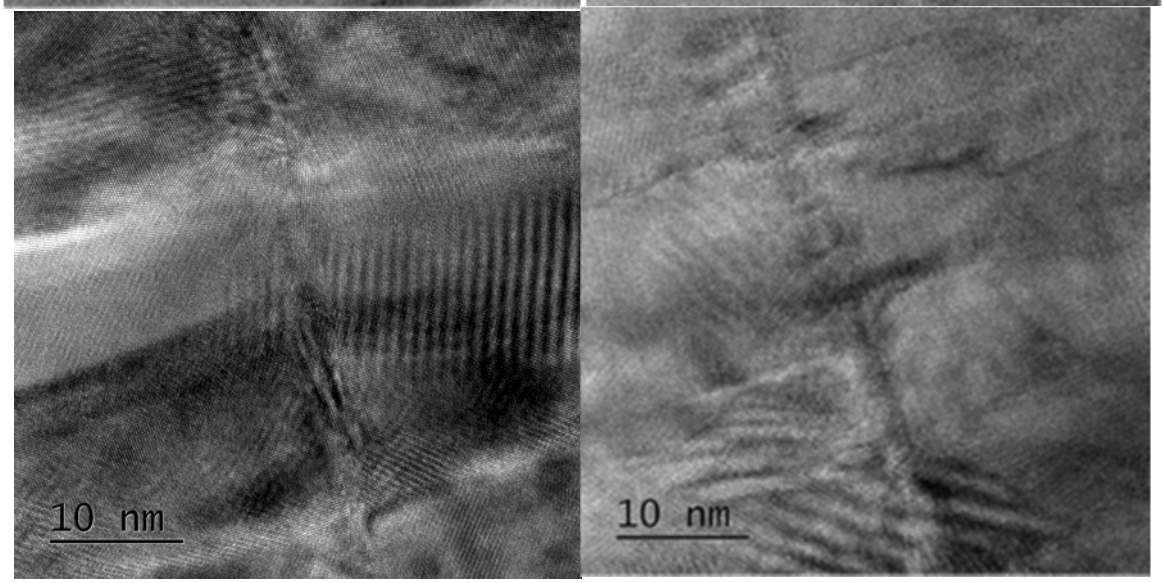

Figure 37: High resolution cross-section images taken at the FeCo/NiFe/FeCo interface in region B

84. These high resolution cross-sections show various sets of crossed lattice fringes, such as the example shown in Figure 38 below. For example, in Figure 38, the zoomed-in area in the yellow square shows prominent patterns of crossed fringes. These lattice fringes arise when the forward scattered (central) beam and the diffracted beam corresponding to one family of crystal planes both lie within the objective aperture and so contribute to the final image. These

CONTAINS CONFIDENTIAL ATTORNEY EYES ONLY
INFORMATION SUBJECT TO PROTECTIVE ORDER

two beams will then "beat" together in the image, resulting in a pattern of fringes that have the spacing of that family of planes, and which align parallel to them. When several diffracted beams are allowed through the objective aperture, each contributes a set of fringes, so that a crossed fringe pattern can be seen in the image. The more diffracted beams that are used to form this lattice image, the closer it will be to an image representing the actual atomic arrangement in the crystal.[14]

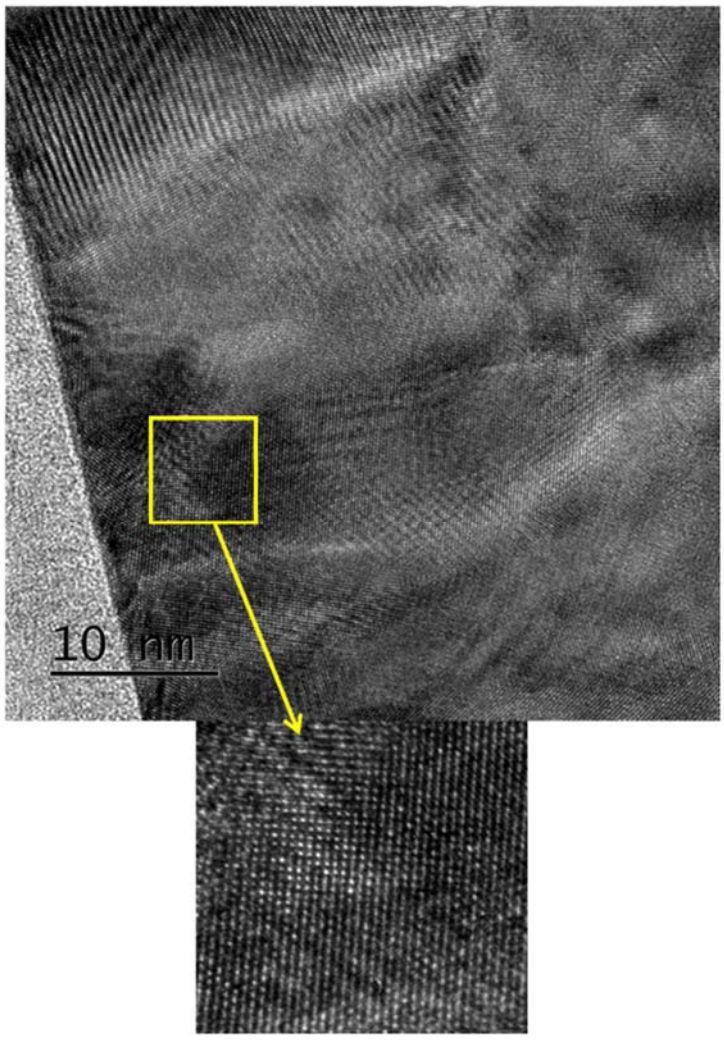

Figure 38: Example showing zoomed-in crossed lattice fringes from a high resolution cross-section from region A as discussed above.

[14] *Transmission Electron Microscopy,* D.B. Williams and C.B. Carter, Springer, (2009), p. 389 et seq.

CONTAINS CONFIDENTIAL ATTORNEY EYES ONLY
INFORMATION SUBJECT TO PROTECTIVE ORDER

85. Additionally, a high resolution cross-section taken in region B is shown in Figure 39 below. This region consists of two FeCo layers with a thin layer of NiFe in between. Like the high resolution cross-section from region A in Figure 38 above, this image also shows crossed lattice fringes, with an example in the region in the yellow box shown enlarged in Figure 40 below.

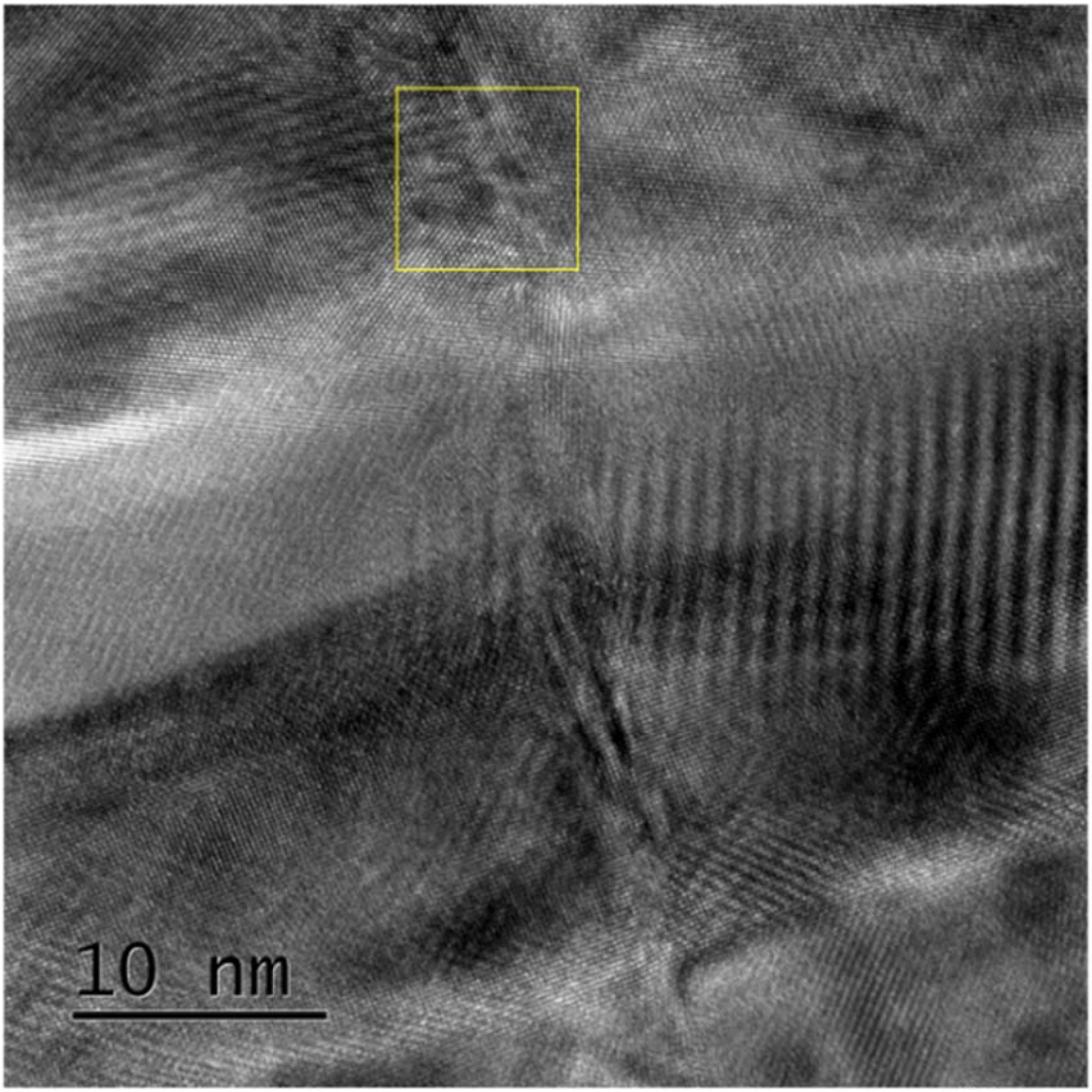

Figure 39: Example high resolution cross-section from region B. The area marked with the yellow square is shown zoomed-in in Figure 40 below.

CONTAINS CONFIDENTIAL ATTORNEY EYES ONLY INFORMATION SUBJECT TO PROTECTIVE ORDER

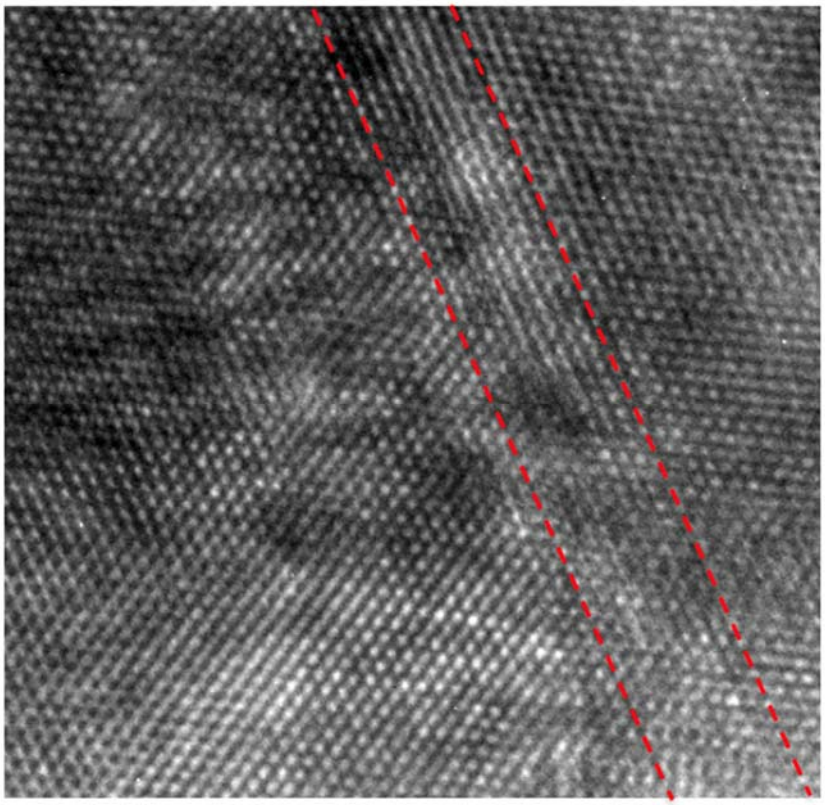

Figure 40: Zoomed-in area from Figure 39 above showing crossed lattice fringes.

86. Several sets of lattice fringes are seen here, as are the FeCo/NiFe interfaces, which are marked with a red dashed line. The fringes that run parallel to the red dashed line are present on both sides of the NiFe, and in the NiFe layer itself, indicating that the orientation of the FeCo is maintained on both sides of the NiFe. The continuity of these fringes across all three layers show that there is an orientation relationship between the FeCo and the NiFe. From the FFTs (as discussed in Section F.1.a.3 below) and the hexagonal arrangement of spots in the FeCo lattice image, looking down into the cross-section (i.e., into the page) shows a $\{111\}_{BCC}$ plane, and a $<110>_{BCC}$ direction is normal to the interface (as is the case at the template/FeCo interface in region A, as discussed in Section F.1.a.3 below).

(3) FFT on TEM high resolution images of cross-sections

CONTAINS CONFIDENTIAL ATTORNEY EYES ONLY
INFORMATION SUBJECT TO PROTECTIVE ORDER

87. The principles behind FFTs are discussed generally in Section E.2.i. above. FFTs were taken at selected points in high resolution cross-section images. For instance, a high resolution cross-section taken in region A is shown in Figure 41 below, with a number of points along the lower NiFe/ lower FeCo interface marked with numbers. At each numbered point, FFTs were taken: (a) in the lower NiFe layer at the location of the numbered point; and (b) in the lower FeCo immediately to the right of the numbered point. Since a diffraction pattern of a sample is just the Fourier transform of its structure,[15] FFTs taken of the image generate the information found in diffraction patterns, and can be used to determine crystal structure. The FFTs can be generated using a number of programs including ImageJ, MIPAR, or Desktop Microscopist; the FFTs here were generated using ImageJ. In Figure 41 below, the area sampled for each FFT was confined to an area of the size indicated by the red square, which was chosen to be small enough to ensure sampling information from the template and excluding information from the surrounding layers.

[15] *The Analytical Theory of Heat, J. B. Fourier*, (1878) [1822], translated by Alexander Freeman, The University Press (translated from French).

CONTAINS CONFIDENTIAL ATTORNEY EYES ONLY
INFORMATION SUBJECT TO PROTECTIVE ORDER

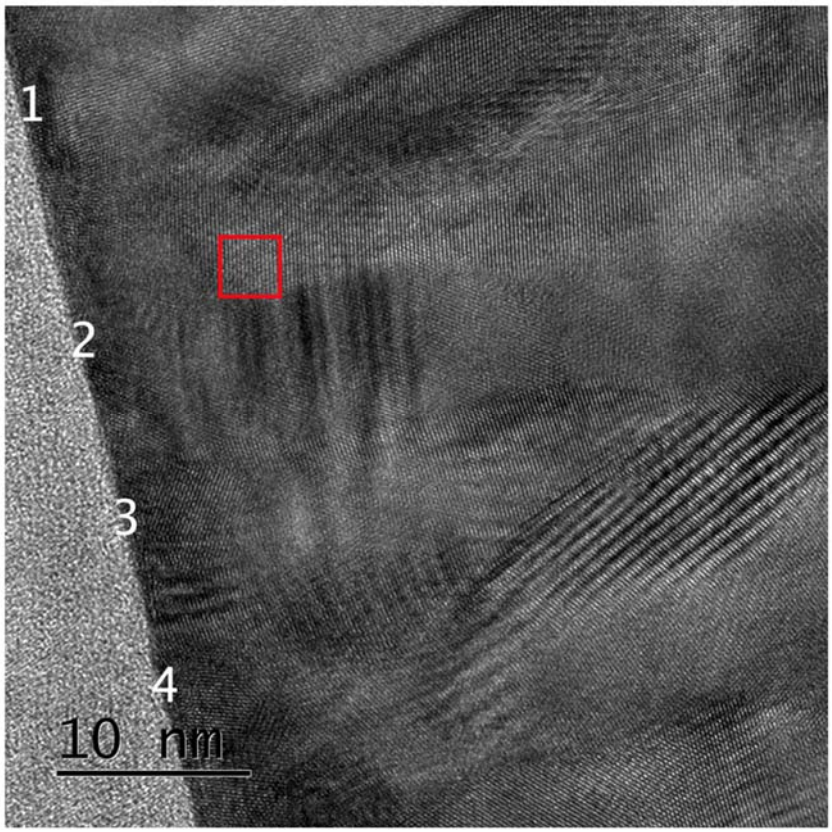

Figure 41: Example high resolution cross-section from region A. The numbered points indicate where FFTs were taken.

88. For example, FFTs taken at point 2 are shown in Figure 42 below. The FFT on the left is from the lower NiFe layer and the FFT on the right is from the lower FeCo directly on the lower NiFe layer. Analysis of the FFTs was performed by measuring the diffraction spot spacings and the angles between rows of diffraction spots and comparing that information with the standard diffraction patterns[16] shown in Figure 42 below their respective FFTs.

[16] *Transmission Electron Microscopy,* D.B. Williams and C.B. Carter, Springer, (2009), pp. 299-301.

CONTAINS CONFIDENTIAL ATTORNEY EYES ONLY
INFORMATION SUBJECT TO PROTECTIVE ORDER

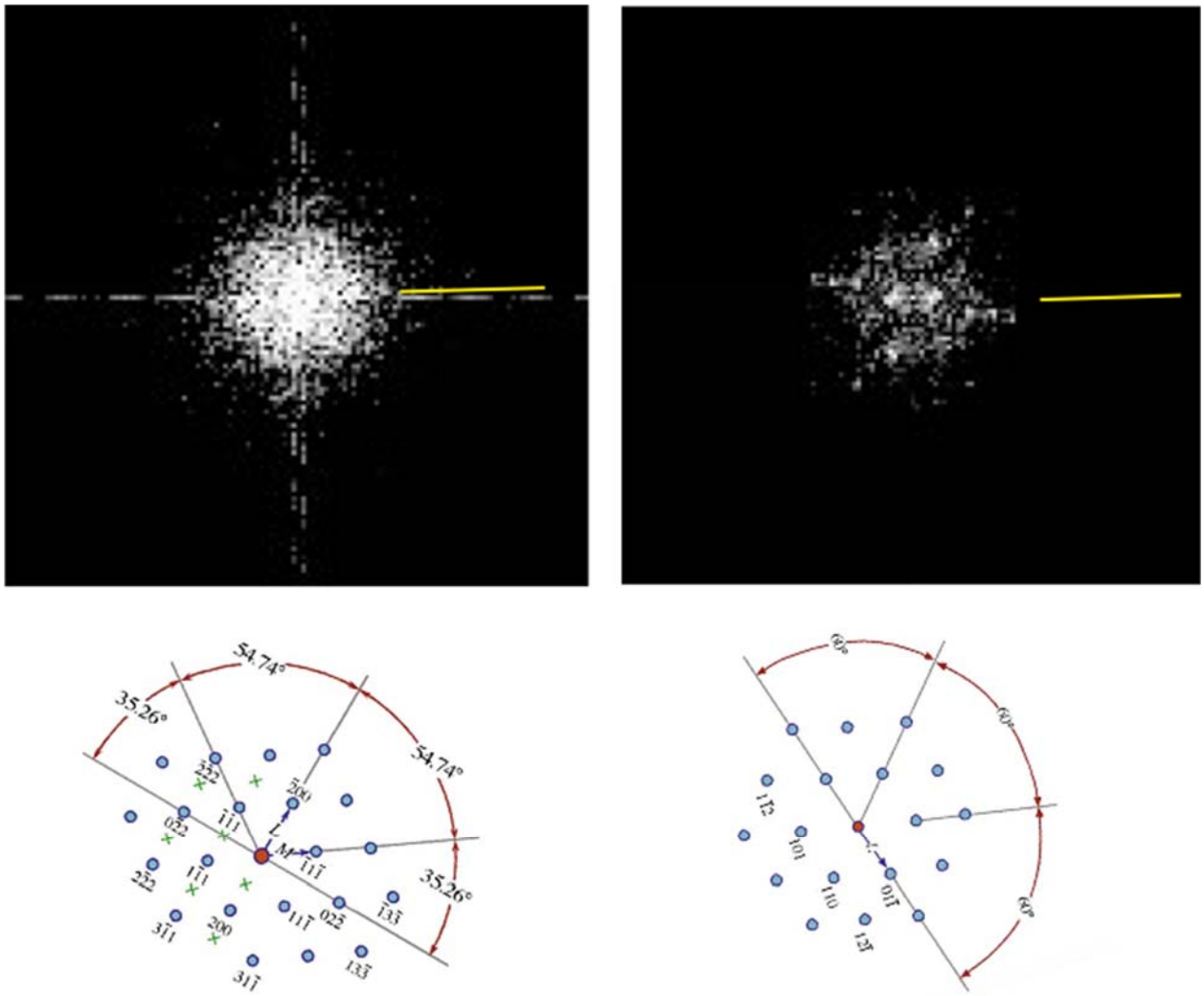

Figure 42: above: FFTs from the NiFe layer (left) and FeCo layer (right); below: standard diffraction patterns rotated into similar orientations as respective FFTs shown immediately above.

89. For the left-hand FFT from the lower NiFe layer, looking down a {110} direction into the page, this analysis indicates that the diffraction pattern is $\{110\}_{FCC}$. The FFT is shown on the top left, and the standard $\{110\}_{FCC}$ diffraction pattern is shown below it, rotated into a similar orientation. Note that a few overlapping spots from the lower FeCo layer can be seen, which are indicative of the differences between the NiFe pattern and the FeCo pattern. Thus, this FFT indicates that the crystal structure of the NiFe layer is FCC. Further, from the high

resolution cross-sections above, because we can see that the lattice fringes are continuous along the lower NiFe layer, this is indicative of the crystal structure of the extent of the lower NiFe layer.

90. For the right-hand FFT from the lower FeCo layer, looking down a {111} direction into the page, this analysis indicates that the diffraction pattern is $\{111\}_{BCC}$. The FFT is shown on the top right, and the standard $\{111\}_{BCC}$ diffraction pattern is shown below it, rotated into a similar orientation. Thus, this FFT indicates that the crystal structure of the lower FeCo layer is BCC. Further, from the high resolution cross-sections above, because we can see that the lattice fringes are continuous along the FeCo layer, this is indicative of the crystal structure of the extent of the FeCo layer.

91. From the discussion above, the two FFT patterns show that there are two parallel directions, one in the lower NiFe layer and one in the lower FeCo layer, pointing out of the page. These are a $<110>_{FCC}$ direction lying parallel to a $<111>_{BCC}$ direction. Further, when analyzing the pattern from the spot spacing and distribution, it can be seen that a $<111>_{FCC}$ direction in the NiFe is also parallel to a $<110>_{BCC}$ in the FeCo, and lie in the plane of the page; both of these directions are indicated by the lines marked on the FFT. The directions are also perpendicular to the lower NiFe/ lower FeCo interface, and so confirm the epitaxial growth in that direction and is evidence of the epitaxial growth of the lower FeCo layer on the lower NiFe layer, which functions as an atomic template. These two mutual orientation relationships are also sufficient to determine the relative orientation of the lower NiFe layer and the lower FeCo layer above it. Therefore, the lower NiFe layer exhibits (111) texture, and the lower FeCo layer exhibits (110) texture.

CONTAINS CONFIDENTIAL ATTORNEY EYES ONLY
INFORMATION SUBJECT TO PROTECTIVE ORDER

92. The parallel directions in the FCC and BCC layers normal to the interface show repeatedly <110> direction in the BCC layers and <111> direction in the FCC layers. Therefore, this analysis shows that the lower NiFe layer has a predominant (111) texture, and the lower FeCo layer has a predominant (110) texture.

93. Since the FFT analysis above shows that the lower NiFe/ lower FeCo relationship is $\{111\}_{FCC}||\{110\}_{BCC}$, as well as $<110>_{FCC}||<111>_{BCC}$, this shows that the Kurdjumov–Sachs orientation relationship is present.

94. Similar analysis was performed on FFTs taken at points other than 2 and each showed similar results as those described above, thereby confirming that the orientational relationships were consistent across the interface between the lower NiFe layer and the lower FeCo layer, and that the same textures were present throughout each layer. These FFTs are contained in Appendix C.[17] Additionally, FFTs were taken on the remaining 4 high-resolution cross sections from region A; annotated cross sections and their accompanying FFTs are also shown in Appendix C and also showed similar results as those described above, further confirming the orientational relationships and textures as described above.

95. To the extent that the FFT results for the lower NiFe layer are inconclusive, I conclude that the lower NiFe layer is FCC and exhibits a predominant (111) texture based further on the discussion of the upper NiFe / FeCo layers below.

[17] FFTs in the Appendix are designated by a frame number that refers to the marked point on the image, followed by a number that refers to the position number on the image, and a letter – T for FFTs taken from the template, and H for those from the FeCo. For example, Frame61T is an FFT from image #6, marked position #1, and in the NiFe template. In cases with three FFTs per point as discussed below, FFTs are designated by a frame number that refers to the marked point on the image, followed by either R, L, or T, showing whether they came from the right side, left side, or the template, respectively.

CONTAINS CONFIDENTIAL ATTORNEY EYES ONLY
INFORMATION SUBJECT TO PROTECTIVE ORDER

96. Additionally, as with the high resolution cross-section in region A, FFTs were taken in region B at a number of points in the example high resolution cross-section shown in Figure 43 below. Here, the two FeCo/NiFe interfaces are indicated by the blue arrows. Also notable, the red arrows show the boundaries between different columnar grains of the FeCo as they grow from right to left, which highlight the elongated nature of the FeCo grains, giving rise to the bamboo structure seen in the low magnification images in Section F.1.b.2 above.

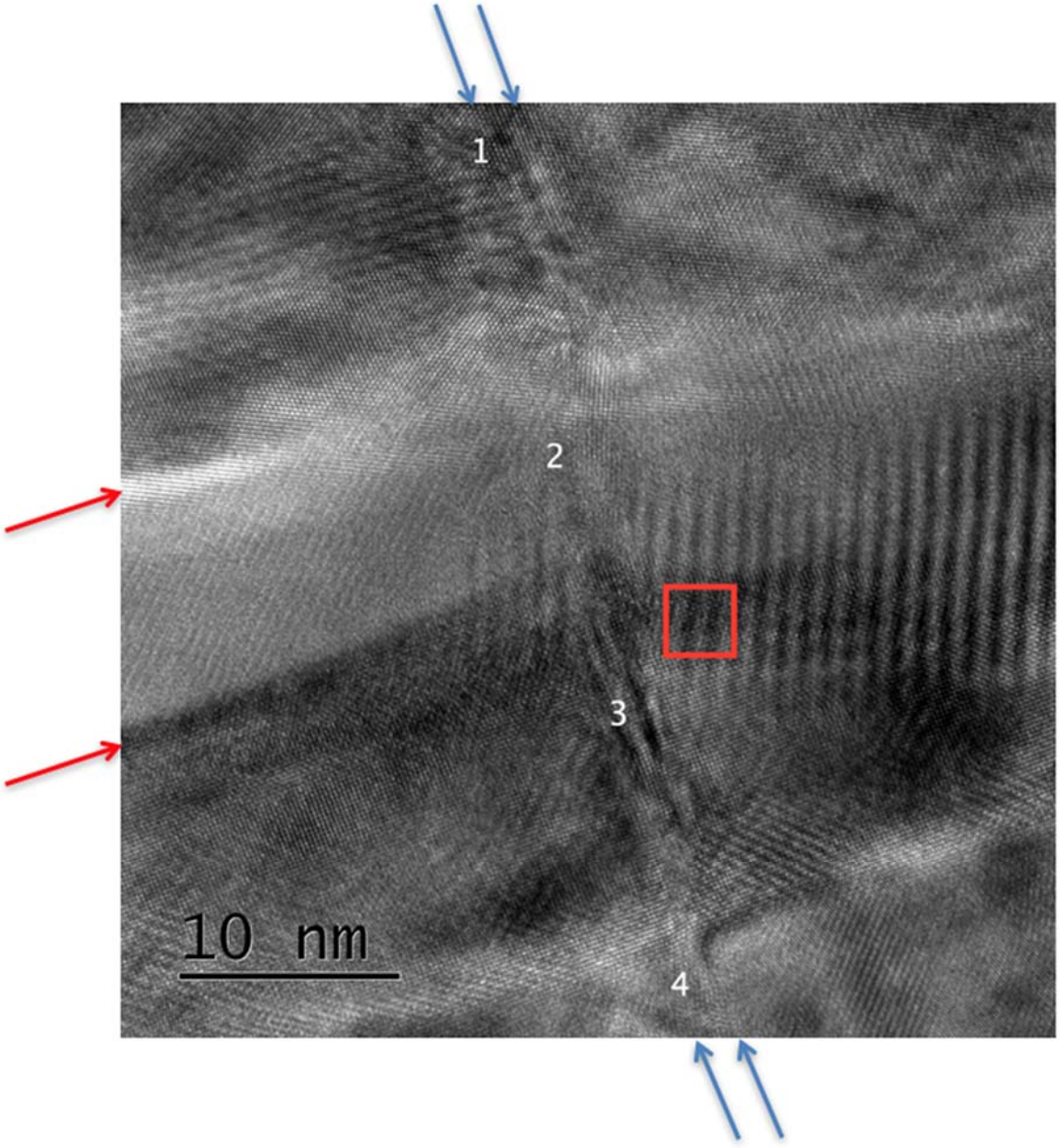

CONTAINS CONFIDENTIAL ATTORNEY EYES ONLY
INFORMATION SUBJECT TO PROTECTIVE ORDER

Figure 43: Example high resolution cross-section from region B. The numbered points indicate where FFTs were taken.

97. Similar to the analysis for the example high resolution cross-section from region A above, at each numbered point, FFTs were taken: (a) in the upper FeCo layer immediately to the left of the upper NiFe layer; (b) in the upper NiFe layer at the location of the numbered point; and (c) in the lower FeCo layer immediate to the right of the upper NiFe layer. Again, the area sampled for each FFT was confined to an area of the size indicated by the red square. For example, the set of FFTs taken around point 1 are shown in Figure 44 below.

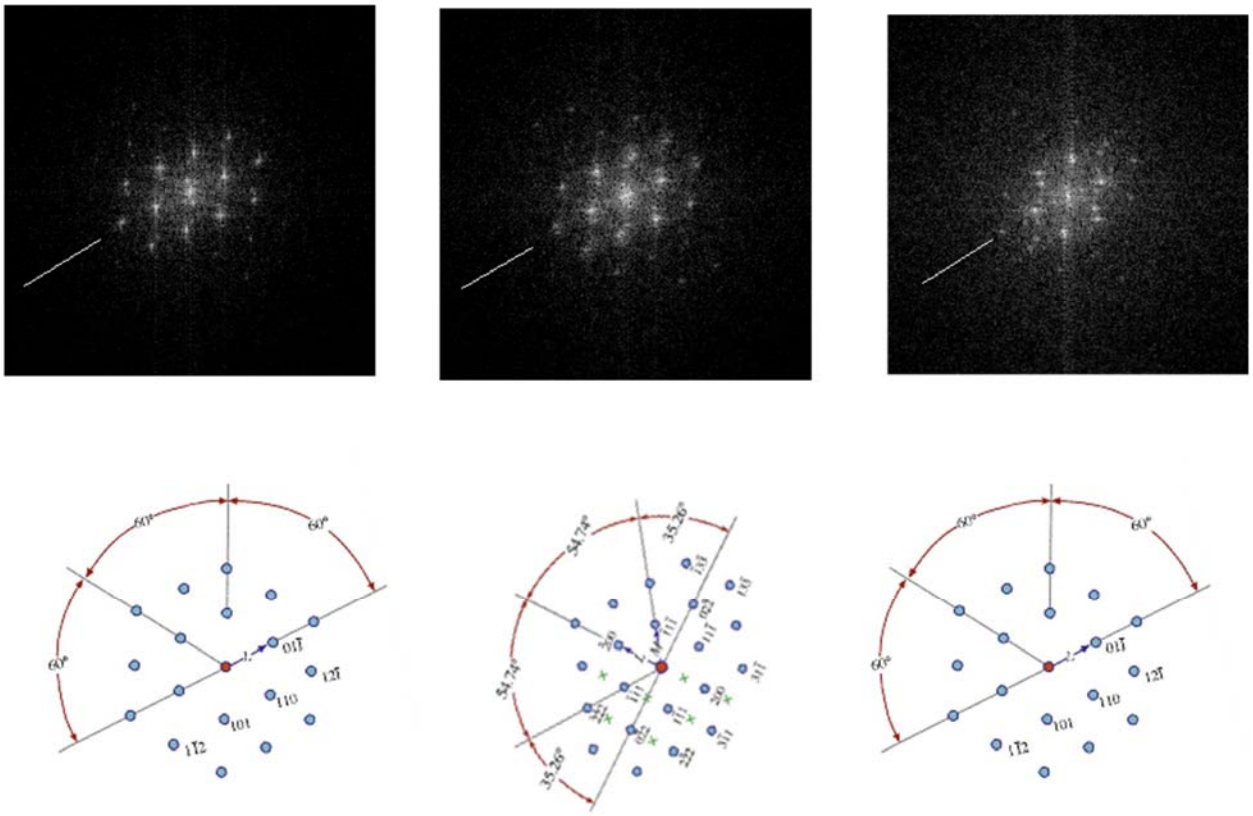

Figure 44: above: FFTs from: (a) the upper FeCo layer to the left of the upper NiFe layer (left); (b) in the upper NiFe layer (center); (c) the lower FeCo layer to the right of the NiFe layer (right); below: standard diffraction patterns rotated into similar orientations as respective FFTs shown immediately above.

98. Again, following the procedures outlined for region A above, the two patterns in the upper and lower FeCo layers are identified as $\{111\}_{BCC}$, while the upper NiFe pattern is

identified as $\{110\}_{FCC}$. These FFTs, like those analyzed above, indicate that the crystal structure of the upper NiFe layer is FCC and the upper and lower FeCo layers is BCC. Likewise, from the high resolution cross-sections above, because we can see that the lattice fringes are continuous, this is indicative of the crystal structure of the extent of the upper NiFe and both FeCo layers.

99. Common directions in all three layers show the persistence of the epitaxial relationship between $<111>_{BCC}$ and $<110>_{FCC}$, as was found at the NiFe/FeCo interface of region A. Again, this is indicative of the upper NiFe layer exhibiting (111) texture, and the FeCo layers exhibiting (110) texture. This also indicates the Kurdjumov-Sachs orientation relationship between the upper NiFe and upper FeCo layers.

100. Again, the parallel directions in the FCC and BCC layers normal to the interface show repeatedly <110> direction in the BCC layers and <111> direction in the FCC layers. Therefore, this analysis shows that the upper NiFe layer has a predominant (111) texture, and the upper FeCo layer has a predominant (110) texture.

101. Further, the FFT patterns show that there are two parallel directions, one in the upper NiFe layer and one each of the adjacent FeCo layers, pointing out of the page. These are a $<110>_{FCC}$ direction lying parallel to a $<111>_{BCC}$ direction. When analyzing the pattern from the spot spacing and distribution, it can be seen that a $<111>_{FCC}$ direction in the NiFe is also parallel to a $<110>_{BCC}$ in the FeCo, and lie in the plane of the page; both of these directions are indicated by the yellow lines marked on the FFT. The directions are also perpendicular to the upper NiFe/FeCo interfaces, and so confirm the epitaxial growth in that direction and is evidence of the epitaxial growth of the lower FeCo layer on the lower NiFe layer, which functions as an atomic template. These two mutual orientation relationships are also sufficient to determine the relative

CONTAINS CONFIDENTIAL ATTORNEY EYES ONLY
INFORMATION SUBJECT TO PROTECTIVE ORDER

orientation of the lower NiFe layer and the lower FeCo layer above it. Therefore, the lower NiFe layer exhibits (111) texture, and the lower FeCo layer exhibits (110) texture.

102. The parallel directions in the FCC and BCC layers normal to the interface show repeatedly <110> direction in the BCC layers and <111> direction in the FCC layers. Therefore, this analysis shows that the lower NiFe layer has a predominant (111) texture, and the lower FeCo layer has a predominant (110) texture.

103. Since the FFT analysis above shows that the upper NiFe / FeCo relationship is $\{111\}_{FCC}\|\{110\}_{BCC}$, as well as $<110>_{FCC}\|<111>_{BCC}$, this shows that the Kurdjumov–Sachs orientation relationship is present with respect to both the lower NiFe / FeCo layers, and the upper NiFe / FeCo layers. Further, as discussed in Section F.1.a.4 below, the microbeam diffraction analysis confirms the presence of Kurdjumov–Sachs orientational variants in the lower FeCo layer. I would not expect such variants but for the lower FeCo layer to be grown upon a predominately (111) FCC NiFe template later.

104. As above, similar analysis was performed on FFTs taken at points other than 1 and each showed similar results as those described above, thereby confirming that the orientational relationships were consistent across the interfaces as described above, and that the same textures were present throughout each layer. These FFTs are contained in Appendix C. Additionally, FFTs were taken on the remaining 4 high-resolution cross sections from region B; annotated cross sections and their accompanying FFTs are also shown in Appendix C and also showed similar results as those described above, further confirming the orientational relationships and textures as described above.

105. I also note that the FFTs taken from various points along the NiFe layers, while they maintain a common direction with the FeCo layers normal to the interface, change

CONTAINS CONFIDENTIAL ATTORNEY EYES ONLY
INFORMATION SUBJECT TO PROTECTIVE ORDER

significantly with position along the interface. These changes in the FFT indicate differences in orientation along the template, and thus the grain size in the template. The grain size in the NiFe template layers is comparable to the width of the FeCo grains, so that the grain sizes in the two are similar. Thus, there is ordinarily only one or two FeCo grains per NiFe template grain.

(4) TEM—microbeam diffraction on plan view samples

106. Microbeam diffraction, as described in Section E.2.d above, was performed on a region of the lower FeCo layer of the write pole as shown by the red square in Figure 45 below. A plan view sample was prepared such that the upper FeCo/NiFe layer pair was removed, leaving the lower FeCo layer of the write pole exposed for microbeam diffraction. From the area indicated by the red square, 1,600 diffraction patterns were obtained by scanning the electron beam incrementally across the area in the box. A typical diffraction pattern is shown on the right. Note that all diffraction patterns below were annotated using Keynote, software available from Apple.

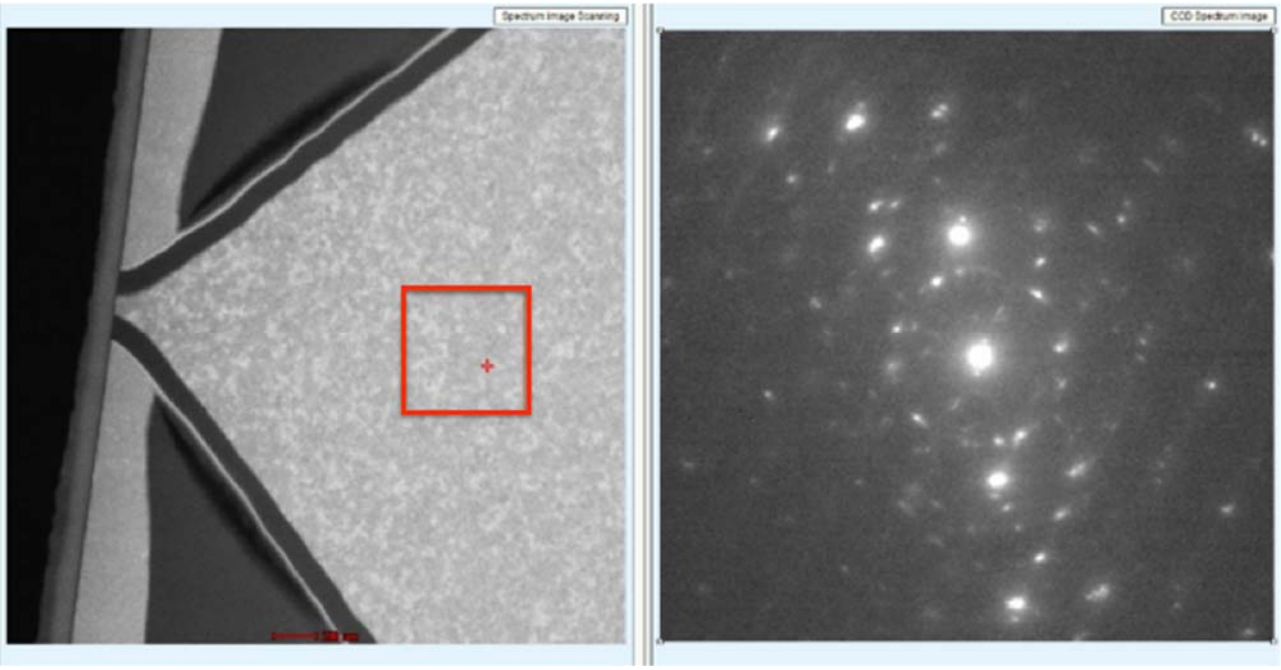

Figure 45: Plan view STEM image of S0GPPC near the pole tip of the write head (left). 1,600 diffraction patterns were taken from the area outlined in red. A typical diffraction pattern is shown on the right.

CONTAINS CONFIDENTIAL ATTORNEY EYES ONLY
INFORMATION SUBJECT TO PROTECTIVE ORDER

107. By defocusing the diffraction pattern image slightly, as shown on the right of Figure 46 below, we obtain an enlarged central spot that contains an image of a portion of the sample. This shows that the image of the plan view sample on the left and the diffraction pattern on the right are in near perfect alignment, to ±10˚. Thus, directions associated with the sample can be related to directions in the diffraction pattern, and those directions may be indexed.

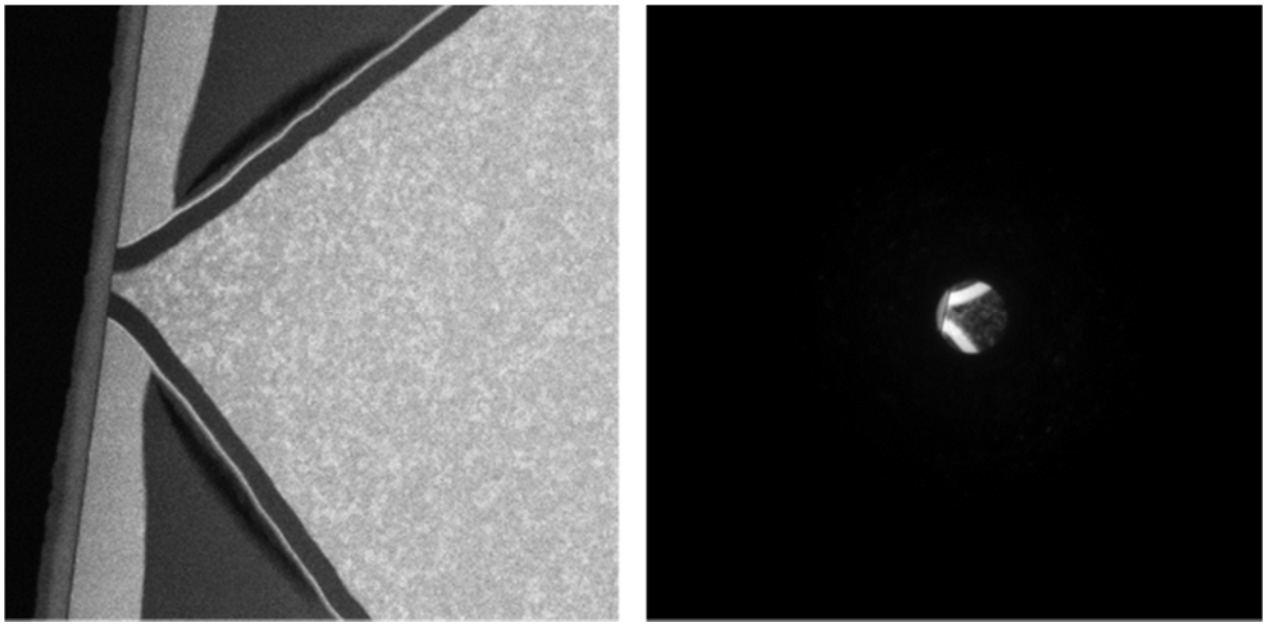

Figure 46: Plan view STEM image of S0GPPC (left), with a de-magnified image of the central spot of its diffraction pattern (as shown in Figure 45 above) in which the image of the head can be seen. This fixes the relative orientation of the image (left) and any diffraction patterns.

108. Individual frames from this set of 1,600 may contain diffraction patterns from one, two, or sometimes more separate FeCo crystallites. Typical single crystal patterns obtained for this analysis are shown in Figure 47 below. These patterns are readily identified and indexed as patterns in the $(110)_{BCC}$ orientation. This is confirmed by measurement of the ratio of the sides of the rectangles, found to be 5.4:3.8 = 1:√2, as required. Further, this is the epitaxial growth direction for the lower FeCo layer on the lower NiFe layer (the atomic template) as expected. These patterns are further confirmation that the FeCo layer is BCC with (110) texture.

CONTAINS CONFIDENTIAL ATTORNEY EYES ONLY
INFORMATION SUBJECT TO PROTECTIVE ORDER

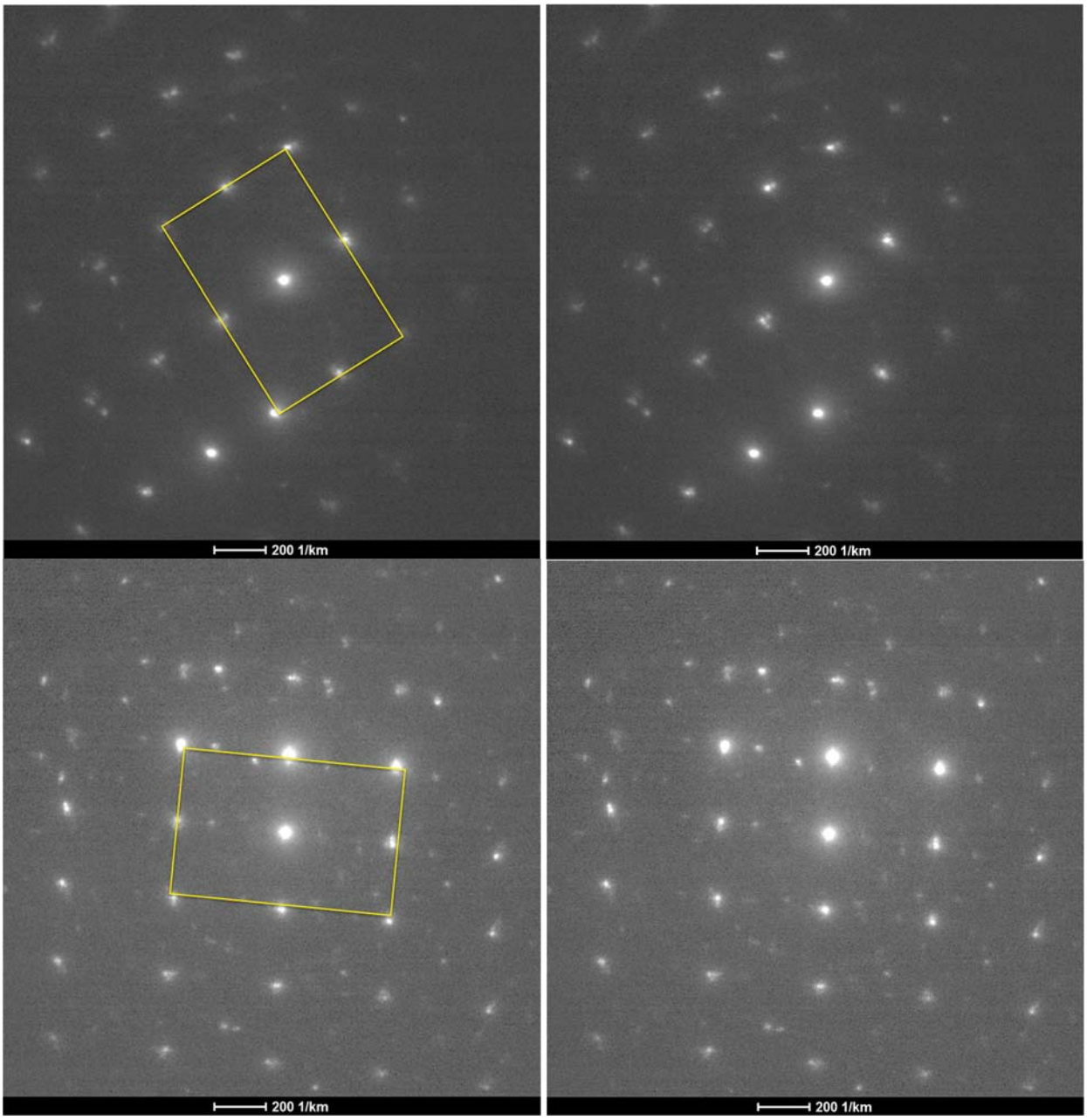

Figure 47: Single crystallite diffraction patterns, frames 722 (upper) and 417 (lower), in the (110) orientation. These patterns visually identify as standard $(110)_{BCC}$ patterns.

109. Figure 48 below shows another example of a single crystallite $(110)_{BCC}$ diffraction pattern. Although there are additional diffraction spots caused by the phenomenon of double diffraction,[18] no orientation other than $(110)_{BCC}$ is apparent. Also note that some spots in the motif are weak or barely detectable. This arises from distortions in the sample, or the sample

[18] Double diffraction arises when the beam passes through overlapping crystals.

CONTAINS CONFIDENTIAL ATTORNEY EYES ONLY
INFORMATION SUBJECT TO PROTECTIVE ORDER

being tilted slightly off of the exact (110) orientation, so that some diffraction spots do not make a perfect intersection with the Ewald sphere, and so are faint or not visible at all. Despite these slight variances, it is readily ascertainable that this is a $(110)_{BCC}$ diffraction pattern as no other orientation describes it.

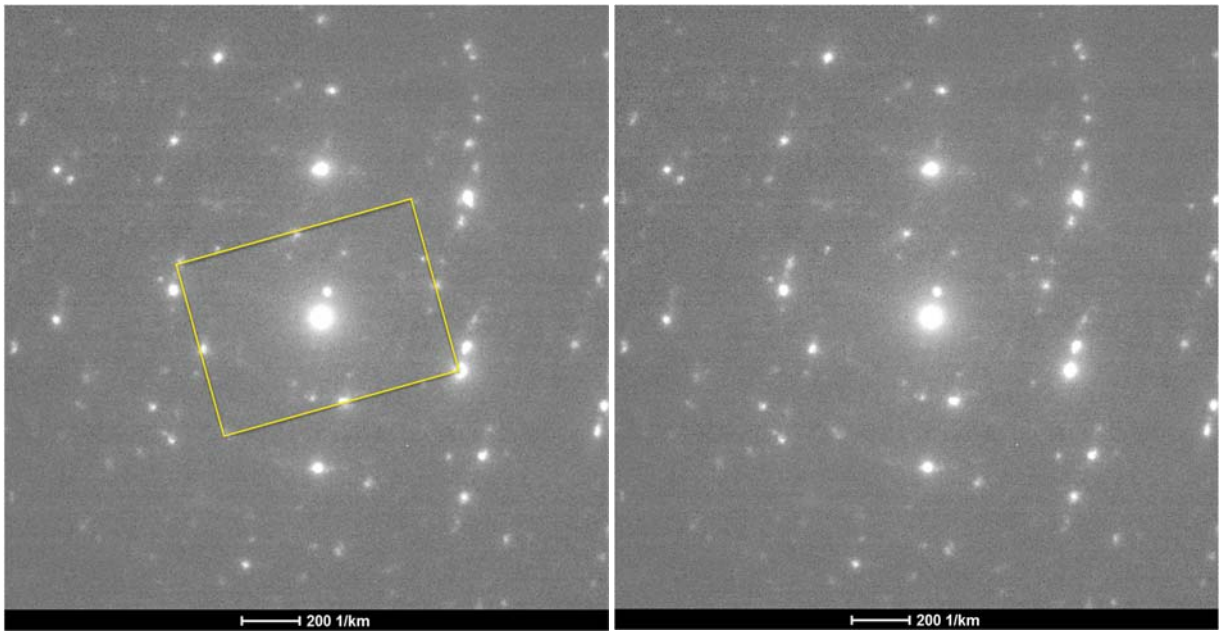

Figure 48: Single crystallite diffraction pattern, frame 837, in the (110) orientation. While there are additional or weak spots, this motif is readily identifiable as a $(110)_{BCC}$ pattern.

110. Figure 49 below shows an example diffraction pattern with two crystallites, both in the $(110)_{BCC}$ orientation, but rotated by ~9˚ about their common $[110]_{BCC}$ direction. This is the separation of two variants in the Kurdjumov-Sachs orientation. The measured ratio of the sides of the motif are 1:√2 as required. Angles were measured directly in Keynote.

CONTAINS CONFIDENTIAL ATTORNEY EYES ONLY
INFORMATION SUBJECT TO PROTECTIVE ORDER

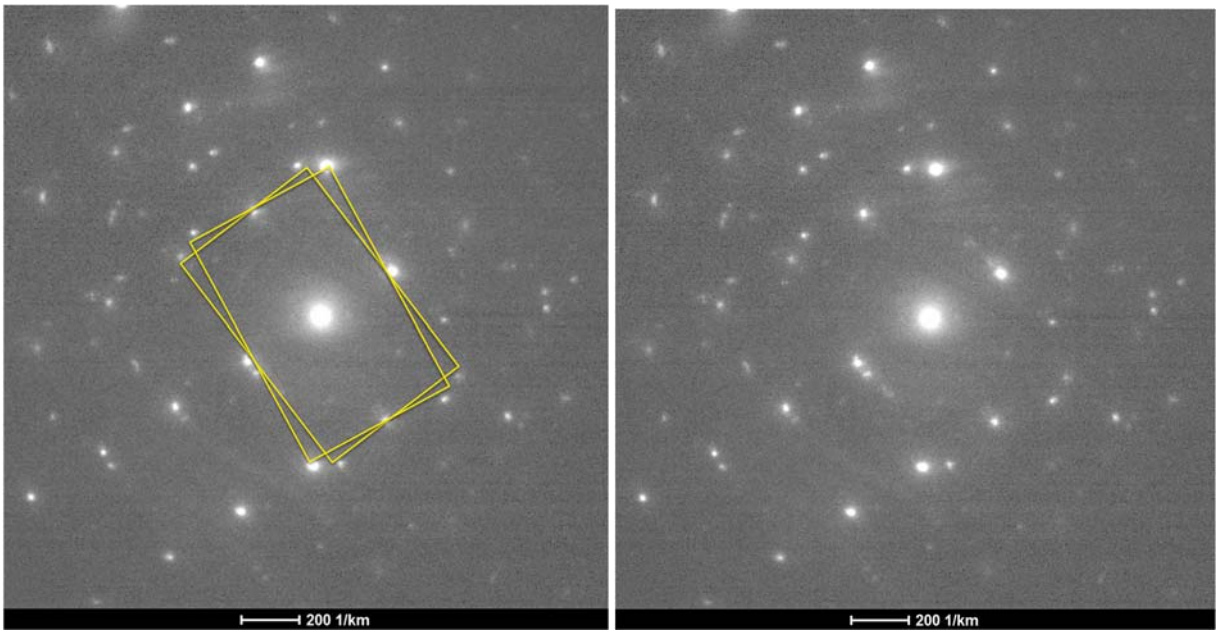

Figure 49: Two crystallites, both in the $(110)_{BCC}$ orientation, frame 721, rotated by ~9˚ about their common $[110]_{BCC}$ direction.

111. Figure 50 below shows another example diffraction pattern with two crystallites, both in the $(110)_{BCC}$ orientation, but rotated by ~11˚ about their common $[110]_{BCC}$ direction. . This is also the separation of two variants in the Kurdjumov-Sachs orientation. The measured ratio of the sides of the motif is 1:√2 as required.

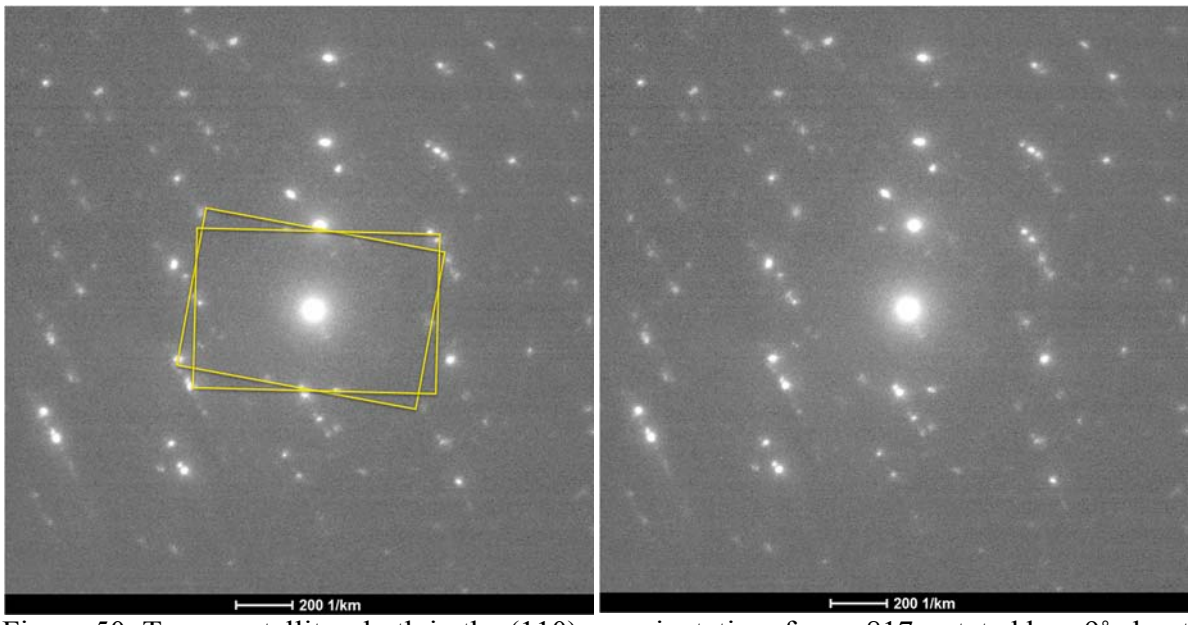

Figure 50: Two crystallites, both in the $(110)_{BCC}$ orientation, frame 817, rotated by ~9˚ about their common $[110]_{BCC}$ direction.

CONTAINS CONFIDENTIAL ATTORNEY EYES ONLY
INFORMATION SUBJECT TO PROTECTIVE ORDER

112. Figure 51 below shows two diffraction patterns each showing two crystallites both in the $(110)_{BCC}$ orientation, rotated about their common $[110]_{BCC}$ direction by ~70.53˚. This is also the separation of two variants in the Kurdjmov-Sachs orientation. This also means that the crystallites are in the "twin" orientation, which is alternatively described as a 180˚ rotation about their common <211> direction (circled in red below), or a mirror reflection in the <211> plane (dashed line).

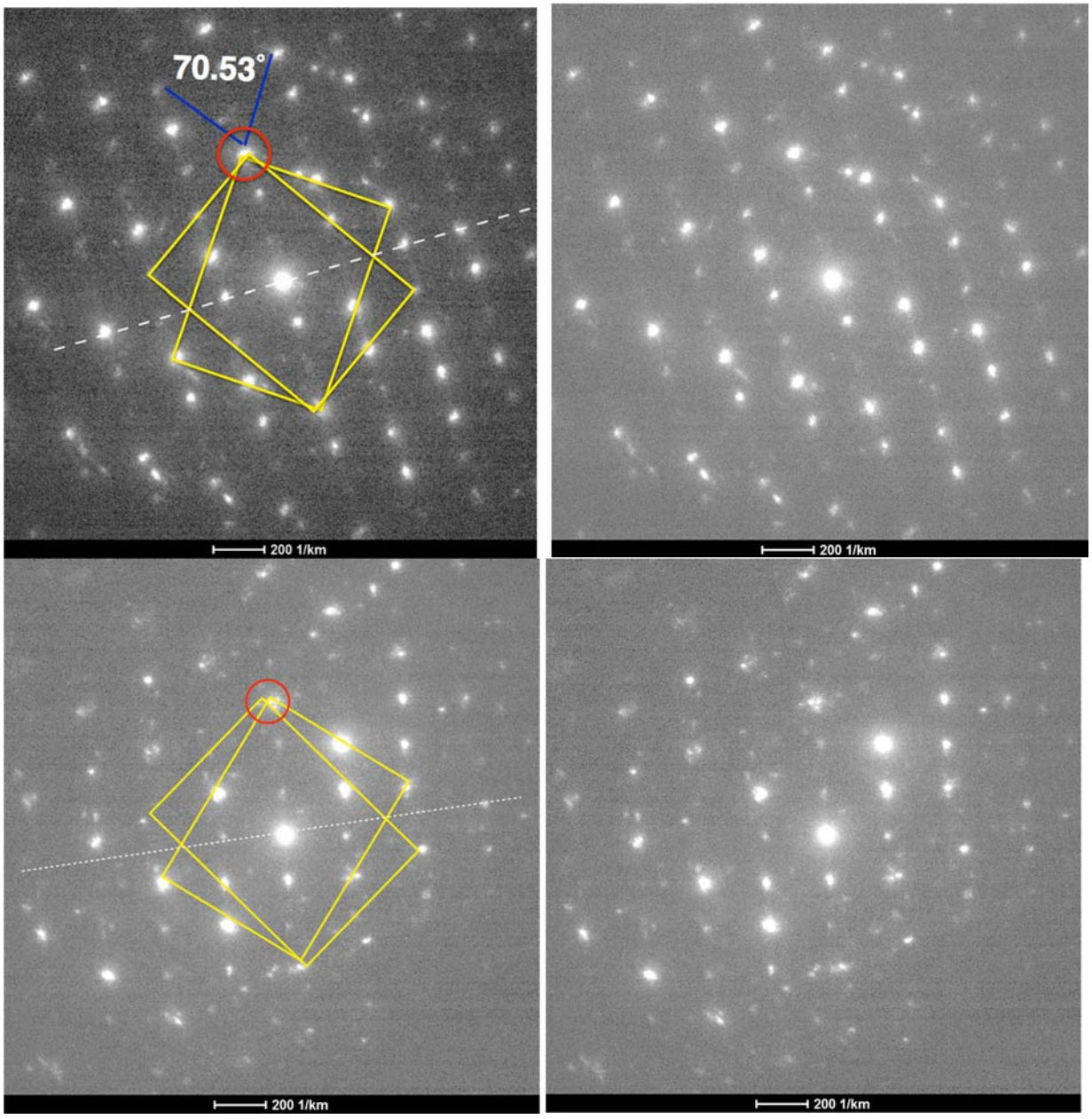

CONTAINS CONFIDENTIAL ATTORNEY EYES ONLY
INFORMATION SUBJECT TO PROTECTIVE ORDER

Figure 51: Both patterns, frames 726 (upper) and 802 (lower), show two crystallites both in the $(110)_{BCC}$ twin orientation, rotated by ~70.53˚ about their common $[110]_{BCC}$ direction

113. Figure 52 below shows a complex diffraction pattern, which arises when more than two crystallites contribute to the pattern. In the example of Figure 52 below, there are two variants of $(110)_{BCC}$ rotated with respect to each other by ~4˚, and a third at ~71˚ from the first.

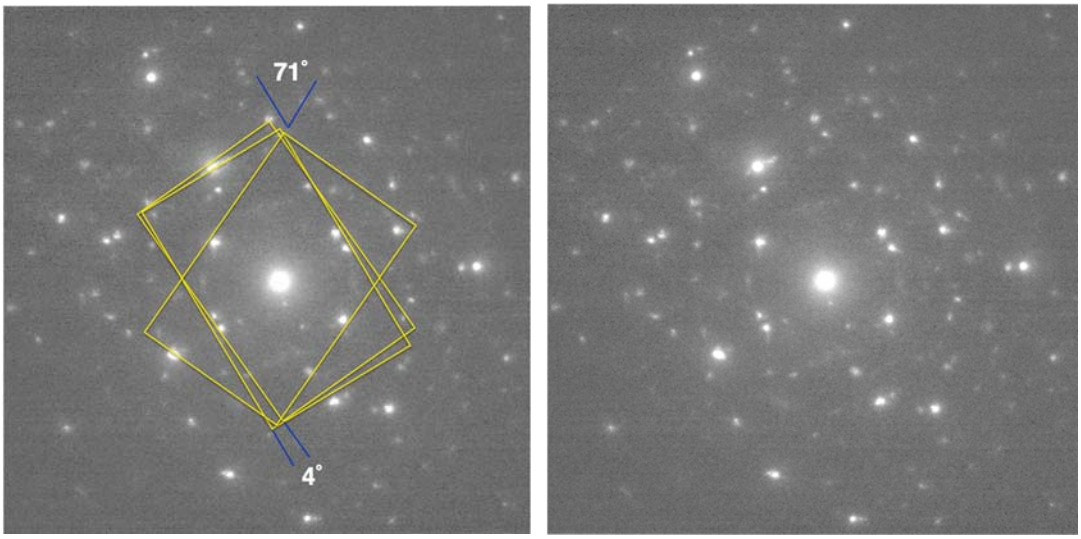

Figure 52: Diffraction pattern, frame 1487, showing three crystallites in the $(110)_{BCC}$ orientation. Two crystallites are rotated with respect to each other by ~4˚, and the third is at ~71˚ from the first.

114. In addition to the analysis of individual patterns, 100 out of the 1600 diffraction patterns were selected using a random number generator. These 100 were categorized as either a) showing no recognizable pattern, b) showing a single {110} patterns, c) showing two or three {110} patterns, d) showing {110} twins, or e) showing a pattern other than {110}. The results show the following numbers in each category – 27 showed no recognizable pattern, 30 showed a single {110} pattern, and 44 showed two or three {110} patterns (including twins).

115. Thus, microbeam diffraction imaging results confirm that the lower FeCo layer is BCC and contains variants with the expected orientation relationship for the Kurdjumov-Sachs six variant system. Typical FeCo diffraction patterns exhibit the $(110)_{BCC}$ orientation, consistent with the epitaxial growth relationship of $(110)_{FeCo}$ on $(111)_{NiFe}$.

CONTAINS CONFIDENTIAL ATTORNEY EYES ONLY INFORMATION SUBJECT TO PROTECTIVE ORDER

(5) Dark field image analysis

116. The principles behind dark field imaging and analysis are discussed in Section E.2.f above. Figure 53below shows the area from the write head of S0GPPC where the diffraction data was taken on the left (this plan view sample is the same as that analyzed regarding microbeam diffraction above, exposing the FeCo layer), and a defocused diffraction ring pattern on the right which reveals an image of the sample in the central spot, similar to that discussed in Section F.1.a.4 above. This provides the orientation of the write head with respect to the diffraction pattern, as seen in Figure 53 below. From this image, it is clear that the diffraction pattern and the tip of the sample are almost exactly parallel, with less than 10˚ rotation from one to the other.

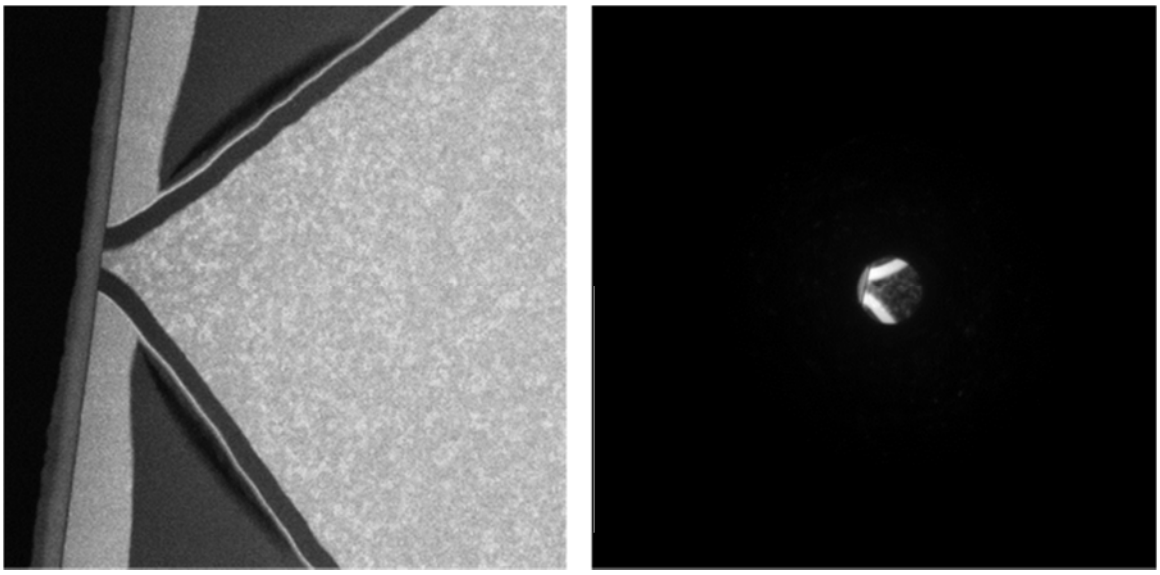

Figure 53: Defocused diffraction pattern (right) reveals alignment with sample (left) to be almost exactly parallel.

117. First, a small objective aperture is inserted to enclose a segment of the {200} diffraction ring, as shown on the left in Figure 54 below. Next, a dark field image of an area of the lower FeCo layer is obtained, as shown on the right in Figure 54 below. Where crystallites show up bright in the dark field image, it indicates that their {200} planes are oriented so as to

CONTAINS CONFIDENTIAL ATTORNEY EYES ONLY
INFORMATION SUBJECT TO PROTECTIVE ORDER

diffract into the direction enclosed by the objective aperture. The yellow arrow in the annotated image points in the direction of the objective aperture from the center of the diffraction pattern. This means that the bright crystallites have their <200> directions aligned parallel to the arrow, i.e., perpendicular to the long axis of the write head. Also note that the sample is oriented such that the $<110>_{BCC}$ directions are antiparallel to the electron beam.

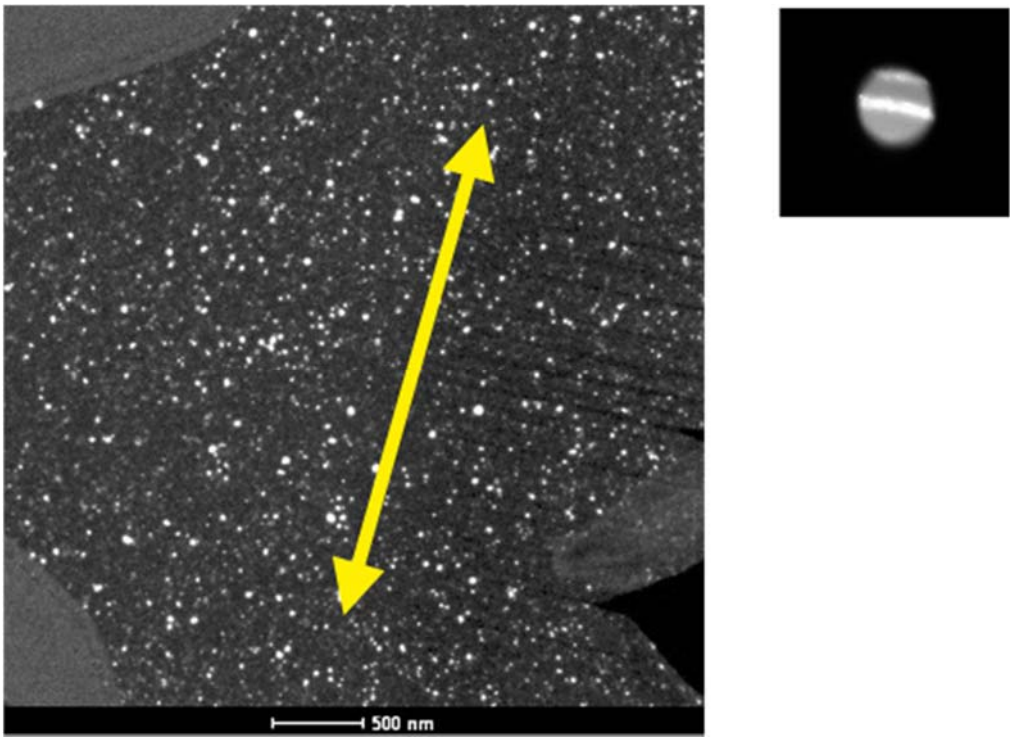

Figure 54: Dark field image showing crystallites with <200> directions aligned parallel to the yellow arrow (left). Enclosed segment of {200} diffraction ring (right).

118. In contrast to Figure 54 above, an image taken with the objective aperture at roughly 90˚ to the position above, as shown on the right in Figure 55 below, produces an image in which significantly fewer of the crystallites are illuminated as shown on the left in Figure 55, indicating that a smaller fraction of crystallites have their <200> directions aligned parallel to the long axis of the head.

CONTAINS CONFIDENTIAL ATTORNEY EYES ONLY
INFORMATION SUBJECT TO PROTECTIVE ORDER

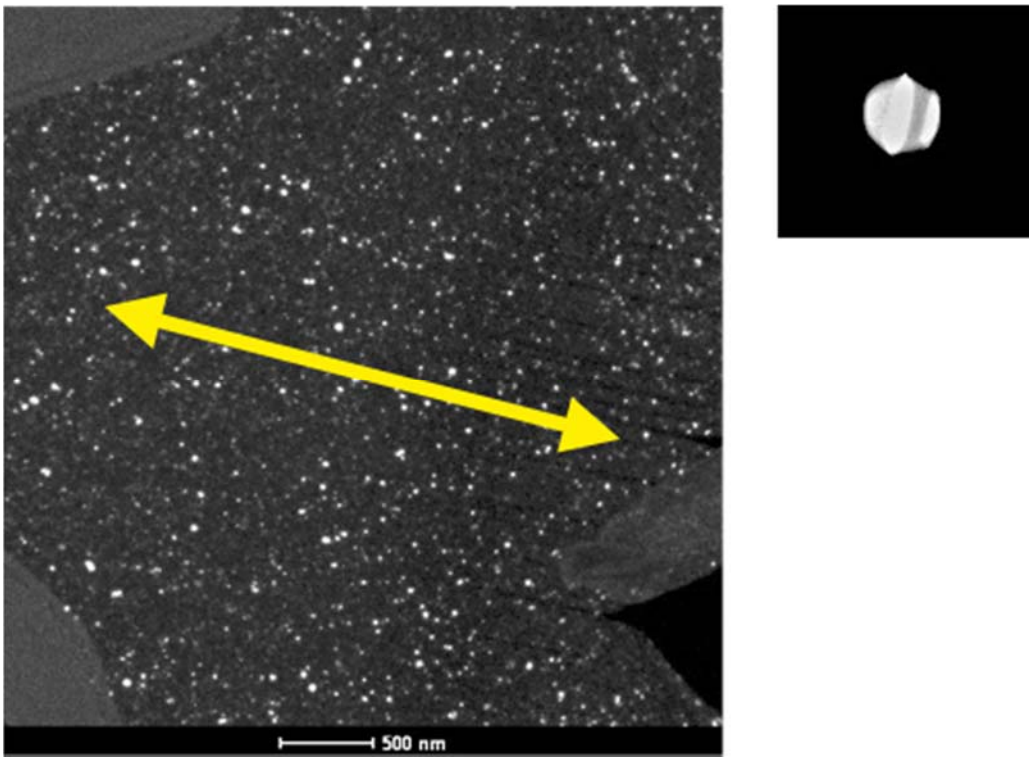

Figure 55: Dark field image showing crystallites with <200> directions aligned parallel to the yellow arrow (left). Enclosed segment of {200} diffraction ring (right).

119. This procedure is repeated at 10˚ intervals around the diffraction ring in at least a 180˚ rotation, producing dark field images similar to shows in Figures 54-55 above. To analyze these images, first, a large area of the dark field image is separated. The size and location of this area for sample S0GPPC is shown in the red box of Figure 56 below.

CONTAINS CONFIDENTIAL ATTORNEY EYES ONLY
INFORMATION SUBJECT TO PROTECTIVE ORDER

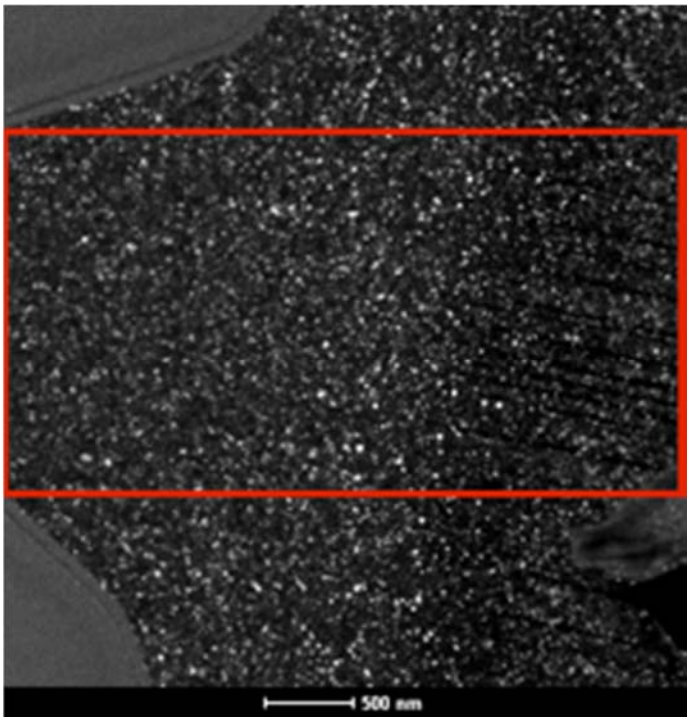

Figure 56: Dark field image with area under analysis shown enclosed by the red box (left) and extracted image (right).

120. Next, to analyze these images, a standard stereological computer program is used. I used ImageJ in my analysis. For each image, a threshold is applied to the isolated area as described by Figure 56 in order to produce a binary black and white image shown in Figure 57 below.

CONTAINS CONFIDENTIAL ATTORNEY EYES ONLY INFORMATION SUBJECT TO PROTECTIVE ORDER

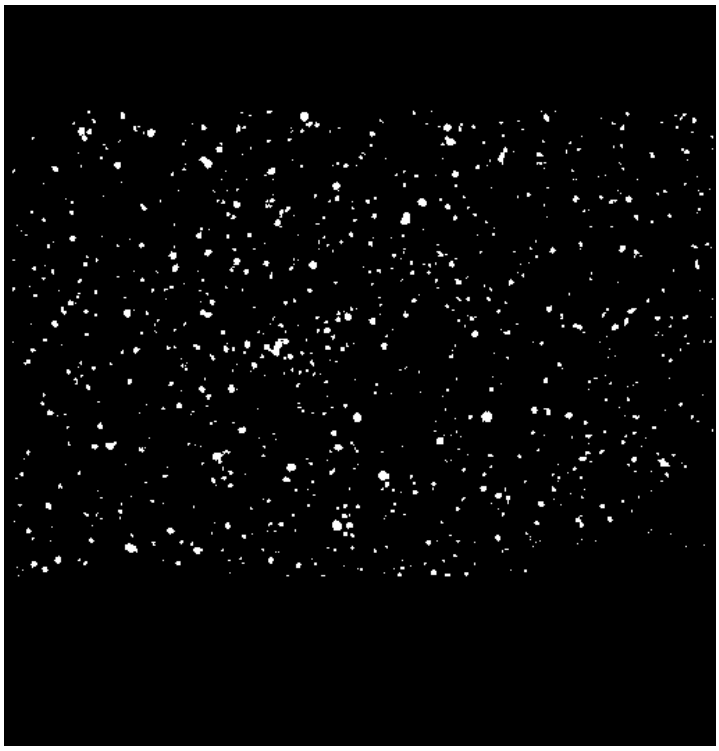

Figure 57: Binary black and white image of the area described by the red box of Figure 56 above.

121. This image is operated on by ImageJ to measure the area fraction of crystallites that are white – that is, the area fraction of crystallites that scatter into the objective aperture at that particular position – and that area fraction for that particular position is tabulated. The image created by ImageJ enumerating the white crystallites is shown in Figure 58 below. The area fraction for each enumerated crystallite is shown in Appendix C.

CONTAINS CONFIDENTIAL ATTORNEY EYES ONLY INFORMATION SUBJECT TO PROTECTIVE ORDER

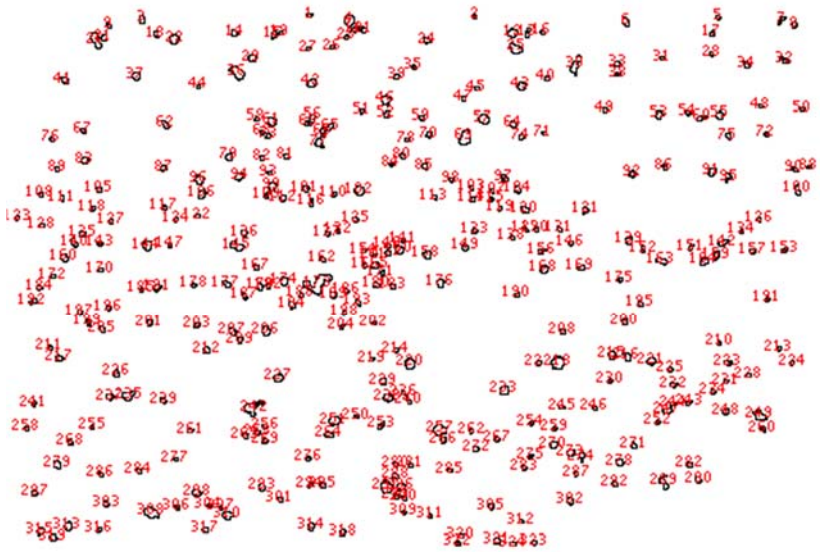

Figure 58: Image enumerating the white crystallites from Figure 57 above. Note that ImageJ enumerates each crystallite individually, and then calculates the relative area occupied by each crystallite.

122. Finally, the area fractions are added for each 10˚ increment to arrive at the total area of white crystallites for that particular increment, and the results for all positions are then tabulated. The results for S0GPPC are shown in Table 1 and graphed in Figure 59 below. The full results of this dark field analysis are attached as Appendix C.

Angle	%Area
0	2.3
10	2.137
20	2.163
30	2.129
40	1.501
50	1.404
60	1.661
70	1.533

CONTAINS CONFIDENTIAL ATTORNEY EYES ONLY
INFORMATION SUBJECT TO PROTECTIVE ORDER

80	1.527
90	1.421
100	1.362
110	1.156
120	1.576
130	1.269
140	1.372
150	1.724
160	1.748
170	2.103
180	2.306

Table 1: Number and area fractions of white crystallites at each angle in 180 degrees of rotation.

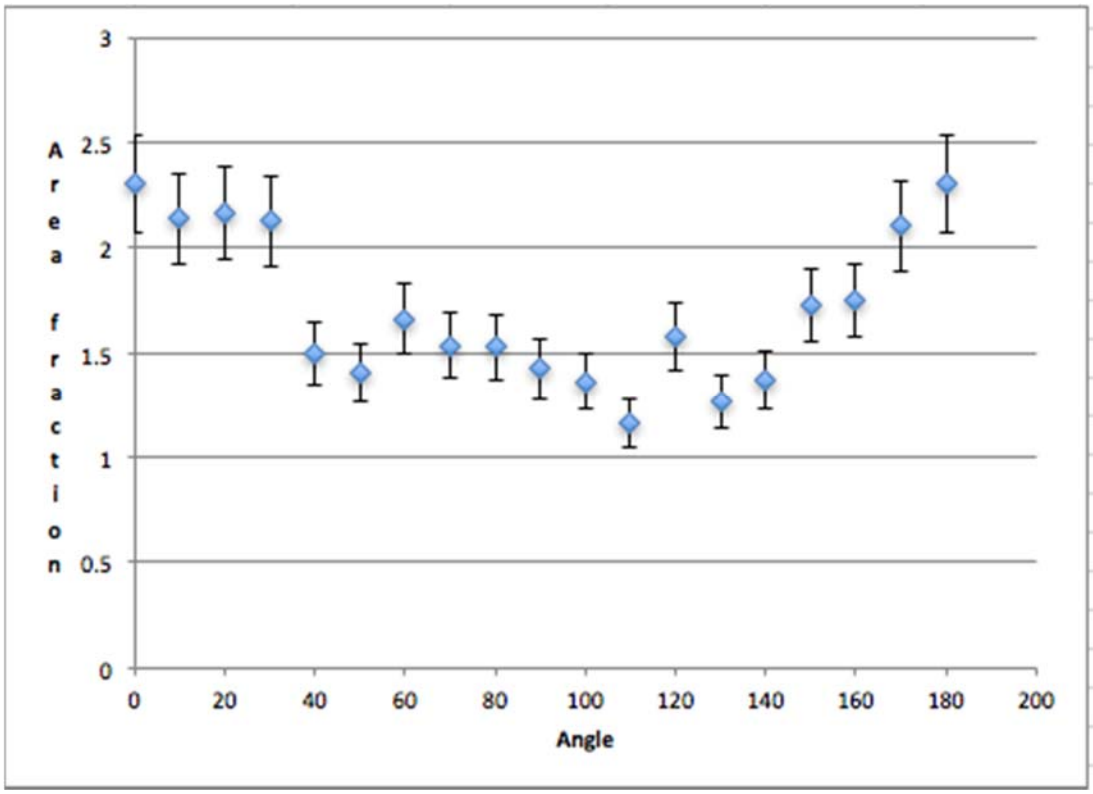

Figure 59: Area fraction of white crystallites vs. angle, where 0 degrees is perpendicular to the long axis of the write head. Error bars also shown.

123. These results indicate that there is a maximum area at 0 degrees, indicating that more crystallites are oriented with their <200> (easy) directions perpendicular to the long axis of the write head.

CONTAINS CONFIDENTIAL ATTORNEY EYES ONLY
INFORMATION SUBJECT TO PROTECTIVE ORDER

124. Further, as I explained in Section F.1.a.3, the sizes of the grains in the NiFe template layers and FeCo layers are similar, such that there are only one or two FeCo grains per NiFe template grain for the great majority of NiFe template grains. Further, this dark field analysis, in conjunction with the microbeam diffraction analysis discussed above, shows that the various FeCo grains on top of the various NiFe template layer grains have members of the six-variant system preferentially aligned such that there is an unequal amount of the six variants in the FeCo layer. Given the relative grain sizes in the FeCo layer and NiFe template layer, there are no NiFe template grains that have six different overlying grains in the FeCo layer, let alone that each of the six different overlying grains would have equal area and each represent a different variant from the six-variant system present in the FeCo layer.

b) **S2MMMC**

(1) EDS analysis

125. The principles behind EDS are discussed generally in Section E.3 above. EDS color maps are shown in Figures 60-64 below and indicate the concentration of elements in the area indicated by the color assigned to that element. Overviews are first shown in Figures 60-61, and individual elemental mappings are shown in Figures 62-64. These mappings indicate the composition of individual layers in the write pole.

CONTAINS CONFIDENTIAL ATTORNEY EYES ONLY
INFORMATION SUBJECT TO PROTECTIVE ORDER

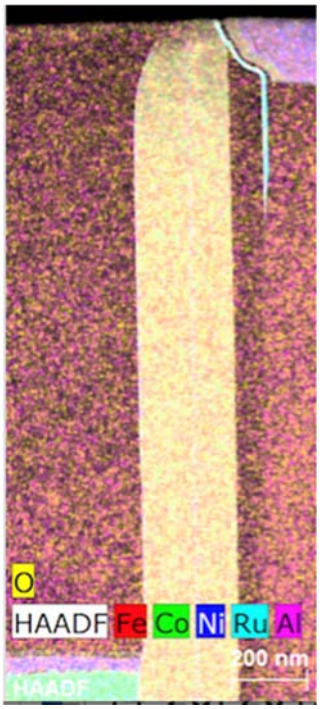

Figure 60: Overall EDS map. Note that the growth direction in the EDS maps for S2MMMC is from left to right.

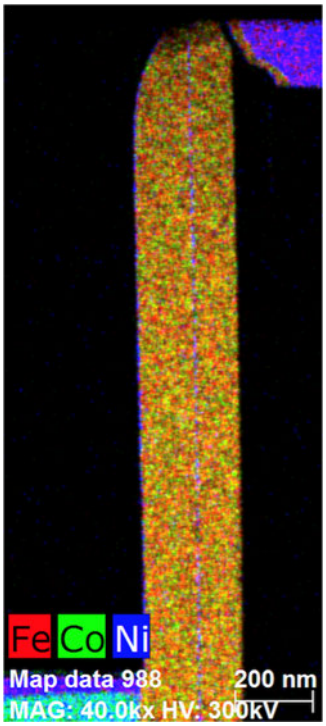

Figure 61: EDS map of Fe, Ni, and Co.

CONTAINS CONFIDENTIAL ATTORNEY EYES ONLY
INFORMATION SUBJECT TO PROTECTIVE ORDER

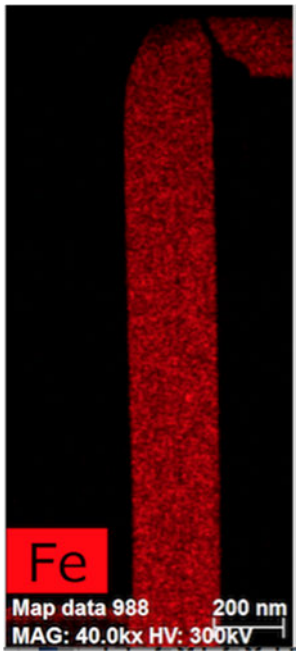

Figure 62: EDS map showing just Fe.

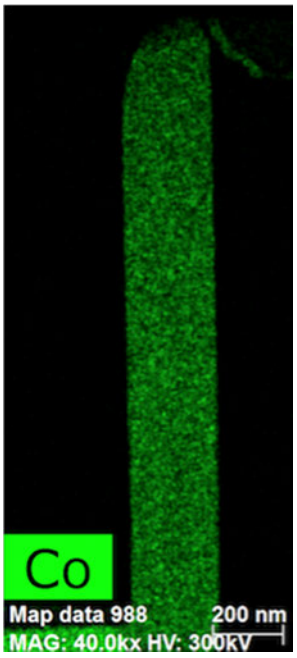

Figure 63: EDS map showing just Co.

CONTAINS CONFIDENTIAL ATTORNEY EYES ONLY INFORMATION SUBJECT TO PROTECTIVE ORDER

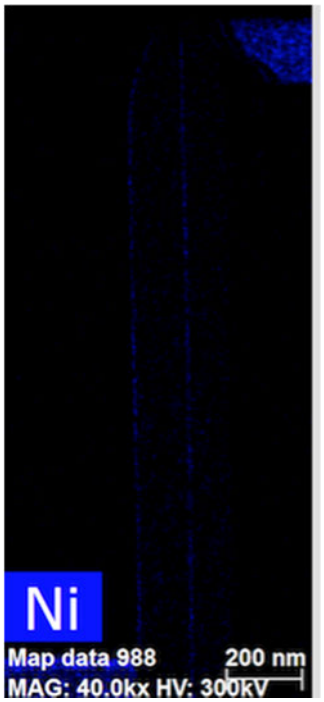

Figure 64: EDS map showing just Ni.

126. Additionally, a quantitative assessment of the composition of the FeCo layers was performed Bruker ESPRIT as shown below.

CONTAINS CONFIDENTIAL ATTORNEY EYES ONLY
INFORMATION SUBJECT TO PROTECTIVE ORDER

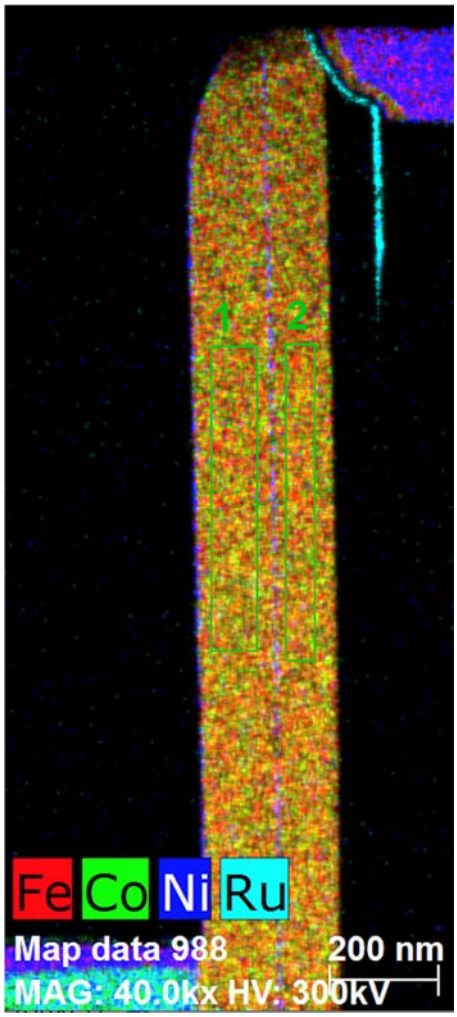

Figure 65: Quantitative assessment performed in the regions enclosed by the green rectangles.

Spectrum: 1

Element	Series	unn. C [wt.%]	norm. C [wt.%]	Atom. C [at.%]	Error (3 Sigma) [wt.%]
Iron	K-series	61.30	61.30	62.58	5.93
Cobalt	K-series	38.06	38.06	36.82	3.86
Nickel	K-series	0.34	0.34	0.33	0.23
Chromium	K-series	0.19	0.19	0.20	0.18
Ruthenium	L-series	0.11	0.11	0.06	0.19
	Total:	100.00	100.00	100.00	

CONTAINS CONFIDENTIAL ATTORNEY EYES ONLY
INFORMATION SUBJECT TO PROTECTIVE ORDER

Spectrum: 2

Element	Series	unn. C [wt.%]	norm. C [wt.%]	Atom. C [at.%]	Error (3 Sigma) [wt.%]
Ruthenium	L-series	0.00	0.00	0.00	0.00
Chromium	K-series	0.14	0.14	0.16	0.19
Iron	K-series	62.67	62.67	63.91	6.21
Cobalt	K-series	36.91	36.91	35.67	3.92
Nickel	K-series	0.27	0.27	0.27	0.24
	Total:	100.00	100.00	100.00	

Figure 66: Output from Bruker ESPRIT showing composition in regions enclosed by the green rectangles.

(2) TEM high resolution images of cross-sections

127. The principles behind TEM imaging are discussed generally in Section E.2 above. High resolution cross-section images were taken using the FEI Titan 80-300 S-Twin microscope ("Titan"), operating in TEM mode at 300 kV, and fitted with an automated image corrector to enhance the spatial resolution.. The high resolution cross-section images were obtained from the circled region of the write pole of S2MMMC as shown in Figure 67 below.

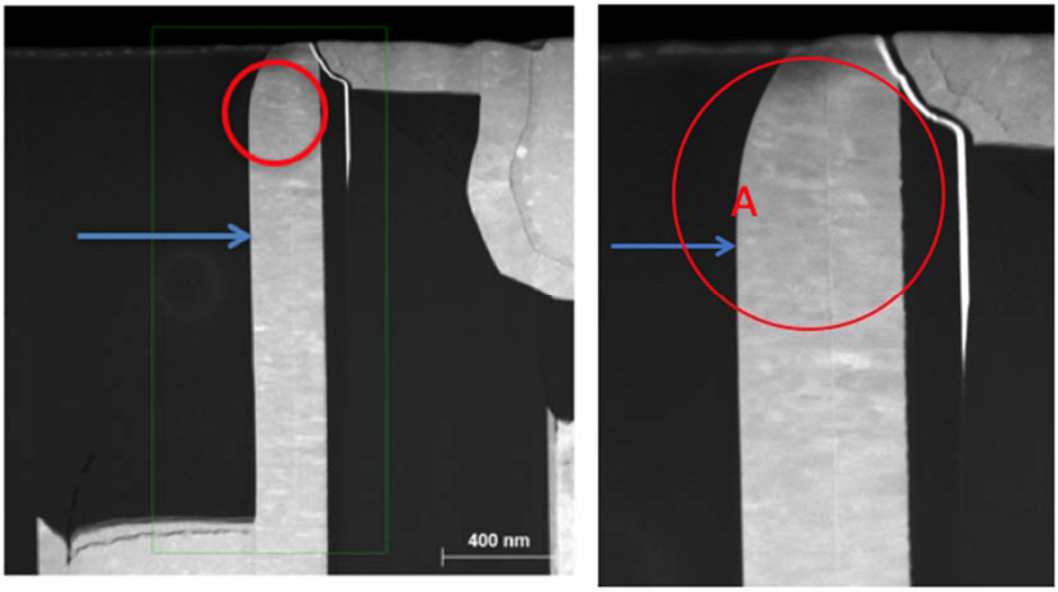

Figure 67: STEM overviews of S2MMMC, with regions where high resolution cross-sections were taken shown in the red circle. The blue arrow indicates the growth direction, the letter indicates the NiFe/FeCo interface. Note the pronounced columnar growth seen in the FeCo region.

CONTAINS CONFIDENTIAL ATTORNEY EYES ONLY
INFORMATION SUBJECT TO PROTECTIVE ORDER

128. The medium magnification image on the right-hand side of Figure 67 shows a grain structure that is elongated perpendicular to the lower NiFe layer normal (in the direction indicated by the blue arrow). Such a morphology is typically referred to as a "bamboo" structure, more formally defined as a grain structure in which the boundaries of the grains tend to be aligned normal to the long axis and to extend through the thickness.[19] The directional nature of this structure modifies the mechanical and electrical properties of a material significantly, by aligning the majority of the grain boundaries parallel to one another, as opposed to being homogeneously distributed. It is very commonly observed in epitaxial growth, where the orientation relationship between the template and the growth layers favors growth in one direction.

129. High resolution images were taken at several points across the sample. Seven such images were taken and are shown below.

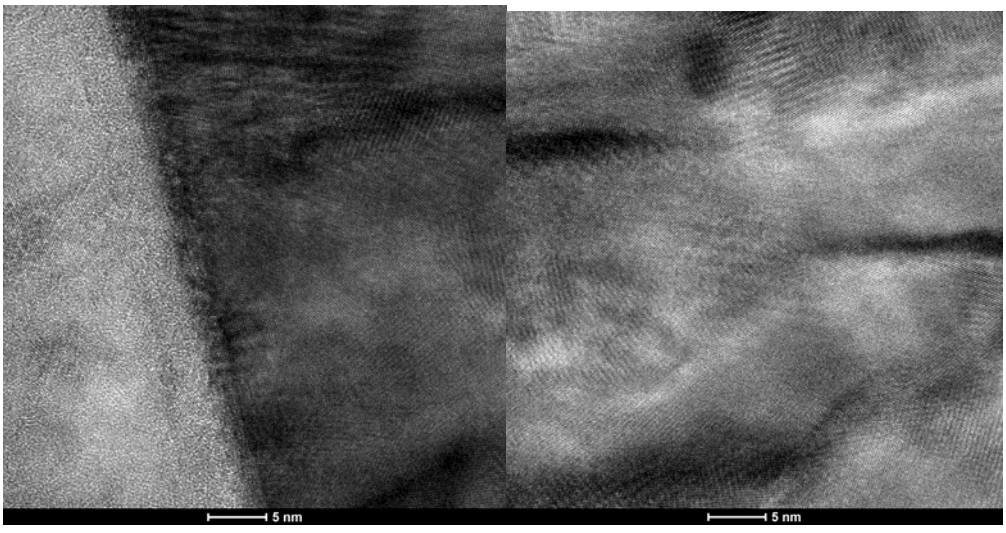

[19] *Analysis of grain-boundary structure in Al–Cu interconnects*, D.P. Field, J.E. Sanchez, P.R. Besser, and D.J. Dingley, J.Appl. Phys., **82** (5), (1997), pp. 2383-2392

CONTAINS CONFIDENTIAL ATTORNEY EYES ONLY
INFORMATION SUBJECT TO PROTECTIVE ORDER

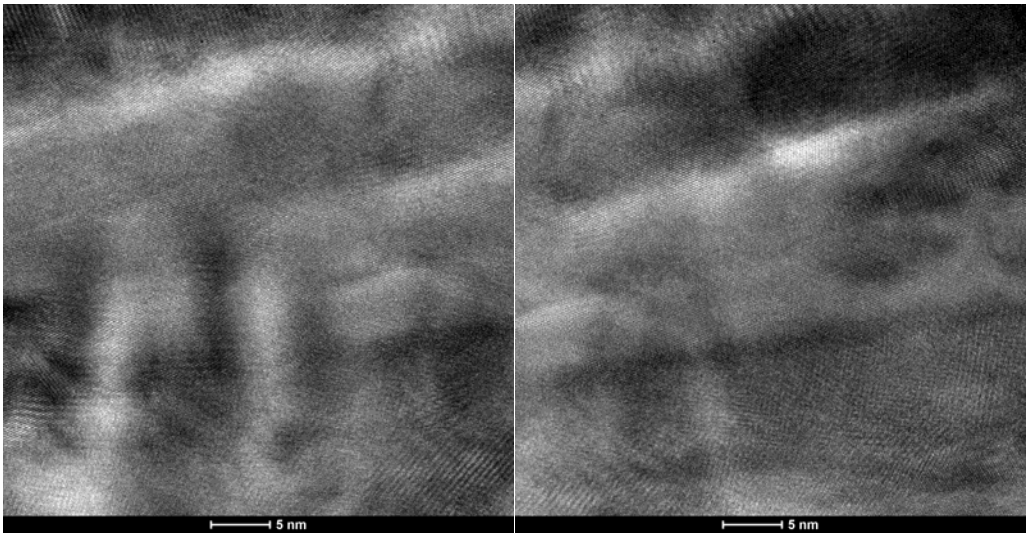

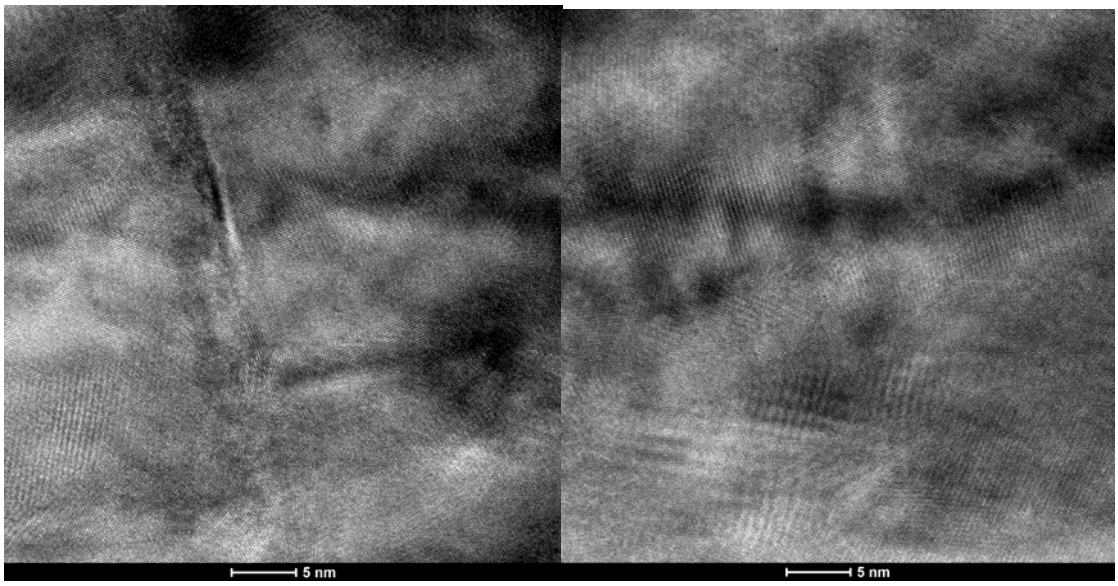

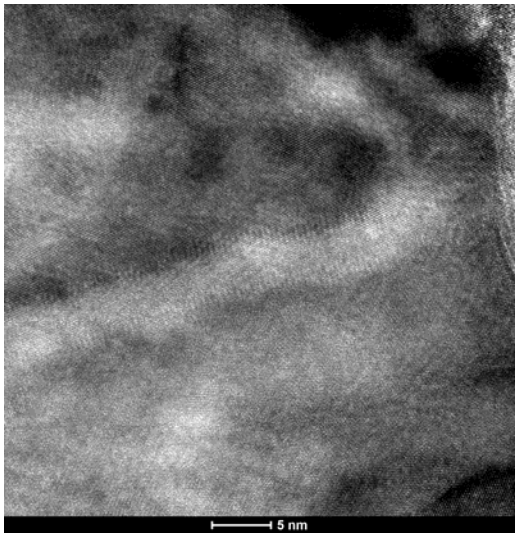

CONTAINS CONFIDENTIAL ATTORNEY EYES ONLY
INFORMATION SUBJECT TO PROTECTIVE ORDER

Figure 68: High resolution cross-section images taken across the sample, beginning from the lower NiFe / lower FeCo interface.

130. These high resolution cross-sections show various sets of crossed lattice fringes, such as the example shown in Figure 69 below. For example, in Figure 69, the zoomed-in area in the red square shows prominent patterns of crossed fringes. These lattice fringes arise when the forward scattered (central) beam and the diffracted beam corresponding to one family of crystal planes both lie within the objective aperture and so contribute to the final image. These two beams will then "beat" together in the image, resulting in a pattern of fringes that have the spacing of that family of planes, and which align parallel to them. When several diffracted beams are allowed through the objective aperture, each contributes a set of fringes, so that a crossed fringe pattern can be seen in the image. The more diffracted beams that are used to form this lattice image, the closer it will be to an image representing the actual atomic arrangement in the crystal.[20]

[20] *Transmission Electron Microscopy,* D.B. Williams and C.B. Carter, Springer, (2009), p. 389 et seq.

CONTAINS CONFIDENTIAL ATTORNEY EYES ONLY
INFORMATION SUBJECT TO PROTECTIVE ORDER

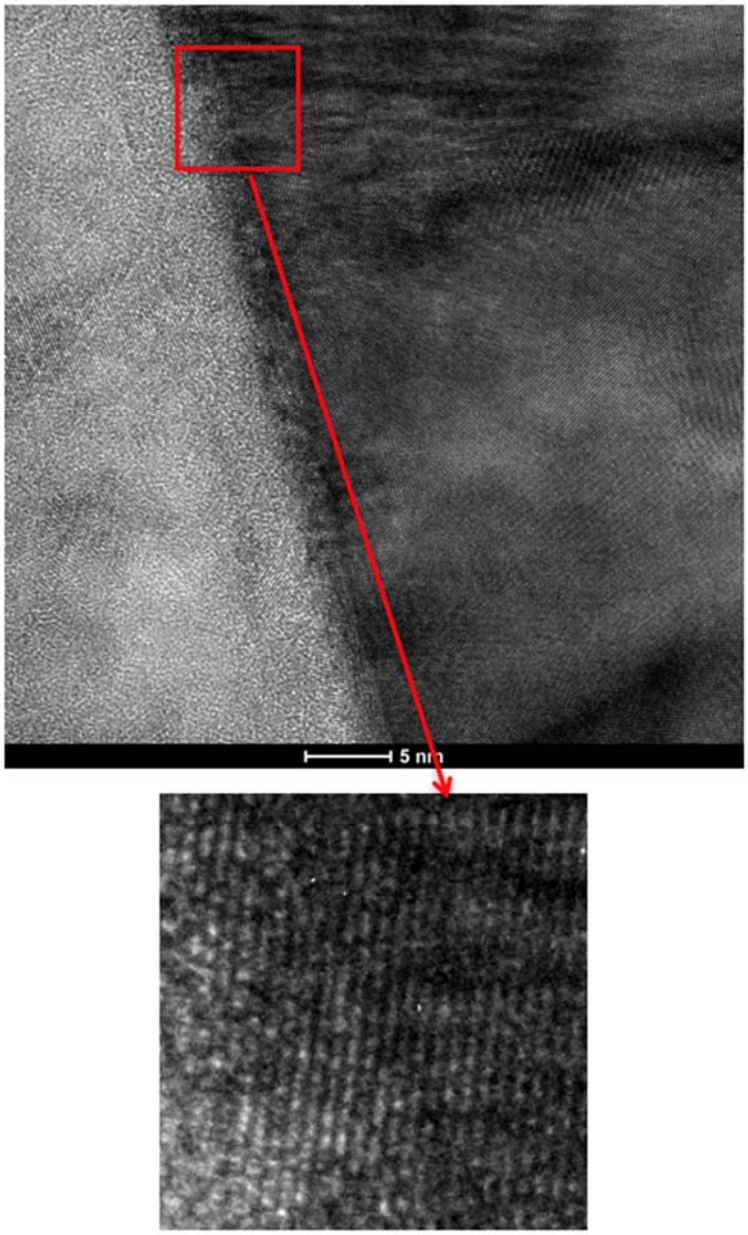

Figure 69: Example showing zoomed-in crossed lattice fringes from a high resolution cross-section from the NiFe/FeCo interface region.

131. Additionally, a high resolution cross-section taken in the region consisting of two FeCo layers with a thin layer of NiFe in between is shown in Figure 70 below. Like the high resolution cross-section in Figure 69 above, this image also shows crossed lattice fringes, with an example in the region in the red box shown enlarged in Figure 70 below.

CONTAINS CONFIDENTIAL ATTORNEY EYES ONLY
INFORMATION SUBJECT TO PROTECTIVE ORDER

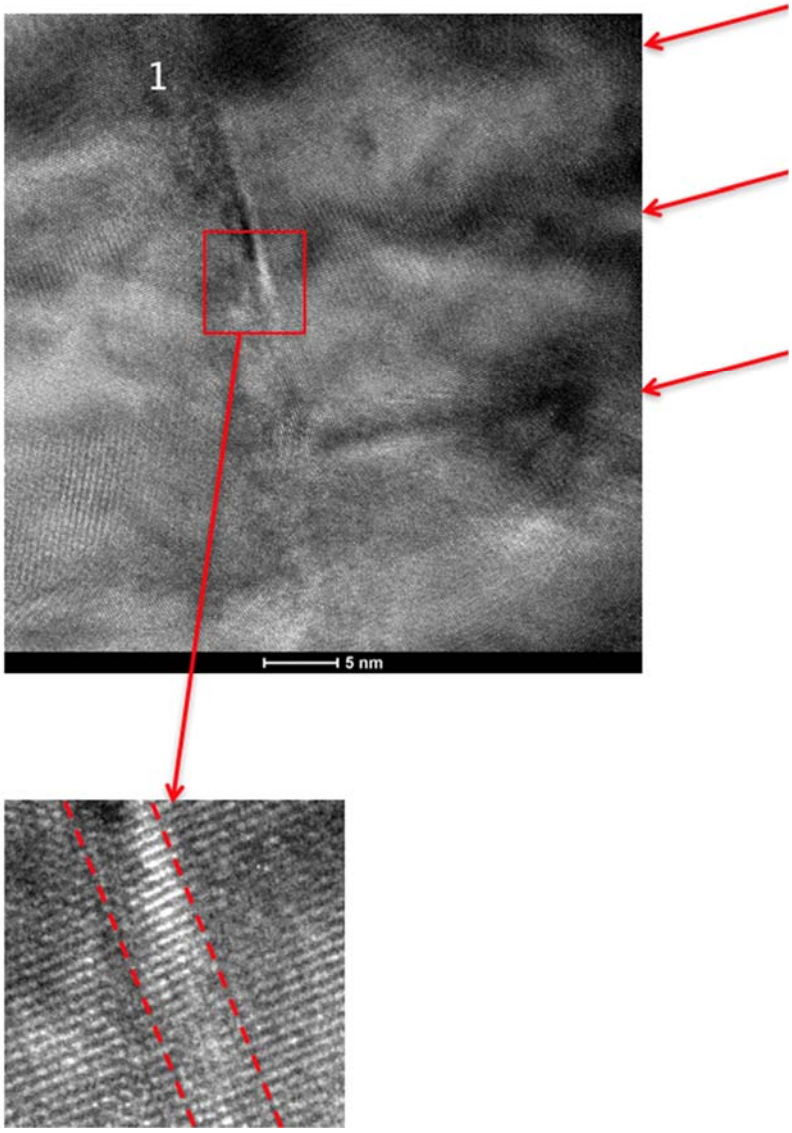

Figure 70: Example high resolution cross-section from NiFe layer in the center of the head (marked by the dashed red lines), with an enlargement showing the continuity of the lattice fringes across the interface.

132. Several sets of lattice fringes are seen here, as are the FeCo/NiFe interfaces, which are marked with a red dashed line. The fringes that run parallel to the red dashed line are present on both sides of the NiFe, and in the NiFe layer itself, indicating that the orientation of the FeCo is maintained on both sides of the NiFe. The continuity of these fringes across all three layers show that there is an orientation relationship between the FeCo and the NiFe. From the FFTs (as discussed in Section F.1.b.3 below) and the hexagonal arrangement of spots in the

CONTAINS CONFIDENTIAL ATTORNEY EYES ONLY
INFORMATION SUBJECT TO PROTECTIVE ORDER

FeCo lattice image, looking down into the cross-section (i.e., into the page) shows a $\{111\}_{BCC}$ plane, and a $<110>_{BCC}$ direction is normal to the interface (as is the case at the template/FeCo interface in region A, as discussed in Section F.1.b.3 below).

(3) FFT on TEM high resolution images of cross-sections

133. The principles behind FFTs are discussed generally in Section E.2.i above. FFTs were taken at selected points in high resolution cross-section images. For instance, a high resolution cross-section taken in region A is shown in Figure 71 below, with a number of points along the lower NiFe/ lower FeCo interface marked with numbers. At each numbered point, FFTs were taken: (a) in the lower NiFe layer at the location of the numbered point; and (b) in the lower FeCo immediately to the left of the numbered point. Since a diffraction pattern of a sample is just the Fourier transform of its structure,[21] FFTs taken of the image generate the information found in diffraction patterns, and can be used to determine crystal structure. The FFTs can be generated using a number of programs including ImageJ, MIPAR, or Desktop Microscopist; the FFTs here were generated using ImageJ. In Figure 71 below, the area sampled for each FFT was confined to an area of the size indicated by the red square, which was chosen to be small enough to ensure sampling information from the template and excluding information from the surrounding layers.

[21] *The Analytical Theory of Heat, J. B. Fourier*, (1878) [1822], translated by Alexander Freeman, The University Press (translated from French).

CONTAINS CONFIDENTIAL ATTORNEY EYES ONLY
INFORMATION SUBJECT TO PROTECTIVE ORDER

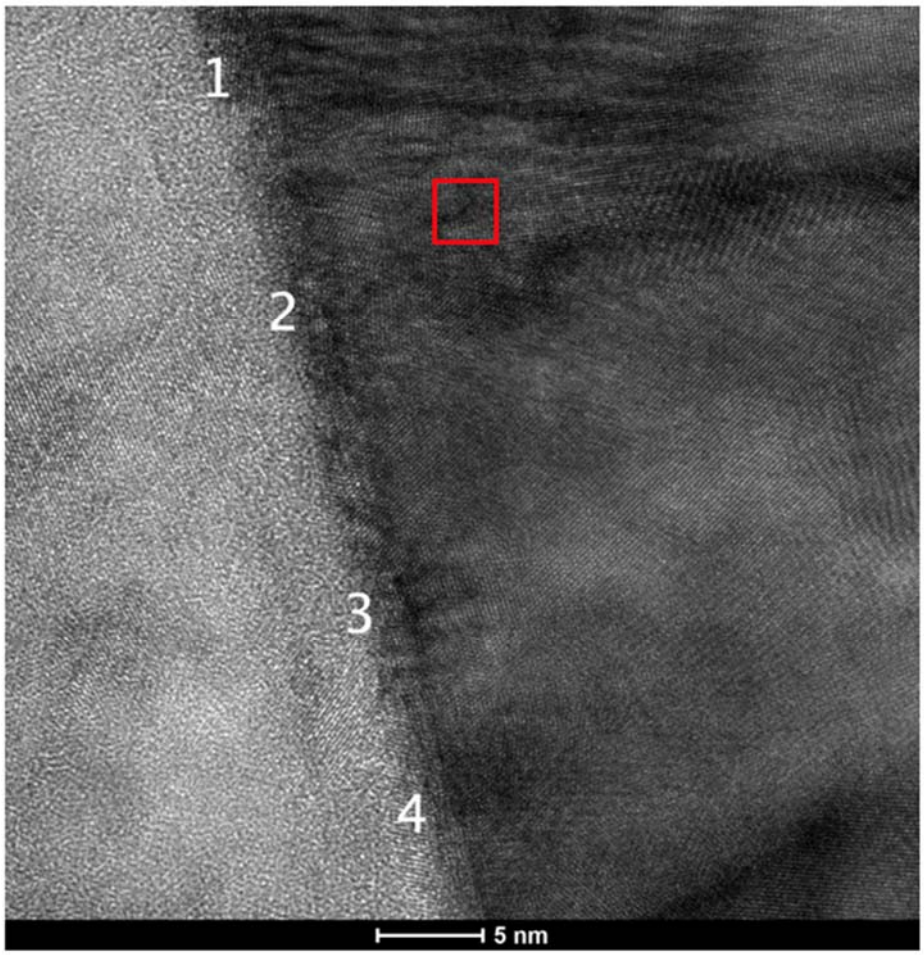

Figure 71: Example high resolution cross-section from circled region. The numbered points indicate where FFTs were taken.

134. For example, FFTs taken at point 1 are shown in Figure 72 below. The FFT on the left is from the lower NiFe layer and the FFT on the right is from the lower FeCo directly on the lower NiFe layer. Analysis of the FFTs was performed by measuring the diffraction spot spacings and the angles between rows of diffraction spots and comparing that information with the standard diffraction patterns[22] shown in Figure 72 below their respective FFTs.

[22] *Transmission Electron Microscopy,* D.B. Williams and C.B. Carter, Springer, (2009), pp. 299-301.

CONTAINS CONFIDENTIAL ATTORNEY EYES ONLY
INFORMATION SUBJECT TO PROTECTIVE ORDER

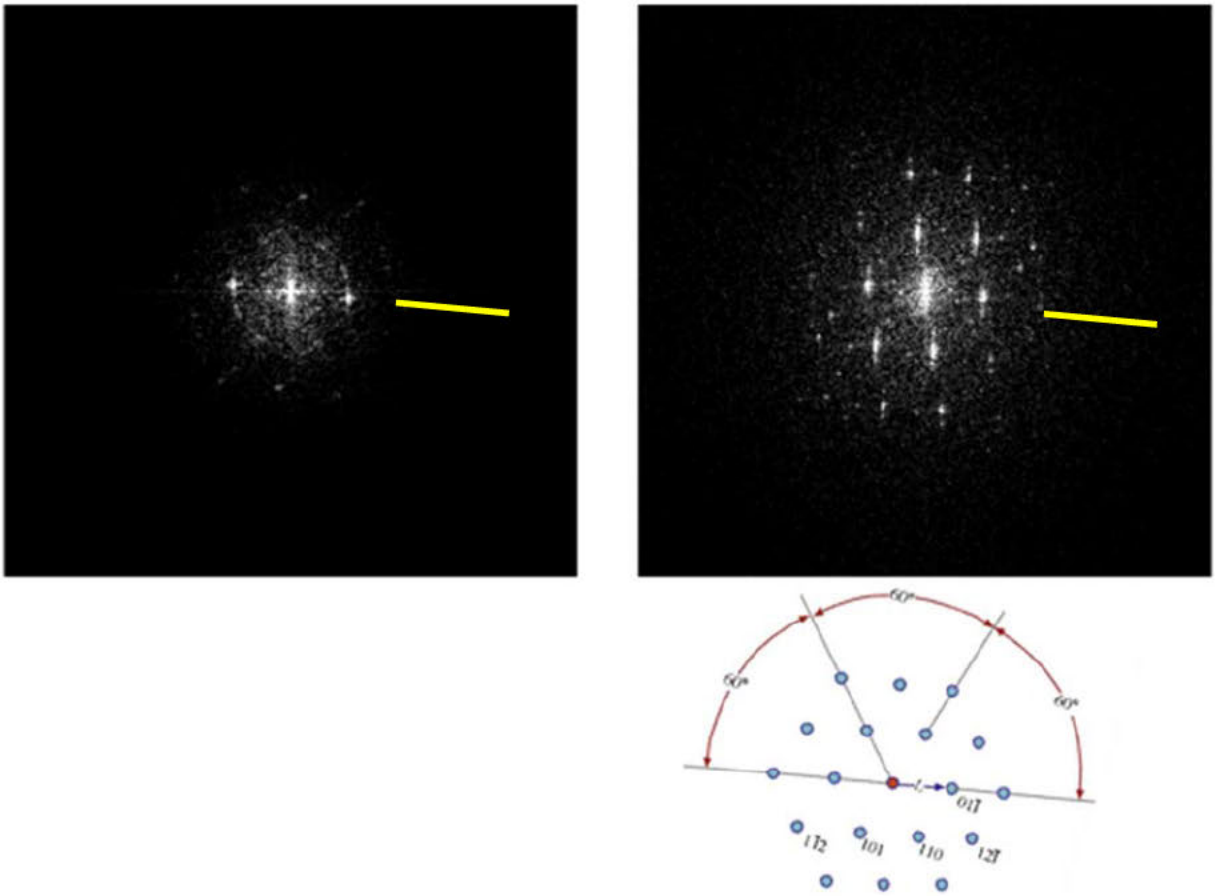

Figure 72: above: FFTs from the NiFe layer (left) and FeCo layer (right) – note that the NiFe pattern is indistinct; below: standard diffraction patterns rotated into similar orientations as respective FFTs shown immediately above.

135. For the right-hand FFT from the lower FeCo layer, looking down a {111} direction into the page, this analysis indicates that the diffraction pattern is $\{111\}_{BCC}$. The FFT is shown on the top right, and the standard $\{111\}_{BCC}$ diffraction pattern is shown below it, rotated into a similar orientation. Thus, this FFT indicates that the crystal structure of the lower FeCo layer is BCC. Further, from the high resolution cross-sections above, because we can see that the lattice fringes are continuous along the FeCo layer, this is indicative of the crystal structure of the extent of the FeCo layer.

136. Although the left hand FFT from the NiFe template is not distinct enough to analyze with certainty, the arrangement of the faint diffraction spots that are visible most closely resemble the $\{110\}_{FCC}$ pattern. Given the evidence for the {110} orientation in the NiFe layer in the mid-region of the sample discussed further below, I conclude that this pattern is $\{110\}_{FCC}$.

137. From the discussion above, the two FFT patterns show that there are two parallel directions, one in the lower NiFe layer and one in the lower FeCo layer, pointing out of the page. These are a $<110>_{FCC}$ direction lying parallel to a $<111>_{BCC}$ direction. Further, when analyzing the pattern from the spot spacing and distribution, it can be seen that a $<111>_{FCC}$ direction in the NiFe is also parallel to a $<110>_{BCC}$ in the FeCo, and lie in the plane of the page; both of these directions are indicated by the yellow lines marked on the FFT. The directions are also perpendicular to the lower NiFe/ lower FeCo interface, and so confirm the epitaxial growth in that direction and is evidence of the epitaxial growth of the lower FeCo layer on the lower NiFe layer, which functions as an atomic template. These two mutual orientation relationships are also sufficient to determine the relative orientation of the lower NiFe layer and the lower FeCo layer above it. Therefore, the lower NiFe layer exhibits (111) texture, and the lower FeCo layer exhibits (110) texture.

138. The parallel directions in the FCC and BCC layers normal to the interface show repeatedly <110> direction in the BCC layers and <111> direction in the FCC layers. Therefore, this analysis shows that the lower NiFe layer has a predominant (111) texture, and the lower FeCo layer has a predominant (110) texture.

139. Since the FFT analysis above shows that the lower NiFe/ lower FeCo relationship is $\{111\}_{FCC}||\{110\}_{BCC}$, as well as $<110>_{FCC}||<111>_{BCC}$, this shows that the Kurdjumov–Sachs orientation relationship is present.

CONTAINS CONFIDENTIAL ATTORNEY EYES ONLY
INFORMATION SUBJECT TO PROTECTIVE ORDER

140. Similar analysis was performed on FFTs taken at points other than 1 and each showed similar results as those described above, thereby confirming that the orientational relationships were consistent across the interface between the lower NiFe layer and the lower FeCo layer, and that the same textures were present throughout each layer. These FFTs are contained in Appendix C. Additionally, FFTs were taken on the remaining high-resolution cross sections; annotated cross sections and their accompanying FFTs are also shown in Appendix C and also showed similar results as those described above, further confirming the orientational relationships and textures as described above.

141. To the extent that the FFT results for the lower NiFe layer are inconclusive, I conclude that the lower NiFe layer is FCC and exhibits a predominant (111) texture based further on the discussion of the upper NiFe / FeCo layers herein.

142. Additionally, as with the high resolution cross-section of the lower NiFe/FeCo layers, FFTs were taken in the upper NiFe/FeCo layers at point 1 in the example high resolution cross-section shown in Figure 73 below. The boundaries between different columnar grains of the FeCo as they grow from right to left can be seen, and highlight the elongated nature of the FeCo grains, giving rise to the bamboo structure seen in the low magnification images in Section F.1.b.2 above.

CONTAINS CONFIDENTIAL ATTORNEY EYES ONLY
INFORMATION SUBJECT TO PROTECTIVE ORDER

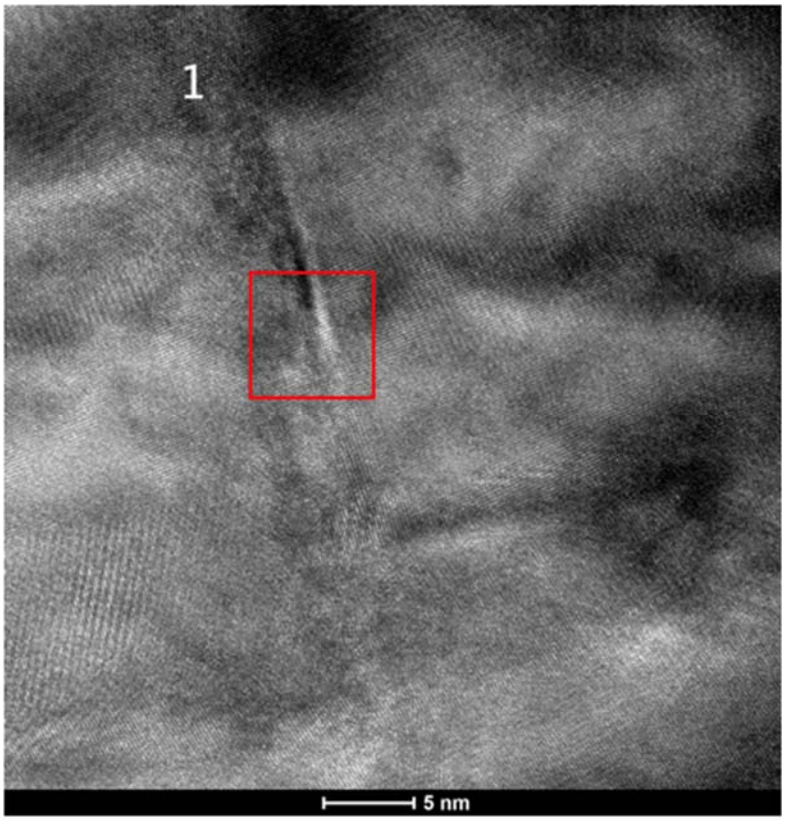

Figure 73: Example high resolution cross-section from the upper NiFe / upper FeCo region. The numbered point indicates where FFTs were taken.

143. Similar to the analysis for the example high resolution cross-section above, at point 1, FFTs were taken: (a) in the upper FeCo layer immediately to the left of the upper NiFe layer; (b) in the upper NiFe layer at the location of the numbered point; and (c) in the lower FeCo layer immediate to the right of the upper NiFe layer. Again, the area sampled for each FFT was confined to an area of the size indicated by the red square. The set of FFTs taken around point 1 are shown in Figure 74 below.

CONTAINS CONFIDENTIAL ATTORNEY EYES ONLY
INFORMATION SUBJECT TO PROTECTIVE ORDER

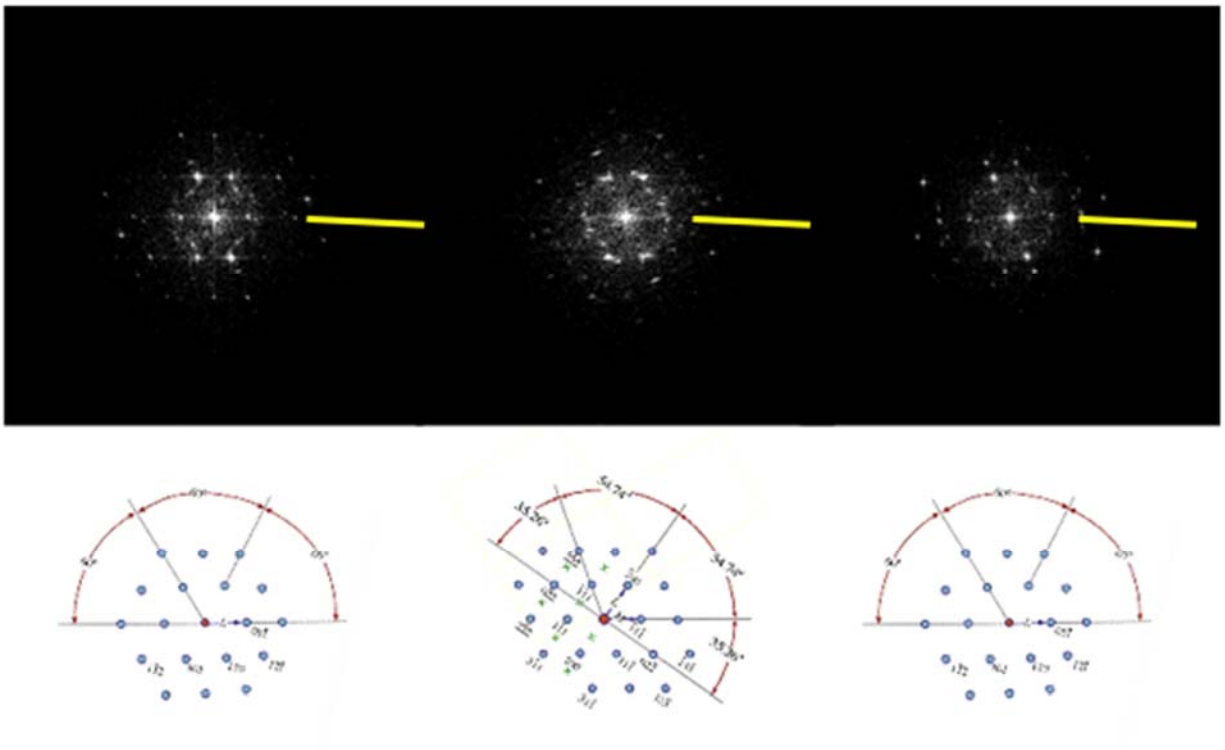

Figure 74: above: FFTs from point 1 from the FeCo layers (left and right) on either side of the upper NiFe layer (center). The FeCo patterns are $\{111\}_{BCC}$, as determined from the ratio of the lengths of the sides of the pattern motif, and the angles between directions, while the NiFe pattern is $\{111\}_{FCC}$.

144. Again, following the procedures outlined above, the two patterns in the upper and lower FeCo layers are identified as $\{111\}_{BCC}$, while the upper NiFe pattern is identified as $\{110\}_{FCC}$. These FFTs indicate that the crystal structure of the upper NiFe layer is FCC and the upper and lower FeCo layers is BCC. Likewise, from the high resolution cross-sections above, because we can see that the lattice fringes are continuous, this is indicative of the crystal structure of the extent of the upper NiFe and both FeCo layers.

145. Common directions in all three layers show the persistence of the epitaxial relationship between $<111>_{BCC}$ and $<110>_{FCC}$, as was found at the lower NiFe/FeCo interface. Again, this is indicative of the upper NiFe layer exhibiting (111) texture, and the FeCo layers

CONTAINS CONFIDENTIAL ATTORNEY EYES ONLY
INFORMATION SUBJECT TO PROTECTIVE ORDER

exhibiting (110) texture. This also indicates the Kurdjumov-Sachs orientation relationship between the upper NiFe and upper FeCo layers.

146. Again, the parallel directions in the FCC and BCC layers normal to the interface show repeatedly <110> direction in the BCC layers and <111> direction in the FCC layers. Therefore, this analysis shows that the upper NiFe layer has a predominant (111) texture, and the upper FeCo layer has a predominant (110) texture.

147. Further, the FFT patterns show that there are two parallel directions, one in the upper NiFe layer and one each of the adjacent FeCo layers, pointing out of the page. These are a $\langle 110 \rangle_{FCC}$ direction lying parallel to a $\langle 111 \rangle_{BCC}$ direction. When analyzing the pattern from the spot spacing and distribution, it can be seen that a $\langle 111 \rangle_{FCC}$ direction in the NiFe is also parallel to a $\langle 110 \rangle_{BCC}$ in the FeCo, and lie in the plane of the page; both of these directions are indicated by the yellow lines marked on the FFT. The directions are also perpendicular to the upper NiFe/FeCo interfaces, and so confirm the epitaxial growth in that direction and is evidence of the epitaxial growth of the lower FeCo layer on the lower NiFe layer, which functions as an atomic template. These two mutual orientation relationships are also sufficient to determine the relative orientation of the lower NiFe layer and the lower FeCo layer above it. Therefore, the lower NiFe layer exhibits (111) texture, and the lower FeCo layer exhibits (110) texture.

148. The parallel directions in the FCC and BCC layers normal to the interface show repeatedly <110> direction in the BCC layers and <111> direction in the FCC layers. Therefore, this analysis shows that the lower NiFe layer has a predominant (111) texture, and the lower FeCo layer has a predominant (110) texture.

149. Since the FFT analysis above shows that the upper NiFe / FeCo relationship is $\{111\}_{FCC} \| \{110\}_{BCC}$, as well as $\langle 110 \rangle_{FCC} \| \langle 111 \rangle_{BCC}$, this shows that the Kurdjumov–Sachs

CONTAINS CONFIDENTIAL ATTORNEY EYES ONLY
INFORMATION SUBJECT TO PROTECTIVE ORDER

orientation relationship is present with respect to both the lower NiFe / FeCo layers, and the upper NiFe / FeCo layers. Further, as discussed in Section F.1.b.4 below, the microbeam diffraction analysis confirms the presence of Kurdjumov–Sachs orientational variants in the lower FeCo layer. I would not expect such variants but for the lower FeCo layer to be grown upon a predominately (111) FCC NiFe template later.

150. I also note that the FFTs taken from various points along the NiFe layers, while they maintain a common direction with the FeCo layers normal to the interface, change significantly with position along the interface. These changes in the FFT indicate differences in orientation along the template, and thus the grain size in the template. The grain size in the NiFe template layers is comparable to the width of the FeCo grains, so that the grain sizes in the two are similar. Thus, there is ordinarily only one or two FeCo grains per NiFe template grain.

(4) TEM—microbeam diffraction on plan view samples

151. Microbeam diffraction, as described in Section E.2.d above, was performed on a region of the lower FeCo layer of the write pole as shown by the red square in Figure 75 below. A plan view sample was prepared such that the upper FeCo/NiFe layer pair was removed, leaving the lower FeCo layer of the write pole exposed for microbeam diffraction. From the area indicated by the red square, 1,600 diffraction patterns were obtained by scanning the electron beam incrementally across the area in the box. A typical diffraction pattern is shown on the right. Note that all diffraction patterns below were annotated using Keynote, software available from Apple.

CONTAINS CONFIDENTIAL ATTORNEY EYES ONLY
INFORMATION SUBJECT TO PROTECTIVE ORDER

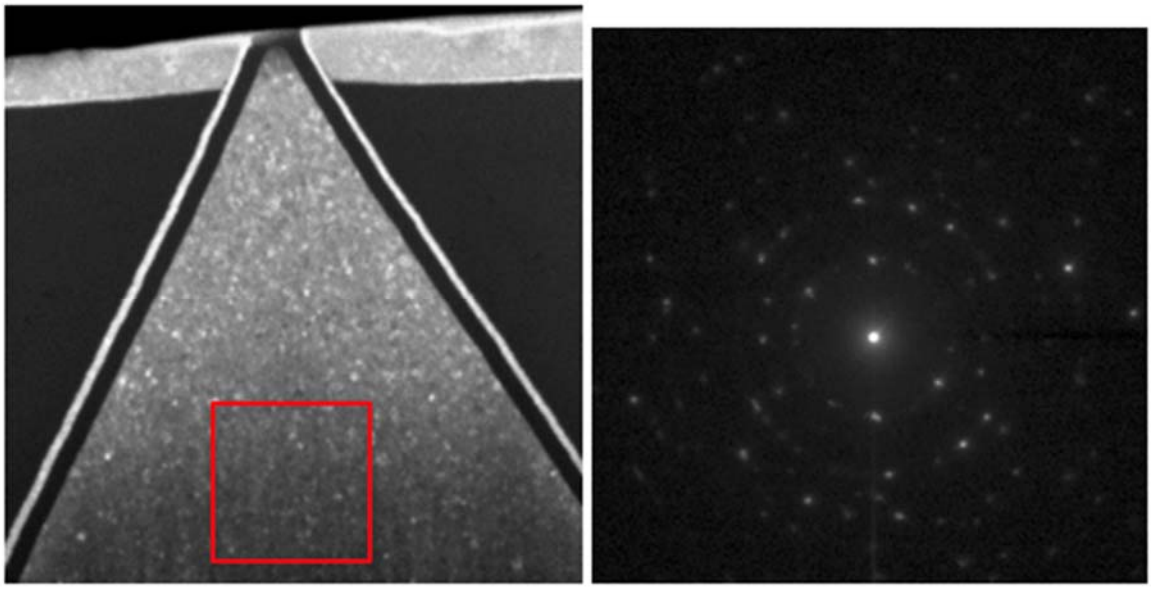

Figure 75: Plan view STEM image of S2MMMC near the pole tip of the write head (left). 1,600 diffraction patterns were taken from the area outlined in red. A typical diffraction pattern is shown on the right.

152. By defocusing the diffraction pattern image slightly, as shown on the right of Figure 76 below, we obtain an enlarged central spot that contains an image of a portion of the sample. This shows that the image of the plan view sample on the left and the diffraction pattern on the right are in near perfect alignment, to ±10˚. Thus, directions associated with the sample can be related to directions in the diffraction pattern, and those directions may be indexed.

CONTAINS CONFIDENTIAL ATTORNEY EYES ONLY
INFORMATION SUBJECT TO PROTECTIVE ORDER

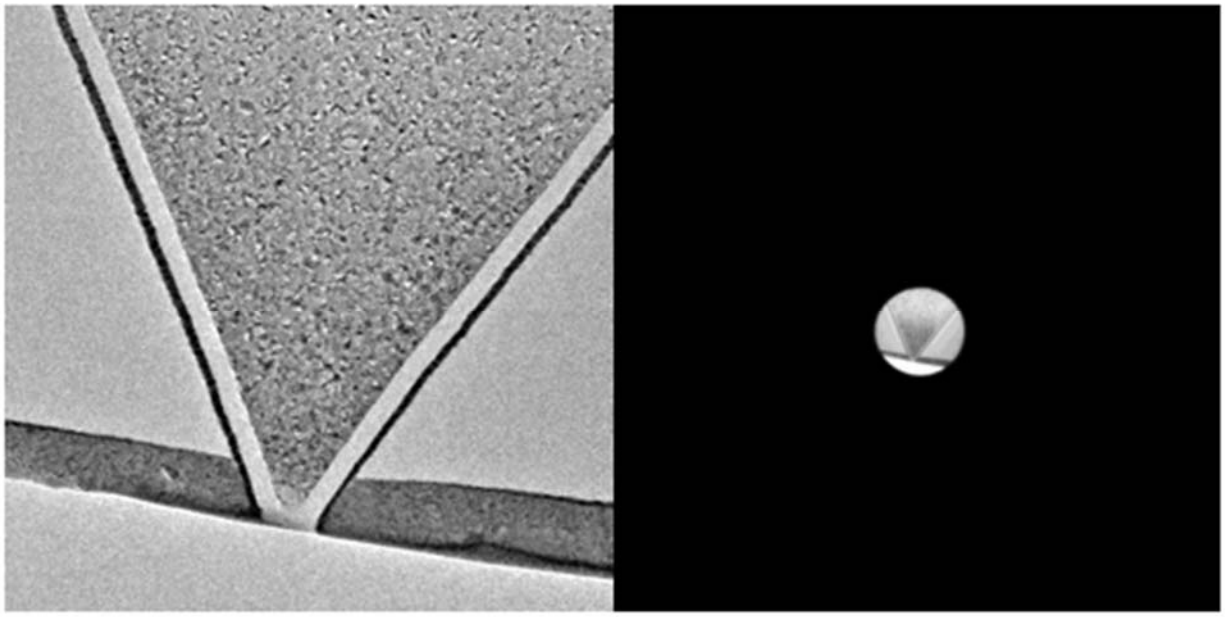

Figure 76: Plan view STEM image of S2MMMC (left), with a de-magnified image of the central spot of its diffraction pattern (as shown in Figure 75 above) in which the image of the head can be seen. This fixes the relative orientation of the image (left) and any diffraction patterns.

153. Individual frames from this set of 1,600 may contain diffraction patterns from one, two, or sometimes more separate FeCo crystallites. Typical single crystal patterns obtained for this analysis are shown in Figure 77 below. These patterns are readily identified and indexed as patterns in the $(110)_{BCC}$ orientation. This is confirmed by measurement of the ratio of the sides of the rectangles, found to be $5.4:3.8 = 1:\sqrt{2}$, as required. Further, this is the epitaxial growth direction for the lower FeCo layer on the lower NiFe layer (the atomic template) as expected. These patterns are further confirmation that the FeCo layer is BCC with (110) texture.

CONTAINS CONFIDENTIAL ATTORNEY EYES ONLY
INFORMATION SUBJECT TO PROTECTIVE ORDER

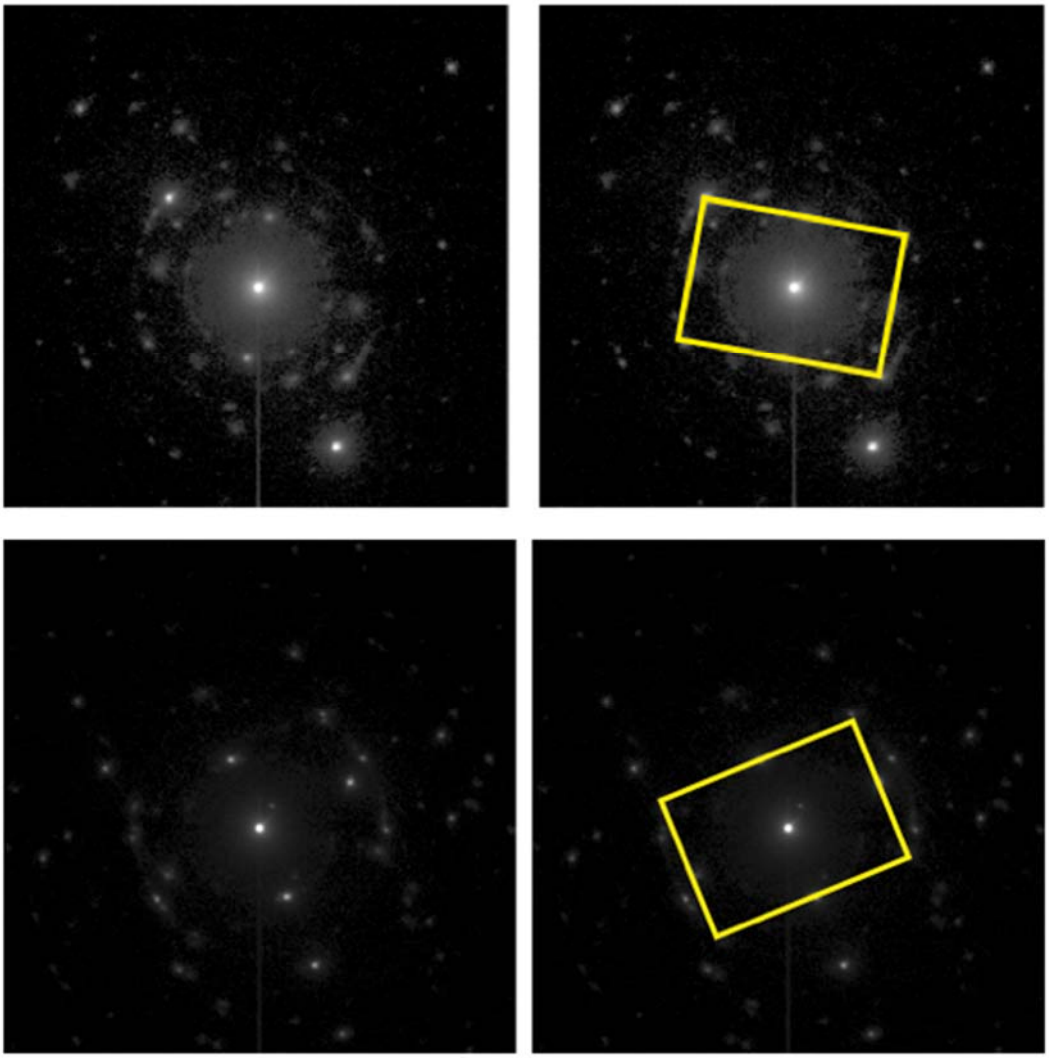

Figure 77: Single crystallite diffraction patterns, frames 419 (upper) and 836 (lower), in the (110) orientation. These patterns visually identify as standard $(110)_{BCC}$ patterns.

154. Figure 78 below shows an example diffraction pattern with two crystallites, both in the $(110)_{BCC}$ orientation, but rotated by ~12˚ about their common $[110]_{BCC}$ direction. This is the separation of two variants in the Kurdjumov-Sachs orientation. The measured ratio of the sides of the motif are 1:√2 as required. Angles were measured directly in Keynote.

CONTAINS CONFIDENTIAL ATTORNEY EYES ONLY
INFORMATION SUBJECT TO PROTECTIVE ORDER

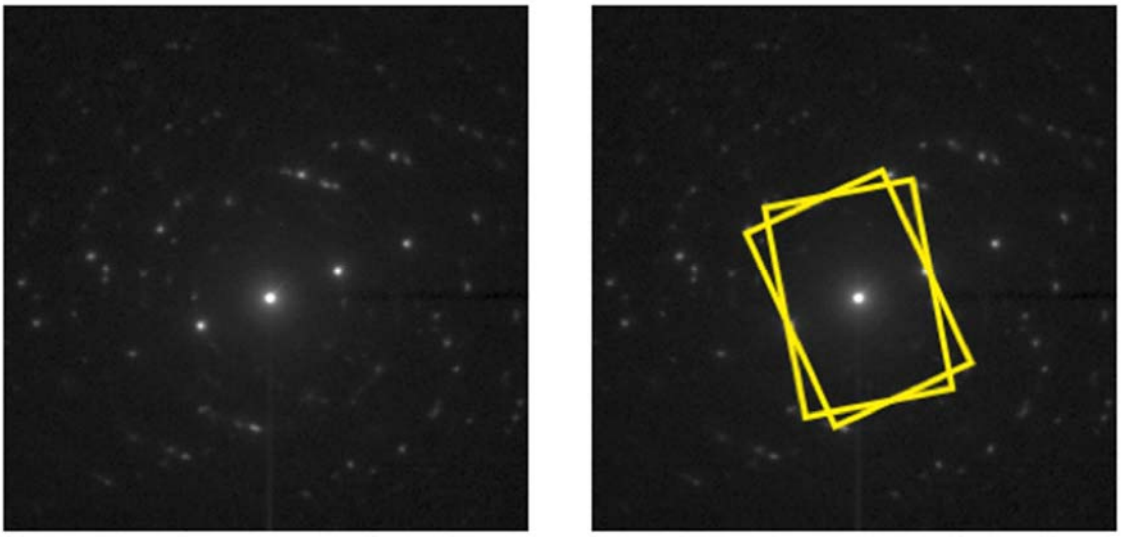

Figure 78: Two crystallites, both in the $(110)_{BCC}$ orientation, frame 137, rotated by ~12˚ about their common $[110]_{BCC}$ direction.

155. Figure 79 below shows two diffraction patterns each showing two crystallites both in the $(110)_{BCC}$ orientation, rotated about their common $[110]_{BCC}$ direction by ~70.53˚. This is also the separation of two variants in the Kurdjmov-Sachs orientation. This also means that the crystallites are in the "twin" orientation, which is alternatively described as a 180˚ rotation about their common <211> direction (circled in red below), or a mirror reflection in the <211> plane (dashed line).

CONTAINS CONFIDENTIAL ATTORNEY EYES ONLY
INFORMATION SUBJECT TO PROTECTIVE ORDER

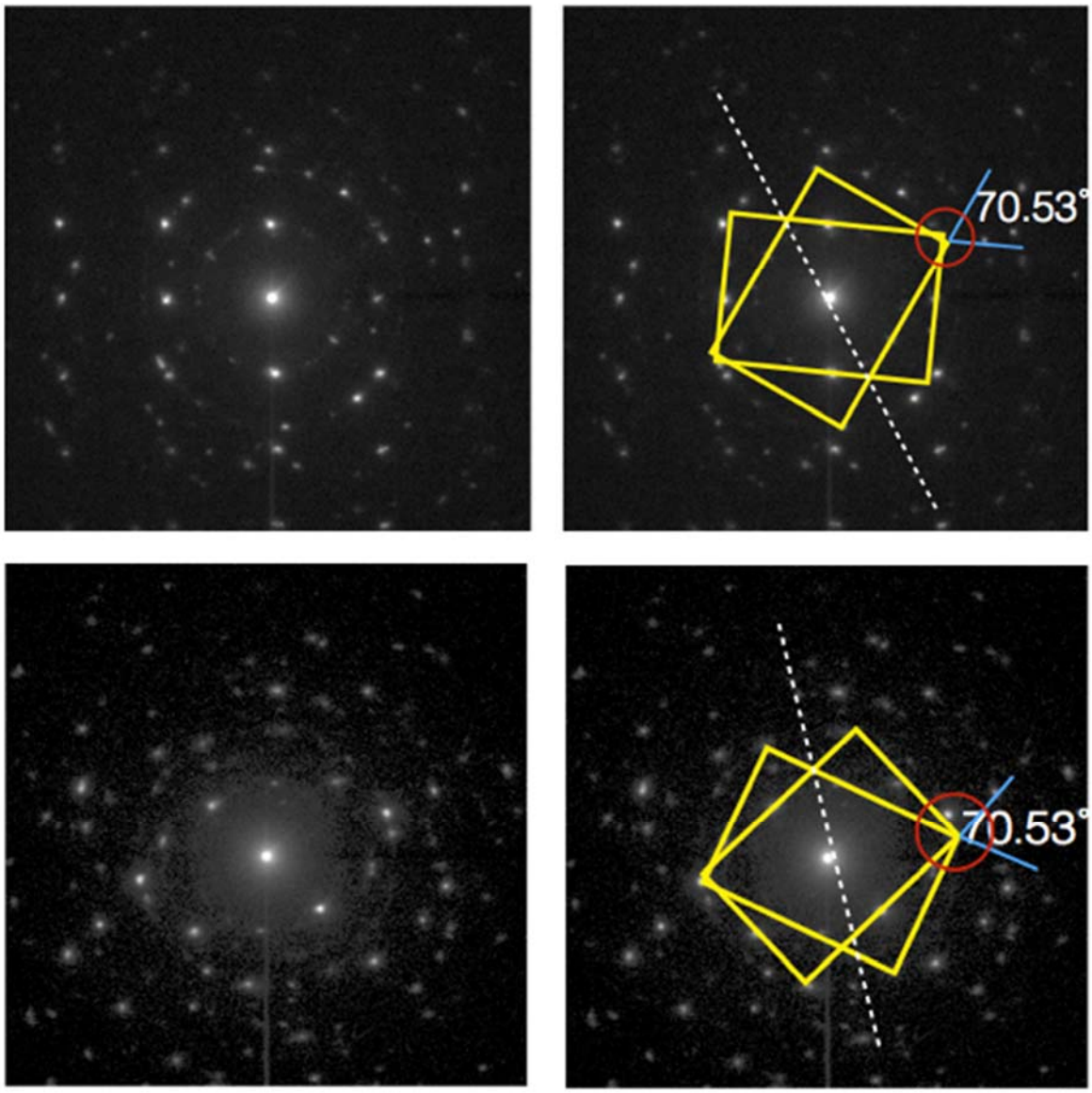

Figure 79: Both patterns, frames 120 (upper) and 669 (lower), show two crystallites both in the $(110)_{BCC}$ twin orientation, rotated by ~70.53˚ about their common $[110]_{BCC}$ direction

156. Figure 80 below shows a complex diffraction pattern, which arises when more than two crystallites contribute to the pattern. In the example of Figure 80below, there are two variants of $(110)_{BCC}$ rotated with respect to each other.

CONTAINS CONFIDENTIAL ATTORNEY EYES ONLY
INFORMATION SUBJECT TO PROTECTIVE ORDER

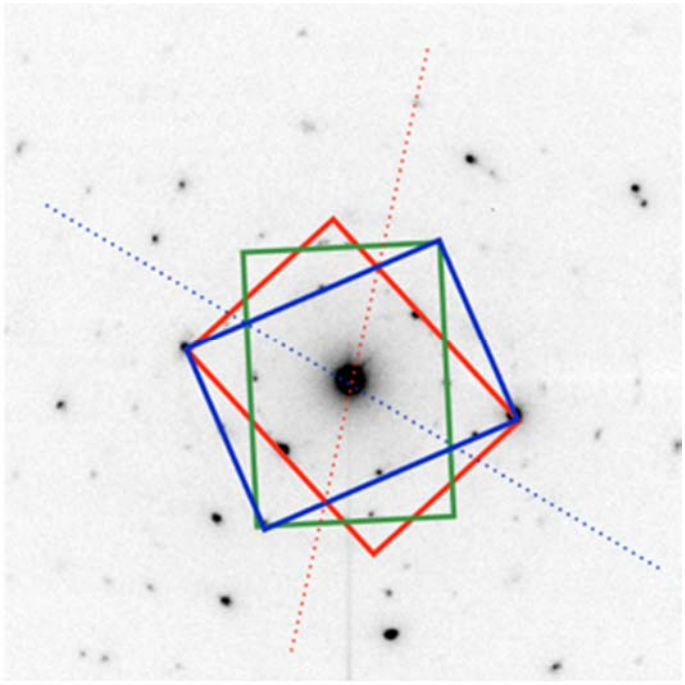

Figure 80: Diffraction pattern, frame 17, showing three crystallites in the $(110)_{BCC}$ orientation.

157. In addition to the analysis of individual patterns, 100 out of the 1600 diffraction patterns were selected using a random number generator. These 100 were categorized as either a) showing no recognizable pattern, b) showing a single {110} patterns, c) showing multiple {110} patterns, d) showing {110} twins, or e) showing a pattern other than {110}. The results show the following numbers in each category – a) 86, b) 9, c) 0, d) 5, e) 0.[23]

158. Thus, microbeam diffraction imaging results confirm that the lower FeCo layer is BCC and contains variants with the expected orientation relationship for the Kurdjumov-Sachs six variant system. Typical FeCo diffraction patterns exhibit the $(110)_{BCC}$ orientation, consistent with the epitaxial growth relationship of $(110)_{FeCo}$ on $(111)_{NiFe}$.

(5) Dark field image analysis

[23] These numbers are influenced by the initial orientation of the sample in the microscope, such that if the sample is precisely aligned so that the predominant $<110>_{BCC}$ direction is not anti-parallel to the electron beam, fewer $\{110\}_{BCC}$ patterns will be observed. This does not indicate, however, that there are in fact fewer $\{110\}_{BCC}$ crystals in the sample, and as discussed herein, I conclude that the FeCo layer is predominately $(110)_{BCC}$.

CONTAINS CONFIDENTIAL ATTORNEY EYES ONLY
INFORMATION SUBJECT TO PROTECTIVE ORDER

159. The principles behind dark field imaging and analysis are discussed in Section E.2.f above. Figure 81 below shows the area from the write head of S2MMMC where the diffraction data was taken on the left (this plan view sample is the same as that analyzed regarding microbeam diffraction above, exposing the FeCo layer), and a defocused diffraction ring pattern on the right which reveals an image of the sample in the central spot, similar to that discussed in Section F.1.b.4 above. This provides the orientation of the write head with respect to the diffraction pattern, as seen in Figure 81 below. From this image, it is clear that the diffraction pattern and the tip of the sample are almost exactly parallel, with less than 10˚ rotation from one to the other.

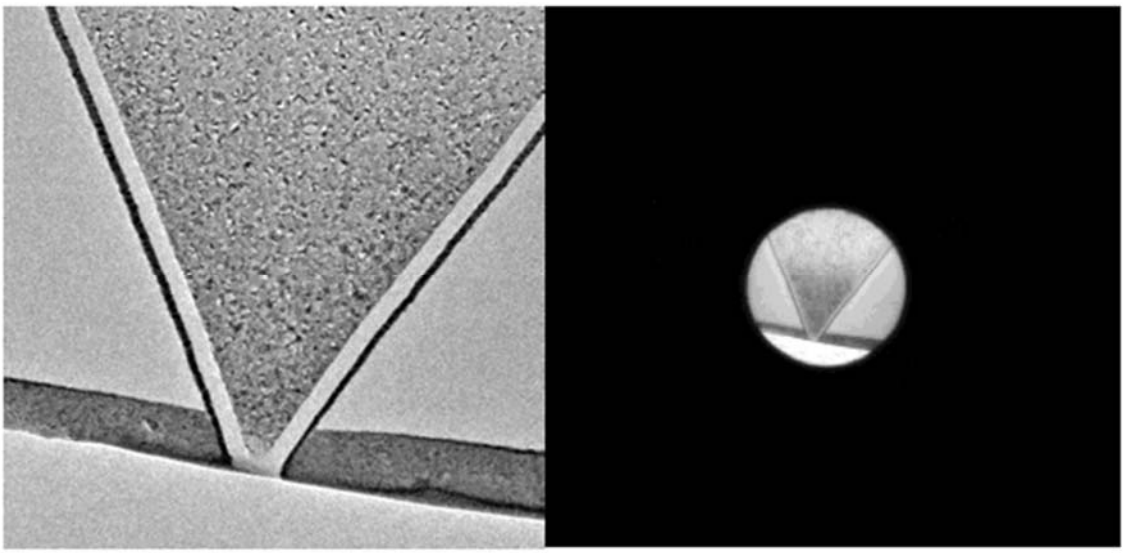

Figure 81: Defocused diffraction pattern (right) reveals alignment with sample (left) to be almost exactly parallel.

160. First, a small objective aperture is inserted to enclose a segment of the {200} diffraction ring, as shown on the right in Figure 82 below. Next, a dark field image of an area of the lower FeCo layer is obtained, as shown on the left in Figure 82 below. Where crystallites show up bright in the dark field image, it indicates that their {200} planes are oriented so as to diffract into the direction enclosed by the objective aperture. The yellow arrow in the annotated

CONTAINS CONFIDENTIAL ATTORNEY EYES ONLY
INFORMATION SUBJECT TO PROTECTIVE ORDER

image points in the direction of the objective aperture from the center of the diffraction pattern. This means that the bright crystallites have their <200> directions aligned parallel to the arrow, i.e., perpendicular to the long axis of the write head. Also note that the sample is oriented such that the $<110>_{BCC}$ directions are antiparallel to the electron beam.

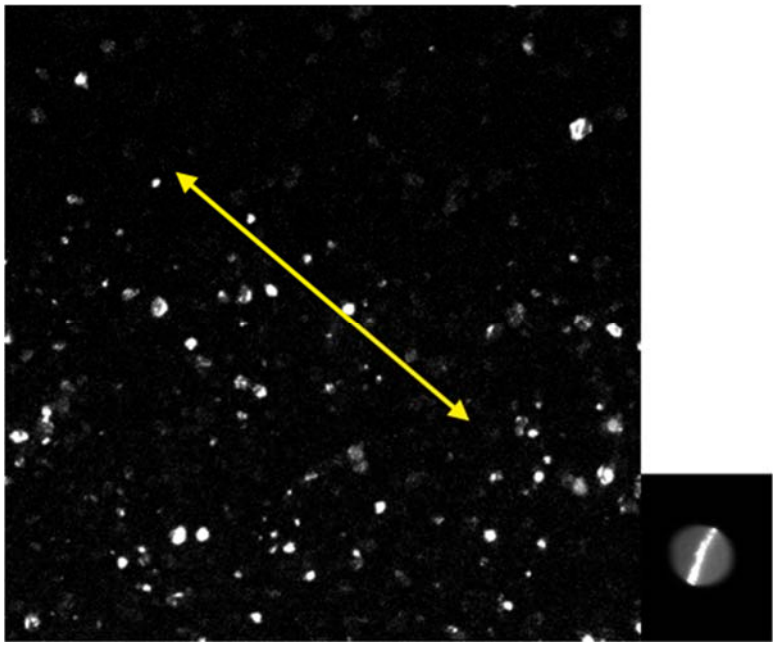

Figure 82: Dark field image showing crystallites with <200> directions aligned parallel to the yellow arrow (left). Enclosed segment of {200} diffraction ring (right).

161. In contrast to Figure 82 above, an image taken with the objective aperture at roughly 90˚ to the position above, as shown on the right in Figure 83 below, produces an image in which significantly fewer of the crystallites are illuminated as shown on the left in Figure 83, indicating that a smaller fraction of crystallites have their <200> directions aligned parallel to the long axis of the head.

CONTAINS CONFIDENTIAL ATTORNEY EYES ONLY
INFORMATION SUBJECT TO PROTECTIVE ORDER

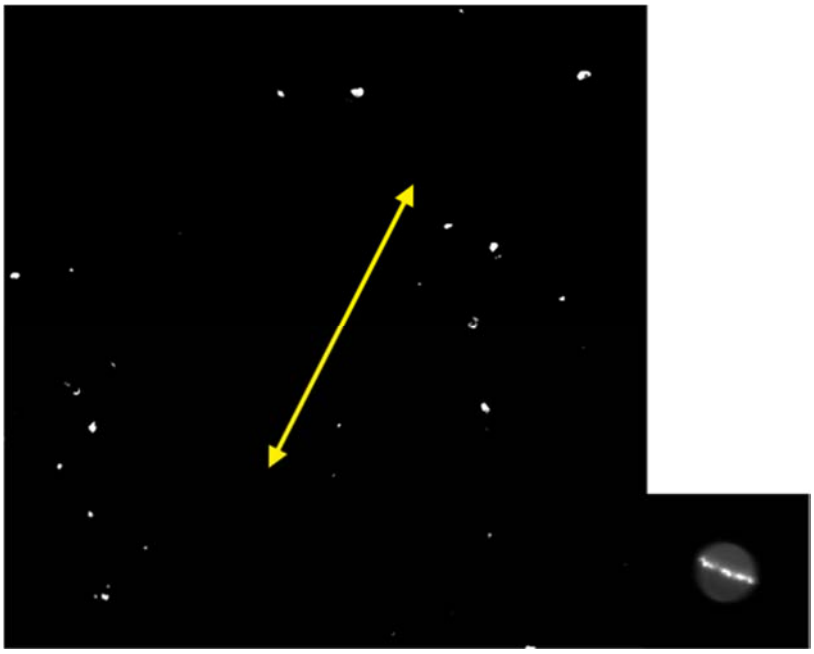

Figure 83: Dark field image showing crystallites with <200> directions aligned parallel to the yellow arrow (left). Enclosed segment of {200} diffraction ring (right).

162. This procedure is repeated at 10˚ intervals around the diffraction ring in at least a 180˚ rotation, producing dark field images similar to shows in Figures 82-83 above. To analyze these images, first, a large area of the dark field image is separated. The size and location of this area for sample S0GPPC is shown in the red box of Figure 84 below.

CONTAINS CONFIDENTIAL ATTORNEY EYES ONLY
INFORMATION SUBJECT TO PROTECTIVE ORDER

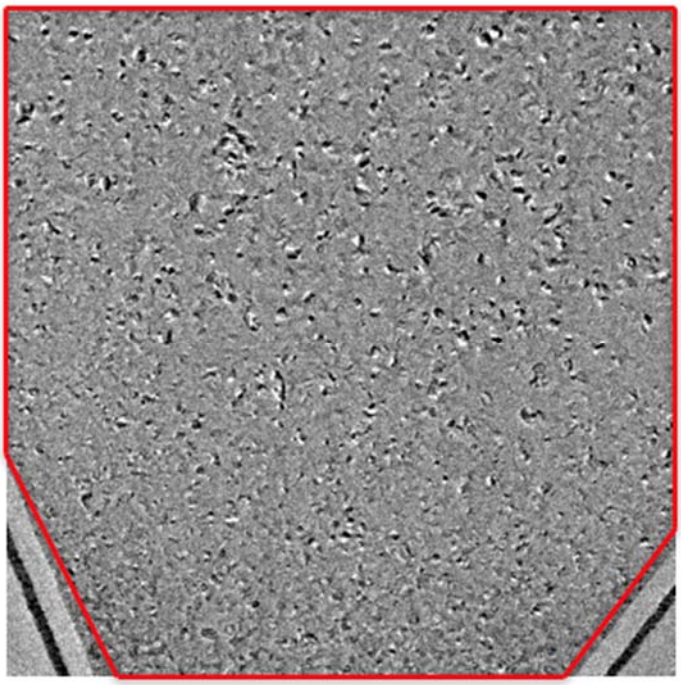

Figure 84: Dark field image with area under analysis shown enclosed by the red box (left) and extracted image (right).

163. Next, to analyze these images, a standard stereological computer program is used. I used ImageJ in my analysis. For each image, a threshold is applied to the isolated area as described by Figure 84 in order to produce a binary black and white image shown in Figure 85 below.

CONTAINS CONFIDENTIAL ATTORNEY EYES ONLY
INFORMATION SUBJECT TO PROTECTIVE ORDER

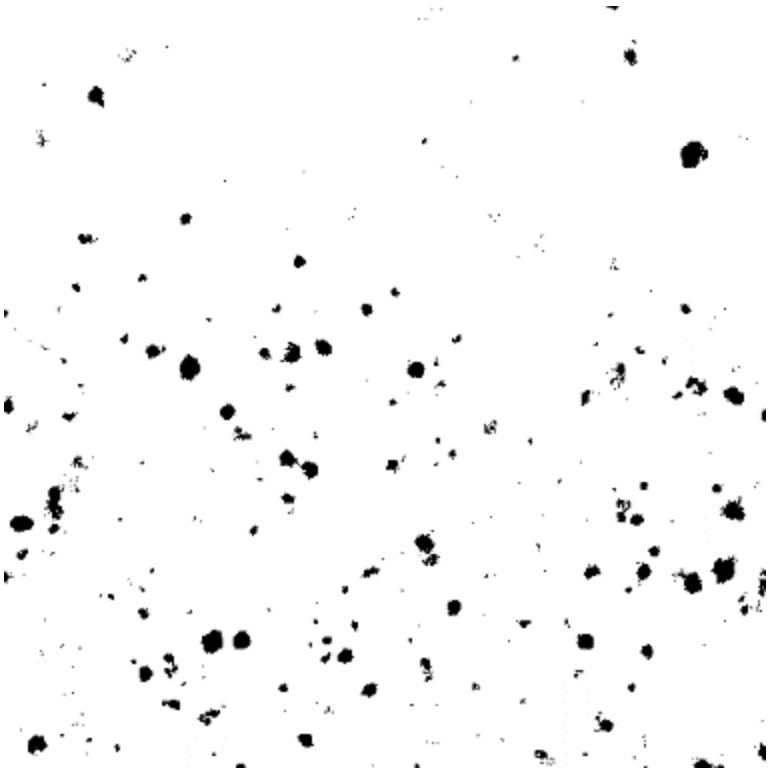

Figure 85: Binary black and white thresholded image of the area described by the red box of Figure 84 above. Note the contrast is reversed from that in the actual image.

164. This image is operated on by ImageJ to measure the area fraction of crystallites that are white – that is, the area fraction of crystallites that scatter into the objective aperture at that particular position – and that area fraction for that particular position is tabulated. The image created by ImageJ enumerating the white crystallites is shown in Figure 86 below. The area fraction for each enumerated crystallite is shown in Appendix C.

CONTAINS CONFIDENTIAL ATTORNEY EYES ONLY INFORMATION SUBJECT TO PROTECTIVE ORDER

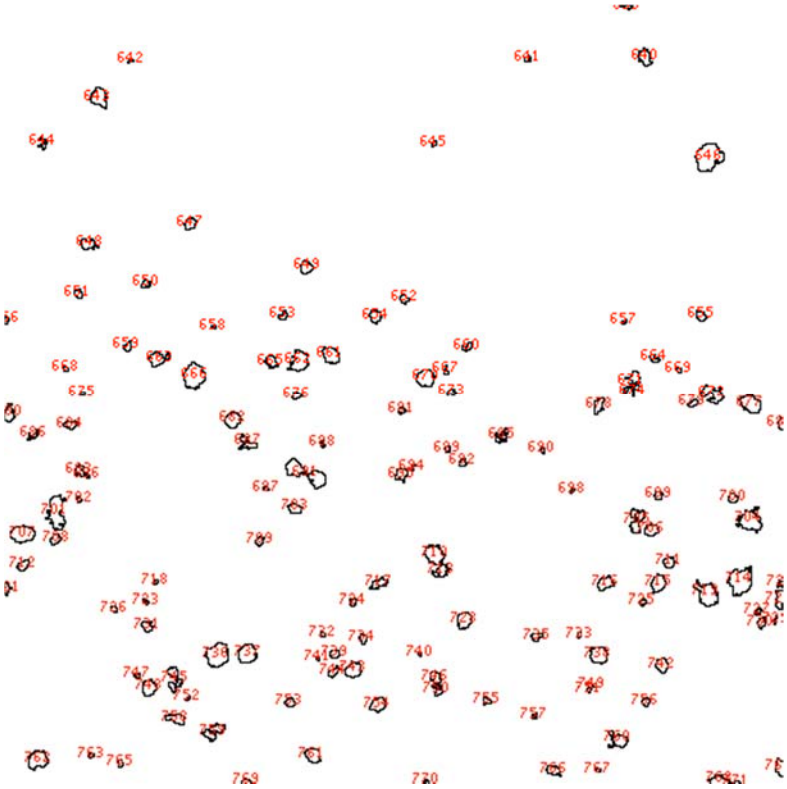

Figure 86: Image enumerating the white crystallites from Figure 85 above. Note that ImageJ enumerates each crystallite individually, and then calculates the relative area occupied by each crystallite.

165. Finally, the area fractions are added for each 10˚ increment to arrive at the total area of white crystallites for that particular increment, and the results for all positions are then tabulated. The results for S2MMMC are shown in Table 2 and graphed in Figure 87 below. The full results of this dark field analysis are attached in Appendix C.

Angle	%Area
0	1.391
10	1.449
20	1.297
30	1.321
40	0.9624
50	1.703
60	1.586
70	1.492
80	1.911
90	2.364

CONTAINS CONFIDENTIAL ATTORNEY EYES ONLY
INFORMATION SUBJECT TO PROTECTIVE ORDER

100	3.022
110	2.225
120	1.642
130	2.139
140	1.217
150	1.175
160	1.699
170	1.17
180	1.194

Table 2: Number and area fractions of white crystallites at each angle in 180 degrees of rotation.

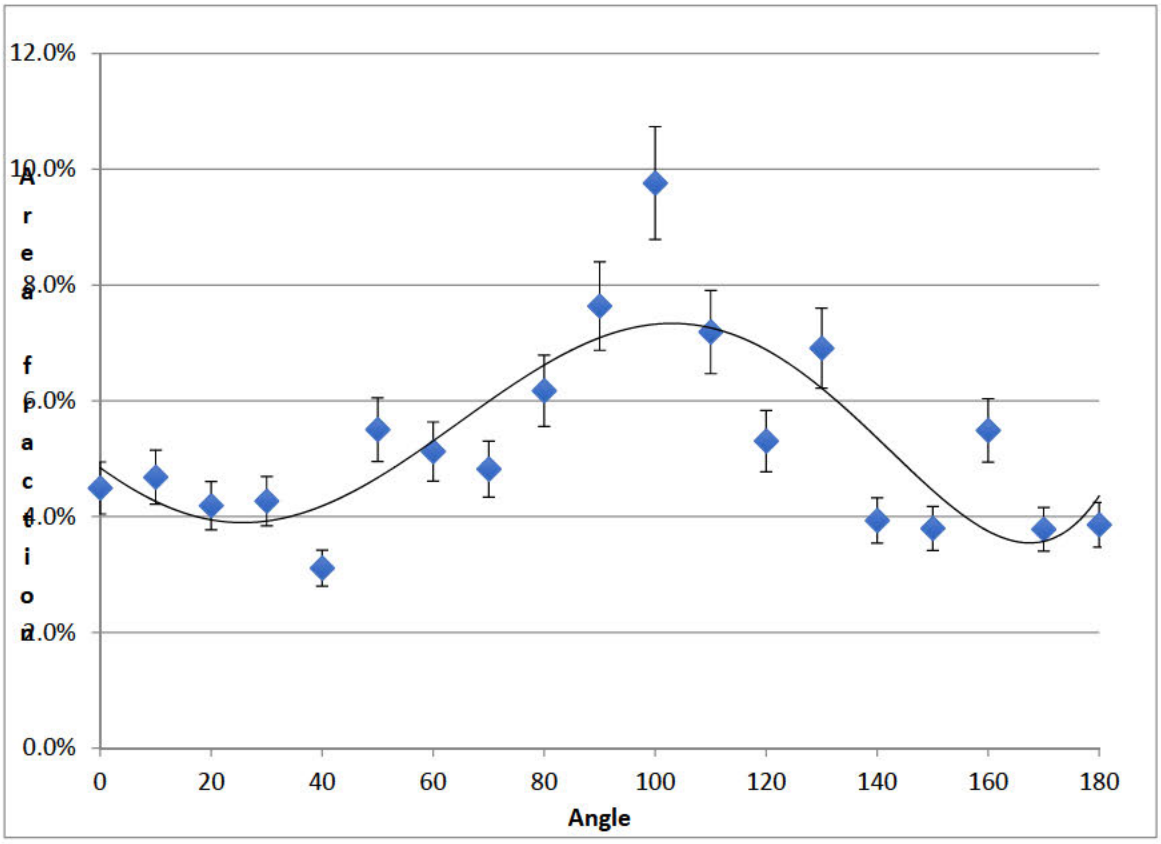

Figure 87: Area fraction of white crystallites vs. angle, where 90 degrees is perpendicular to the long axis of the write head. Error bars also shown.

166. These results indicate that there is a maximum area at 90 degrees, indicating that more crystallites are oriented with their <200> (easy) directions perpendicular to the long axis of the write head.

CONTAINS CONFIDENTIAL ATTORNEY EYES ONLY
INFORMATION SUBJECT TO PROTECTIVE ORDER

167. Further, as I explained in Section F.1.b.3, the sizes of the grains in the NiFe template layers and FeCo layers are similar, such that there is only one or two FeCo grains per NiFe template grain for the great majority of NiFe template grains. Further, this dark field analysis, in conjunction with the microbeam diffraction analysis discussed above, shows that the various FeCo grains on top of the various NiFe template layer grains have members of the six-variant system preferentially aligned such that there is an unequal amount of the six variants in the FeCo layer. Given the relative grain sizes in the FeCo layer and NiFe template layer, there are no NiFe template grains that have six different overlying grains in the FeCo layer, let alone that each of the six different overlying grains would have equal area and each represent a different variant from the six-variant system present in the FeCo layer.

2. **Analysis of [redacted] Products**

a) **SBRD8K**

(1) EDS analysis

168. The principles behind EDS are discussed generally in Section E.3 above. EDS color maps are shown in Figures 88-93 below and indicate the concentration of elements in the area indicated by the color assigned to that element. Overviews are first shown in Figures 88-90, and individual elemental mappings are shown in Figures 91-93. These mappings indicate the composition of individual layers in the write pole.

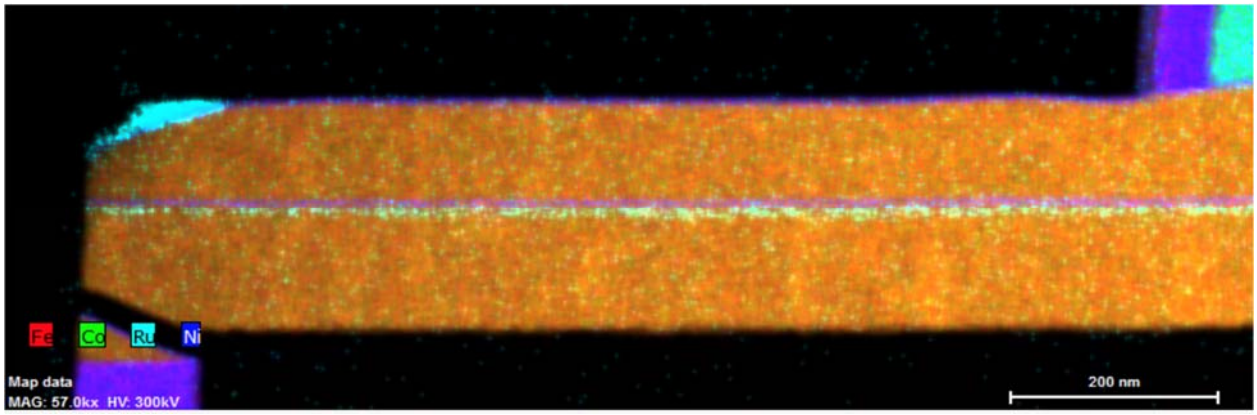

CONTAINS CONFIDENTIAL ATTORNEY EYES ONLY
INFORMATION SUBJECT TO PROTECTIVE ORDER

Figure 88: Overall EDS map. Note that the growth direction in the EDS maps for SBRD8K is from bottom to top.

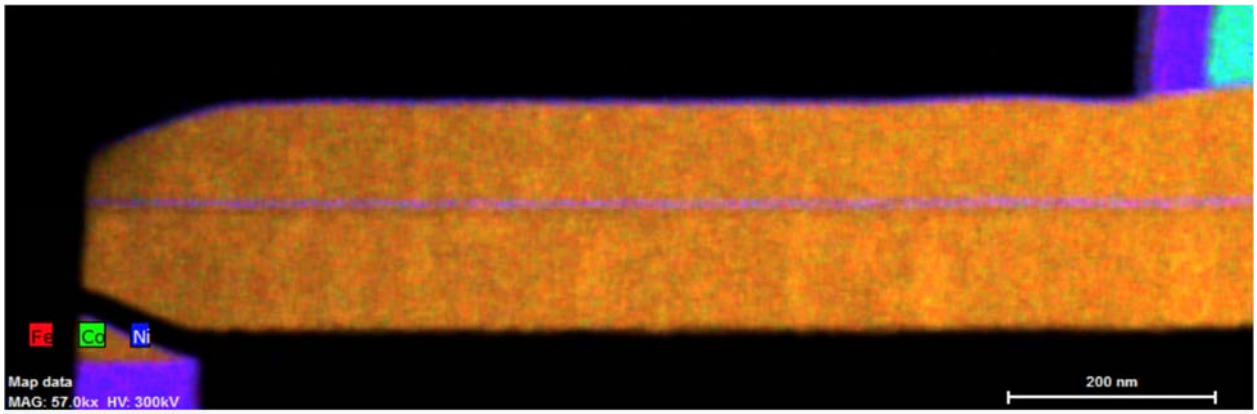

Figure 89: EDS map of Fe, Co, and Ni.

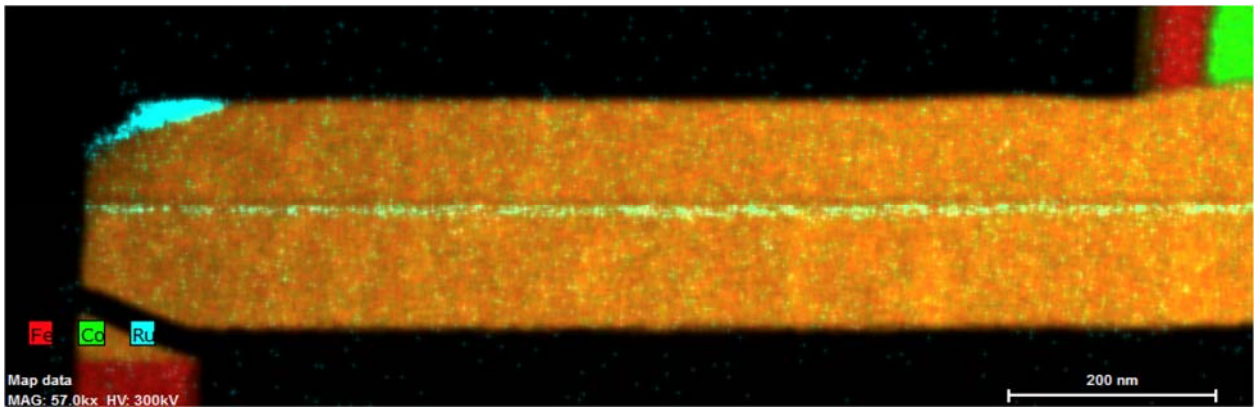

Figure 90: EDS map of Fe, Co, and Ru.

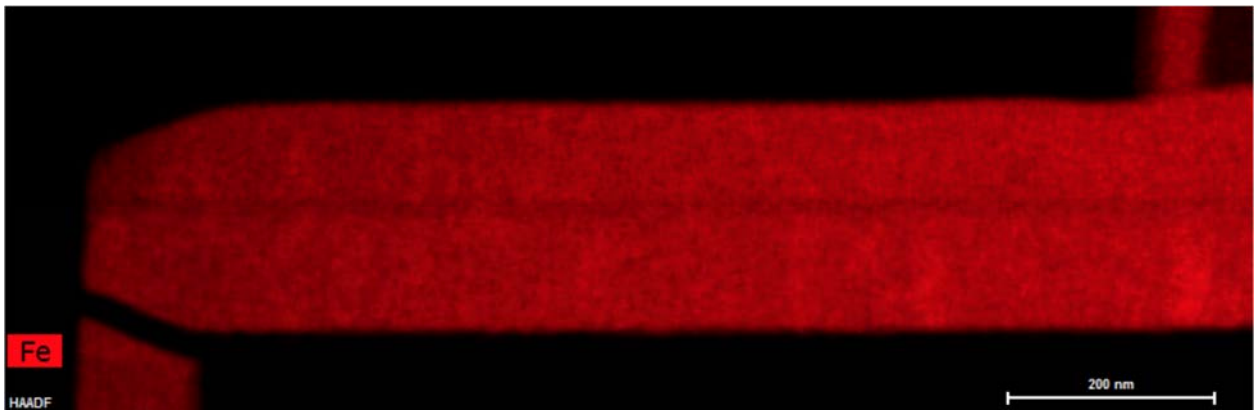

Figure 91: EDS map showing just Fe.

CONTAINS CONFIDENTIAL ATTORNEY EYES ONLY
INFORMATION SUBJECT TO PROTECTIVE ORDER

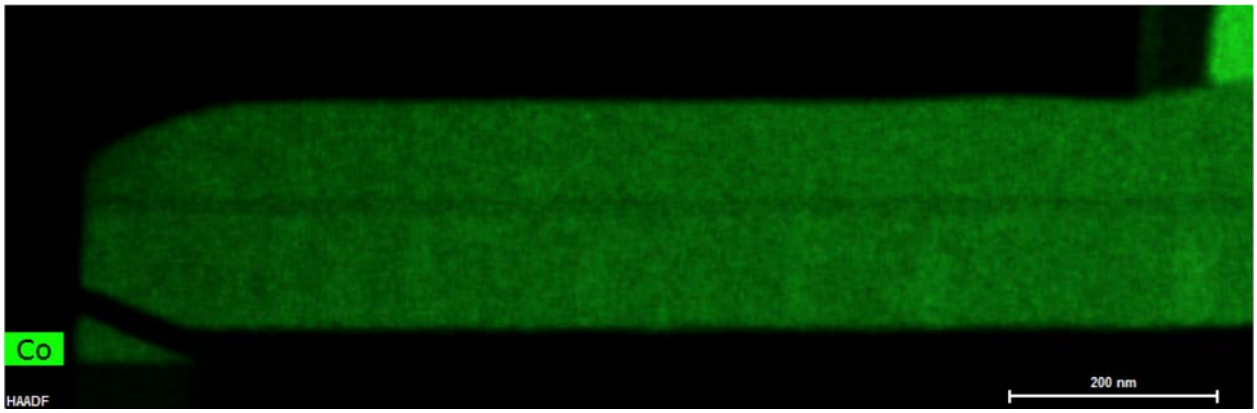

Figure 92: EDS map showing just Co.

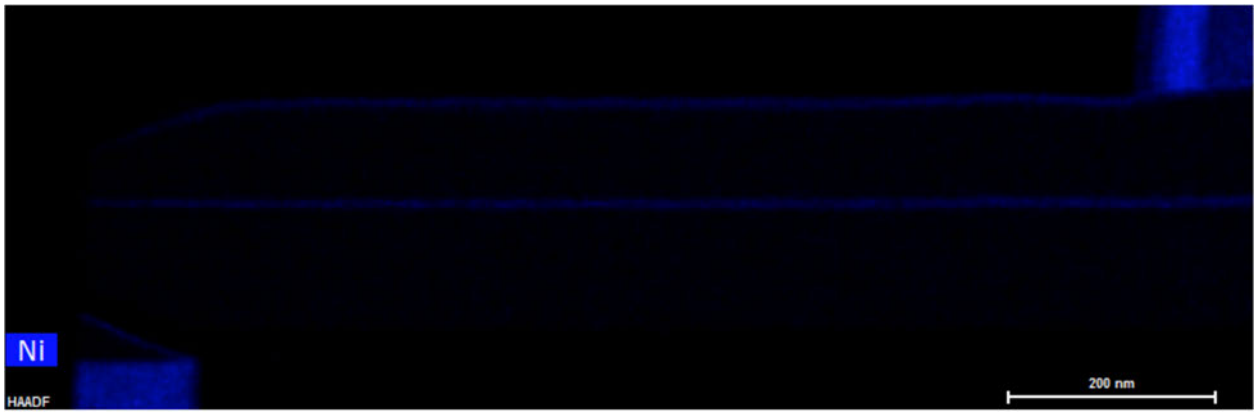

Figure 93: EDS map showing just Ni.

169. Additionally, a quantitative assessment of the composition of the FeCo layers was performed Bruker ESPRIT as shown below.

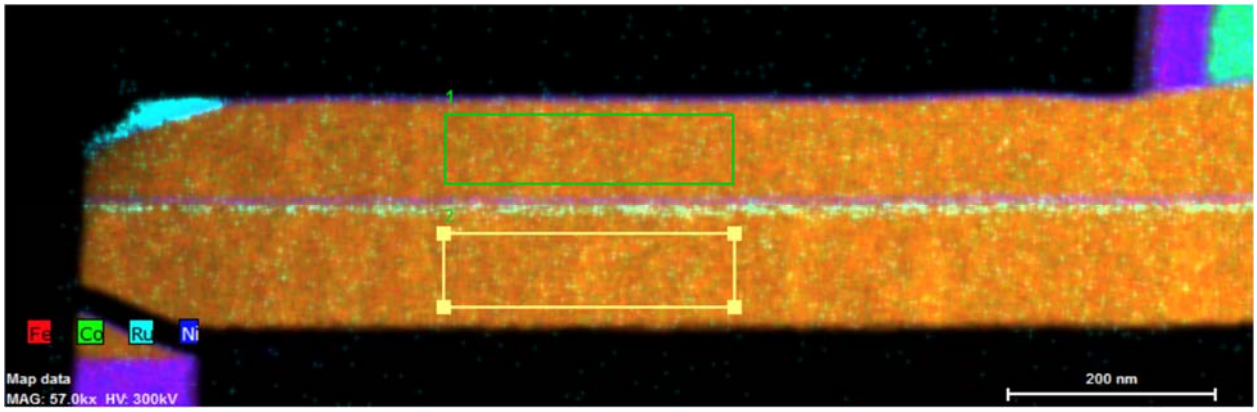

Figure 94: Quantitative assessment performed in the region enclosed by the green and yellow rectangles.

CONTAINS CONFIDENTIAL ATTORNEY EYES ONLY INFORMATION SUBJECT TO PROTECTIVE ORDER

Spectrum: 1

Element	Series	unn. C [wt.%]	norm. C [wt.%]	Atom. C [at.%]	Error (3 Sigma) [wt.%]
Chromium	K-series	0.35	0.35	0.38	0.13
Iron	K-series	61.47	61.47	62.73	5.64
Cobalt	K-series	37.05	37.05	35.83	3.44
Nickel	K-series	1.05	1.05	1.02	0.20
Ruthenium	L-series	0.08	0.08	0.04	0.11
	Total:	100.00	100.00	100.00	

Spectrum: 2

Element	Series	unn. C [wt.%]	norm. C [wt.%]	Atom. C [at.%]	Error (3 Sigma) [wt.%]
Chromium	K-series	0.31	0.31	0.34	0.12
Iron	K-series	61.64	61.64	62.89	5.65
Cobalt	K-series	37.02	37.02	35.79	3.44
Nickel	K-series	0.97	0.97	0.94	0.19
Ruthenium	L-series	0.05	0.05	0.03	0.10
	Total:	100.00	100.00	100.00	

Figure 95: Output from Bruker ESPRIT showing composition in region enclosed by the green and yellow rectangles.

(2) **TEM high resolution images of cross-sections**

170. The principles behind TEM imaging are discussed generally in Section E.2 above. High resolution cross-section images were taken using the FEI Titan 80-300 S-Twin microscope ("Titan"), operating in TEM mode at 300 kV, and fitted with an automated image corrector to enhance the spatial resolution.. The high resolution cross-section images were obtained from the circled region of the write pole of SBRD8K.

CONTAINS CONFIDENTIAL ATTORNEY EYES ONLY
INFORMATION SUBJECT TO PROTECTIVE ORDER

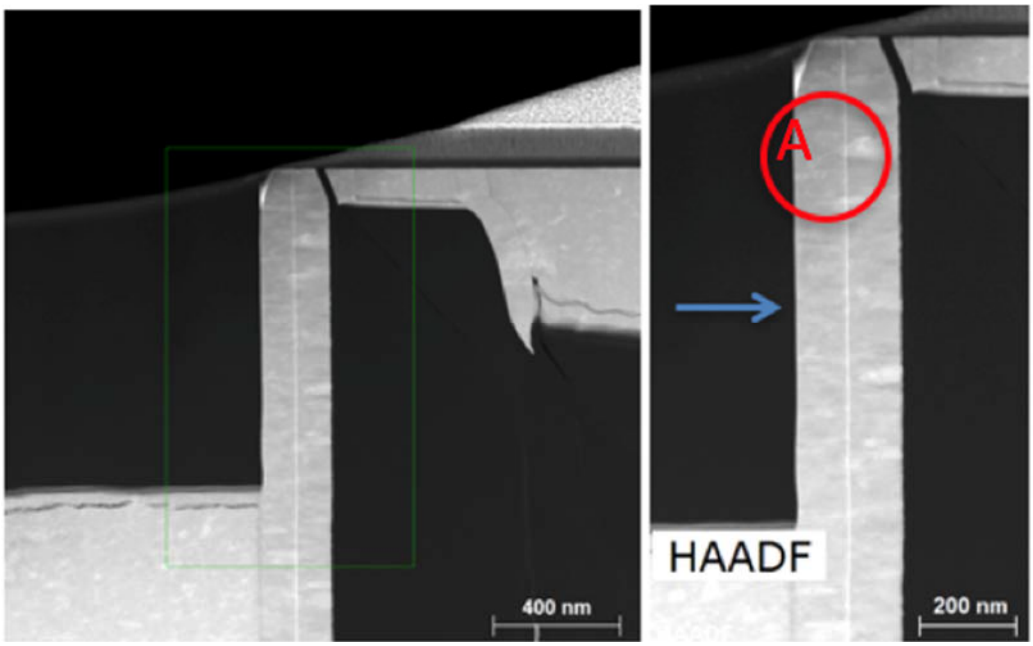

Figure 96: TEM overview of SBRD8K, with regions where high resolution cross-sections were taken shown in the red circle. The blue arrow indicates the growth direction, and A indicates the NiFe template/FeCo interface. Note the pronounced columnar growth seen in both images.

171. The medium magnification image on the right-hand side of Figure 96 shows a grain structure that is elongated perpendicular to the lower NiFe layer normal (in the direction indicated by the blue arrow). Such a morphology is typically referred to as a "bamboo" structure, more formally defined as a grain structure in which the boundaries of the grains tend to be aligned normal to the long axis and to extend through the thickness.[24] The directional nature of this structure modifies the mechanical and electrical properties of a material significantly, by aligning the majority of the grain boundaries parallel to one another, as opposed to being homogeneously distributed. It is very commonly observed in epitaxial growth, where the orientation relationship between the template and the growth layers favors growth in one direction.

[24] *Analysis of grain-boundary structure in Al–Cu interconnects*, D.P. Field, J.E. Sanchez, P.R. Besser, and D.J. Dingley, J.Appl. Phys., **82** (5), (1997), pp. 2383-2392

CONTAINS CONFIDENTIAL ATTORNEY EYES ONLY INFORMATION SUBJECT TO PROTECTIVE ORDER

172. High resolution images were taken at several points along each interface in the circled region in Figure 96 above. Six such images taken are shown below.

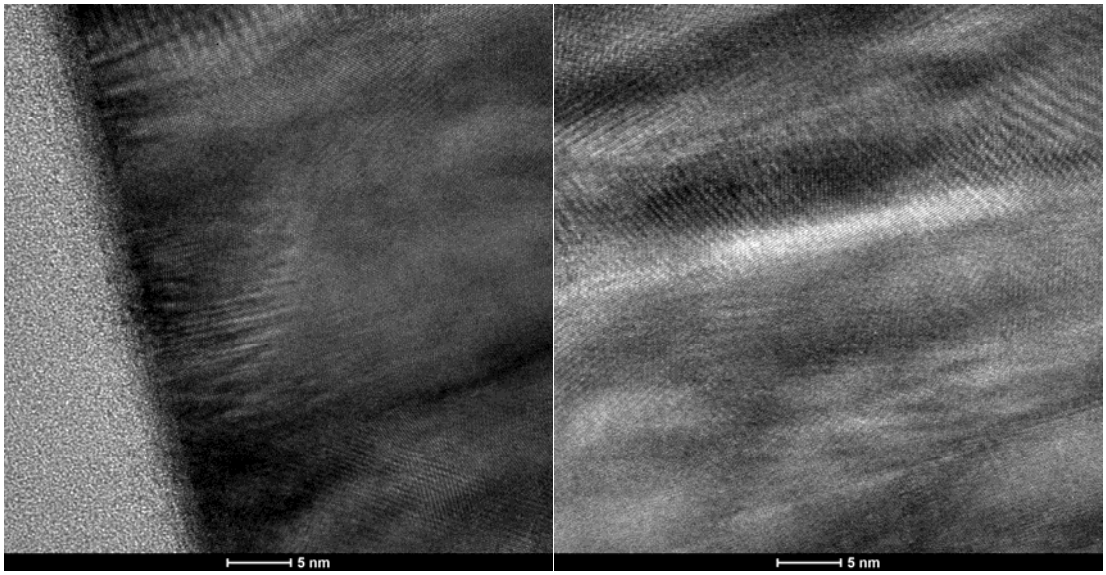

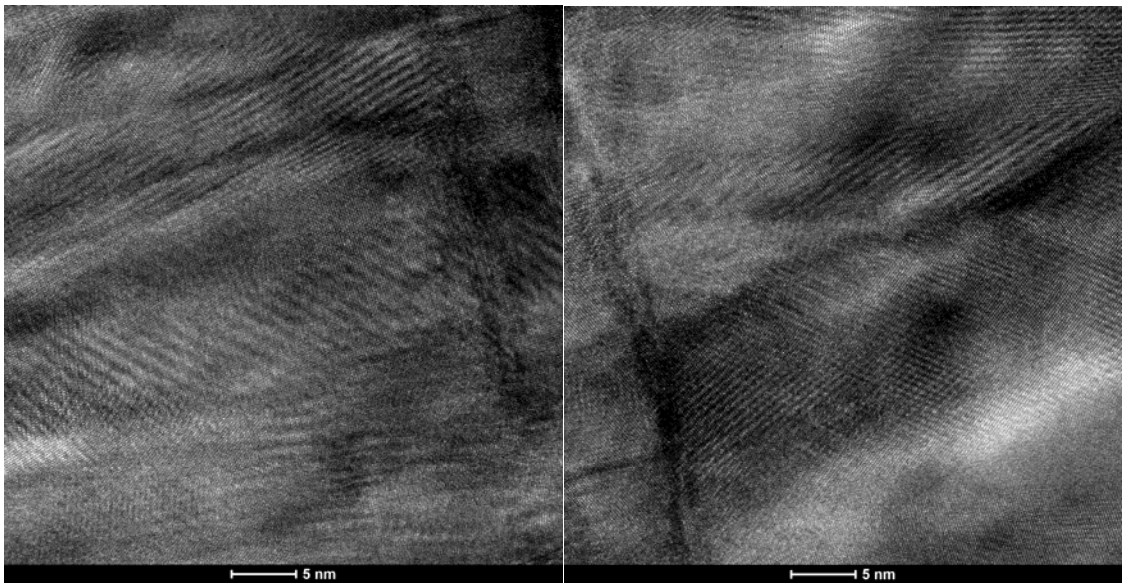

CONTAINS CONFIDENTIAL ATTORNEY EYES ONLY
INFORMATION SUBJECT TO PROTECTIVE ORDER

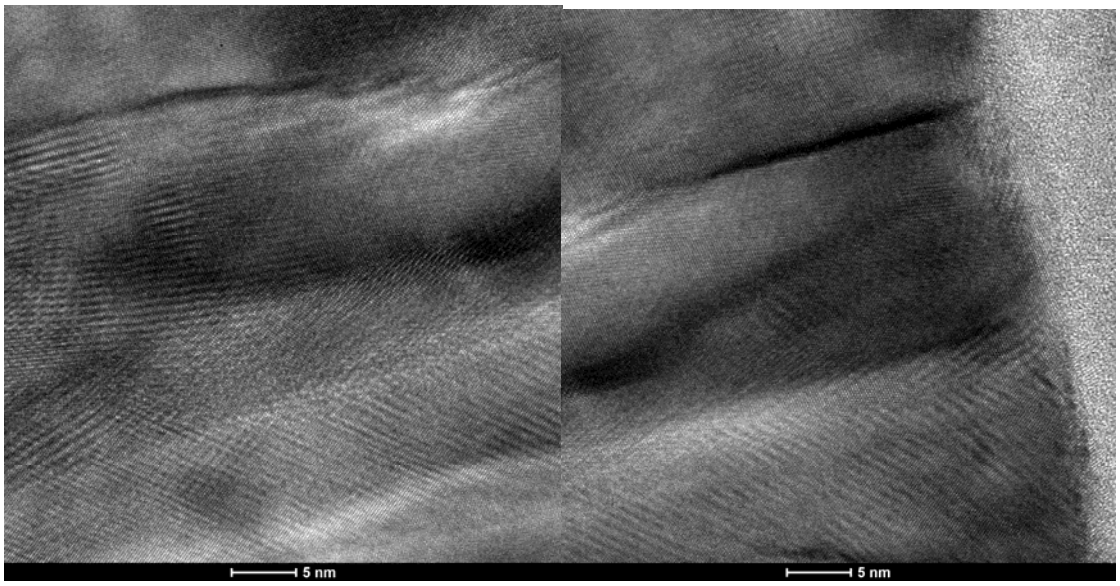

Figure 97: High resolution cross-section images taken across the sample.

173. These high resolution cross-sections show various sets of crossed lattice fringes, such as the example shown in Figure 98 below. For example, in Figure 98, the zoomed-in area in the red square shows prominent patterns of crossed fringes. These lattice fringes arise when the forward scattered (central) beam and the diffracted beam corresponding to one family of crystal planes both lie within the objective aperture and so contribute to the final image. These two beams will then "beat" together in the image, resulting in a pattern of fringes that have the spacing of that family of planes, and which align parallel to them. When several diffracted beams are allowed through the objective aperture, each contributes a set of fringes, so that a crossed fringe pattern can be seen in the image. The more diffracted beams that are used to form this lattice image, the closer it will be to an image representing the actual atomic arrangement in the crystal.[25]

[25] *Transmission Electron Microscopy,* D.B. Williams and C.B. Carter, Springer, (2009), p. 389 et seq.

CONTAINS CONFIDENTIAL ATTORNEY EYES ONLY
INFORMATION SUBJECT TO PROTECTIVE ORDER

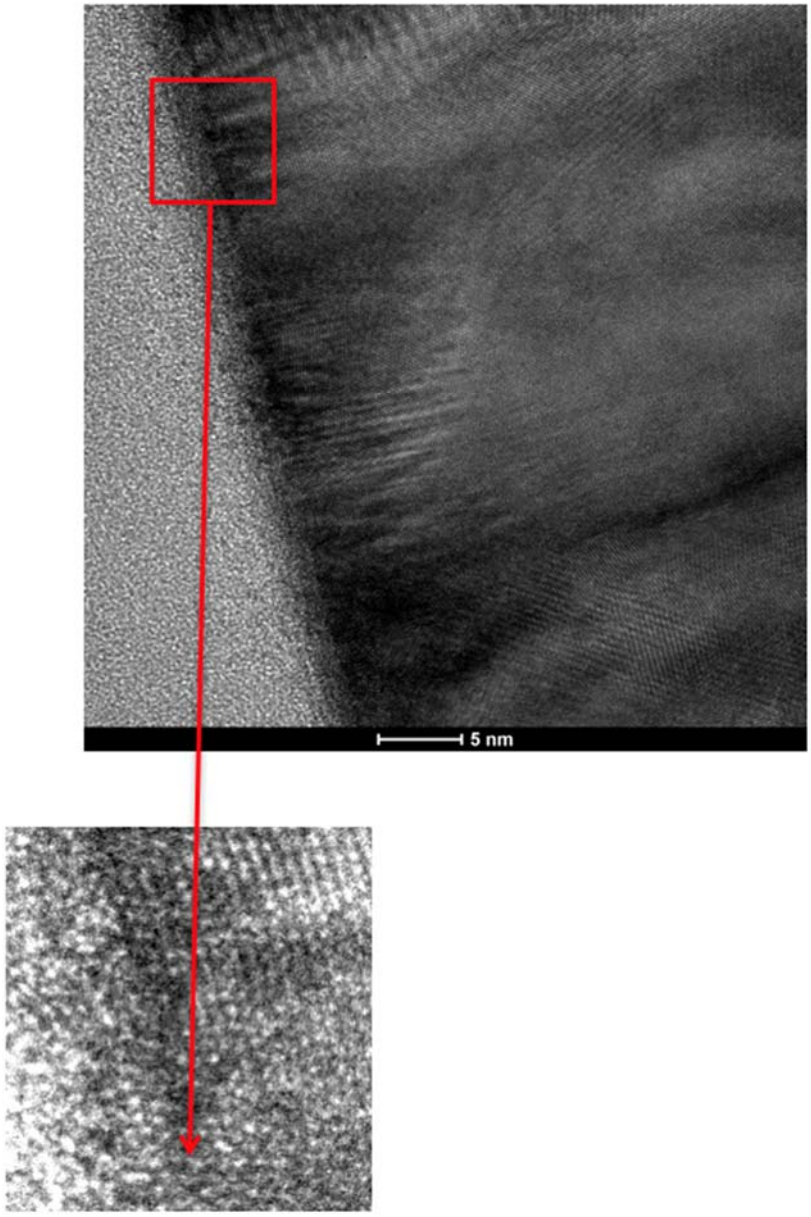

Figure 98: Example showing zoomed-in crossed lattice fringes from a high resolution cross-section from the lower NiFe/FeCo interface region as discussed above.

174. Additionally, a high resolution cross-section taken from the upper NiFe/FeCo interface region is shown in Figure 99 below. This region consists of two FeCo layers with a thin layer of NiFe in between. The NiFe/FeCo interfaces are designated by the blue arrows. Like the high resolution cross-section from the lower NiFe/FeCo interface in Figure 98 above, this image

CONTAINS CONFIDENTIAL ATTORNEY EYES ONLY
INFORMATION SUBJECT TO PROTECTIVE ORDER

also shows crossed lattice fringes, with an example in the region in the red box shown enlarged in Figure 100 below.

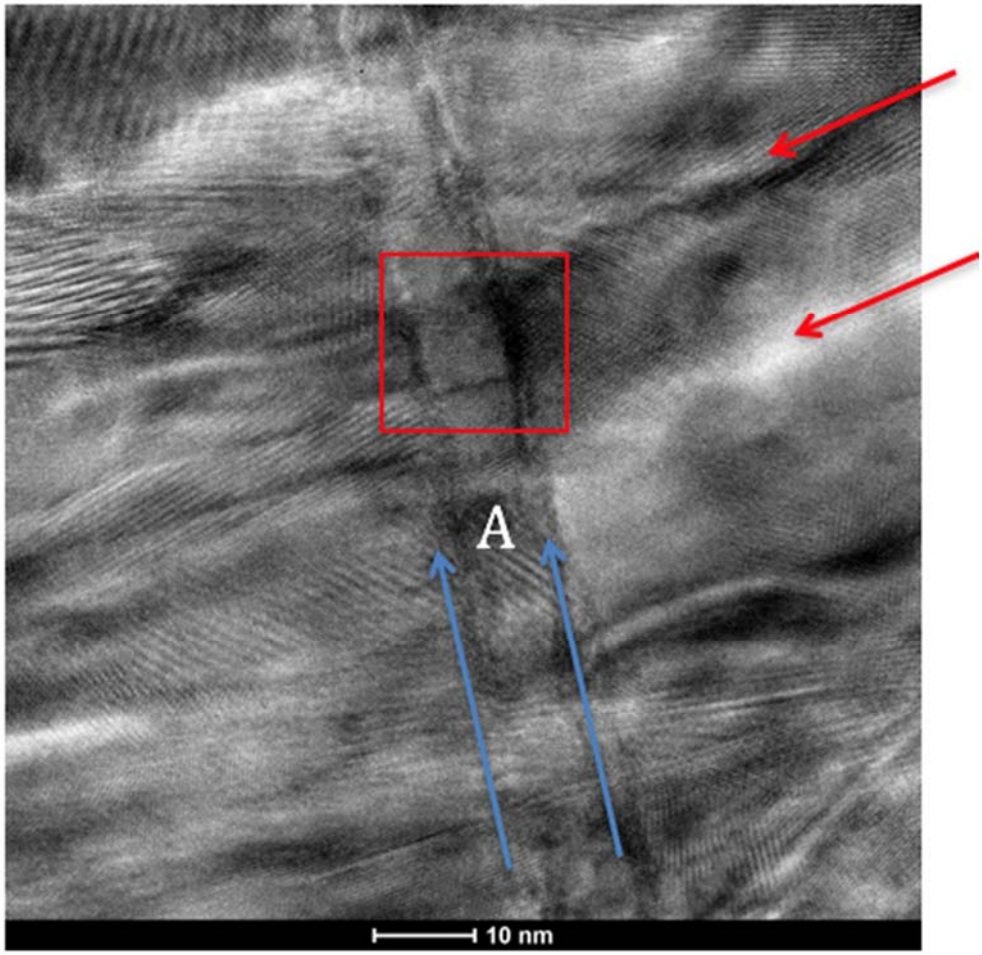

Figure 99: Example high resolution cross-section from the upper NiFe/FeCo/Ru interface area. Area highlighted in red is shown enlarged below.

CONTAINS CONFIDENTIAL ATTORNEY EYES ONLY INFORMATION SUBJECT TO PROTECTIVE ORDER

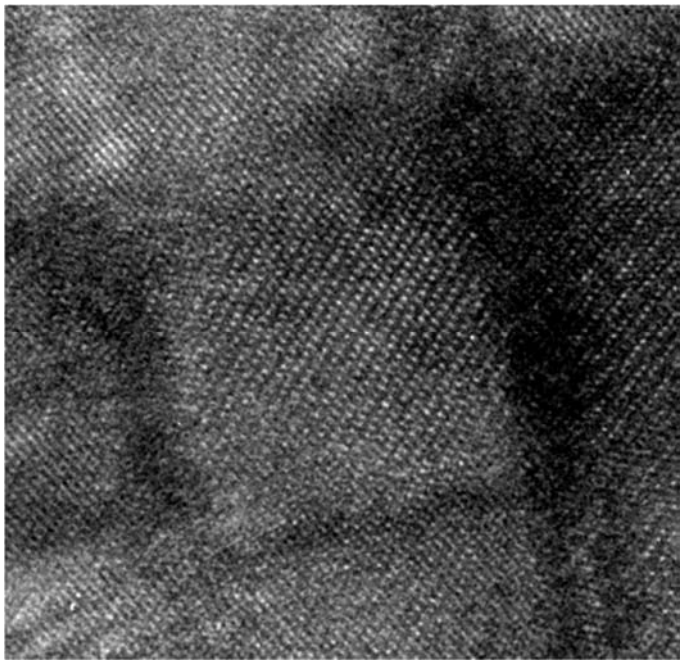

Figure 100: Zoomed-in area from Figure 99 above showing crossed lattice fringes.

175. Several sets of crossed lattice fringes are seen here, as are the FeCo/NiFe/Ru interfaces. The fringes are present on both sides of the NiFe layer, in the NiFe layer itself, and on both sides of the Ru layer, indicating that the orientation of the FeCo is maintained on both sides of the NiFe. The continuity of these fringes across all layers show that there is an orientation relationship between the FeCo and the NiFe. From the FFTs (as discussed in Section F.2.a.3 below) and the hexagonal arrangement of spots in the FeCo lattice image, looking down into the cross-section (i.e., into the page) shows a $\{111\}_{BCC}$ plane, and a $<110>_{BCC}$ direction is normal to the interface (as is the case at the template/FeCo interface in region A, as discussed in Section F.2.a.3 below).

(3) **FFT on TEM high resolution images of cross-sections**

176. The principles behind FFTs are discussed generally in Section E.2.i above. FFTs were taken at selected points in high resolution cross-section images. For instance, a high resolution cross-section taken in region A is shown in Figure 101 below, with a number of points along the lower NiFe/ lower FeCo interface marked with numbers. At each numbered point,

CONTAINS CONFIDENTIAL ATTORNEY EYES ONLY
INFORMATION SUBJECT TO PROTECTIVE ORDER

FFTs were taken: (a) in the lower NiFe layer at the location of the numbered point; and (b) in the lower FeCo immediately to the left of the numbered point. Since a diffraction pattern of a sample is just the Fourier transform of its structure,[26] FFTs taken of the image generate the information found in diffraction patterns, and can be used to determine crystal structure. The FFTs can be generated using a number of programs including ImageJ, MIPAR, or Desktop Microscopist; the FFTs here were generated using ImageJ. In Figure 101 below, the area sampled for each FFT was confined to an area of the size indicated by the red square, which was chosen to be small enough to ensure sampling information from the template and excluding information from the surrounding layers.

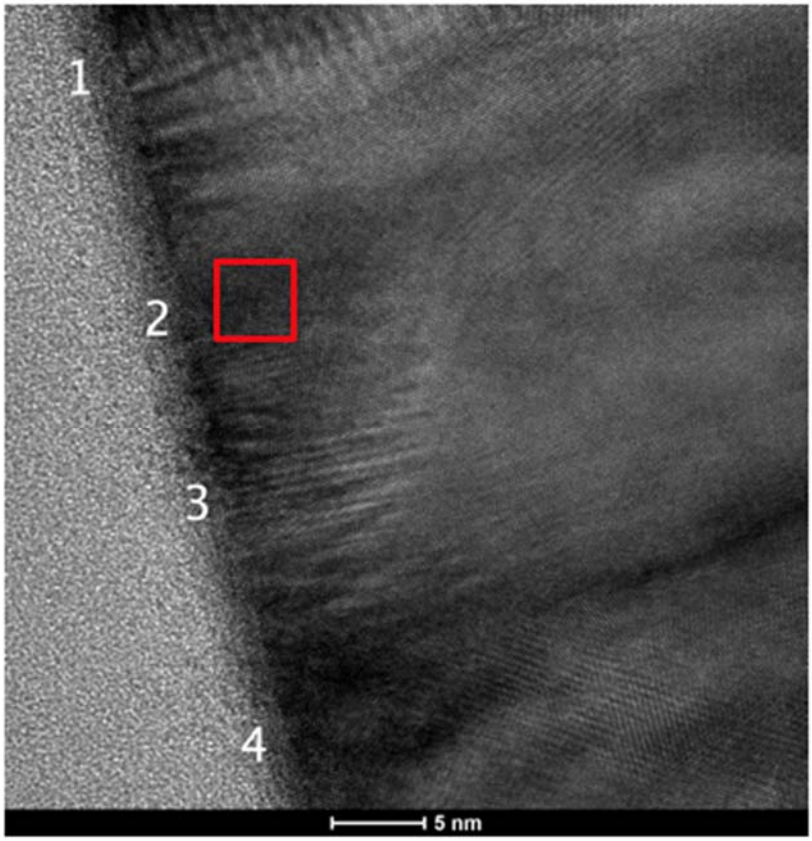

Figure 101: Example high resolution cross-section from the lower NiFe/FeCo interface region. The numbered points indicate where FFTs were taken.

[26] *The Analytical Theory of Heat, J. B. Fourier*, (1878) [1822], translated by Alexander Freeman, The University Press (translated from French).

CONTAINS CONFIDENTIAL ATTORNEY EYES ONLY INFORMATION SUBJECT TO PROTECTIVE ORDER

177. For example, FFTs taken at point 2 are shown in Figure 102 below. The FFT on the left is from the lower NiFe layer and the FFT on the right is from the lower FeCo directly on the lower NiFe layer. Analysis of the FFTs was performed by measuring the diffraction spot spacings and the angles between rows of diffraction spots and comparing that information with the standard diffraction patterns[27] shown in Figure 102 below their respective FFTs.

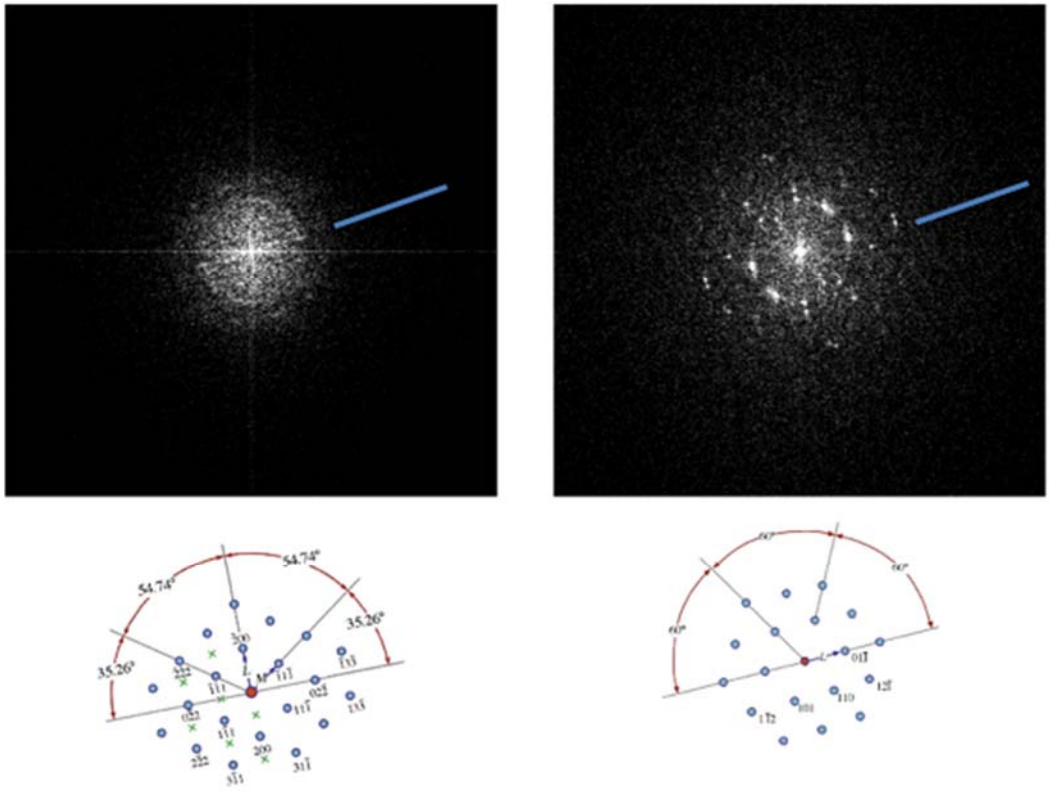

Figure 102: above: FFTs from the NiFe layer (left) and FeCo layer (right); below: standard diffraction patterns rotated into similar orientations as respective FFTs shown immediately above.

178. For the left-hand FFT from the lower NiFe layer, looking down a {110} direction into the page, this analysis indicates that the diffraction pattern is $\{110\}_{FCC}$. The FFT is shown on the top left, and the standard $\{110\}_{FCC}$ diffraction pattern is shown below it, rotated into a

[27] *Transmission Electron Microscopy,* D.B. Williams and C.B. Carter, Springer, (2009), pp. 299-301.

CONTAINS CONFIDENTIAL ATTORNEY EYES ONLY
INFORMATION SUBJECT TO PROTECTIVE ORDER

similar orientation. Note that a few overlapping spots from the lower FeCo layer can be seen, which are indicative of the differences between the NiFe pattern and the FeCo pattern. Thus, this FFT indicates that the crystal structure of the NiFe layer is FCC. Further, from the high resolution cross-sections above, because we can see that the lattice fringes are continuous along the lower NiFe layer, this is indicative of the crystal structure of the extent of the lower NiFe layer.

179. For the right-hand FFT from the lower FeCo layer, looking down a {111} direction into the page, this analysis indicates that the diffraction pattern is $\{111\}_{BCC}$. The FFT is shown on the top right, and the standard $\{111\}_{BCC}$ diffraction pattern is shown below it, rotated into a similar orientation. Thus, this FFT indicates that the crystal structure of the lower FeCo layer is BCC. Further, from the high resolution cross-sections above, because we can see that the lattice fringes are continuous along the FeCo layer, this is indicative of the crystal structure of the extent of the FeCo layer.

180. From the discussion above, the two FFT patterns show that there are two parallel directions, one in the lower NiFe layer and one in the lower FeCo layer, pointing out of the page. These are a $<110>_{FCC}$ direction lying parallel to a $<111>_{BCC}$ direction. Further, when analyzing the pattern from the spot spacing and distribution, it can be seen that a $<111>_{FCC}$ direction in the NiFe is also parallel to a $<110>_{BCC}$ in the FeCo, and lie in the plane of the page; both of these directions are indicated by the lines marked on the FFT. The directions are also perpendicular to the lower NiFe/ lower FeCo interface, and so confirm the epitaxial growth in that direction and is evidence of the epitaxial growth of the lower FeCo layer on the lower NiFe layer, which functions as an atomic template. These two mutual orientation relationships are also sufficient to determine the relative orientation of the lower NiFe layer and the lower FeCo layer above it.

CONTAINS CONFIDENTIAL ATTORNEY EYES ONLY
INFORMATION SUBJECT TO PROTECTIVE ORDER

Therefore, the lower NiFe layer exhibits (111) texture, and the lower FeCo layer exhibits (110) texture.

181. The parallel directions in the FCC and BCC layers normal to the interface show repeatedly <110> direction in the BCC layers and <111> direction in the FCC layers. Therefore, this analysis shows that the lower NiFe layer has a predominant (111) texture, and the lower FeCo layer has a predominant (110) texture.

182. Since the FFT analysis above shows that the lower NiFe/ lower FeCo relationship is $\{111\}_{FCC}||\{110\}_{BCC}$, as well as $<110>_{FCC}||<111>_{BCC}$, this shows that the Kurdjumov–Sachs orientation relationship is present.

183. Similar analysis was performed on FFTs taken at points other than 2 and each showed similar results as those described above, thereby confirming that the orientational relationships were consistent across the interface between the lower NiFe layer and the lower FeCo layer, and that the same textures were present throughout each layer. These FFTs are contained in Appendix C. Additionally, FFTs were taken on the remaining high-resolution cross sections; annotated cross sections and their accompanying FFTs are also shown in Appendix C and also showed similar results as those described above, further confirming the orientational relationships and textures as described above.

184. To the extent that the FFT results for the lower NiFe layer are inconclusive, I conclude that the lower NiFe layer is FCC and exhibits a predominant (111) texture based further on the discussion of the upper NiFe / FeCo layers below.

185. Additionally, as with the high resolution cross-section in the lower NiFe/FeCo interface region, FFTs were taken in the NiFe/FeCo/Ru/FeCo interface region around point A shown in Figure 103 below. Here, the two interfaces are indicated by the blue arrows. Also

CONTAINS CONFIDENTIAL ATTORNEY EYES ONLY
INFORMATION SUBJECT TO PROTECTIVE ORDER

notable, the red arrows show the boundaries between different columnar grains of the FeCo as they grow from right to left, which highlight the elongated nature of the FeCo grains, giving rise to the bamboo structure seen in the low magnification images in Section F.2.a.2 above.

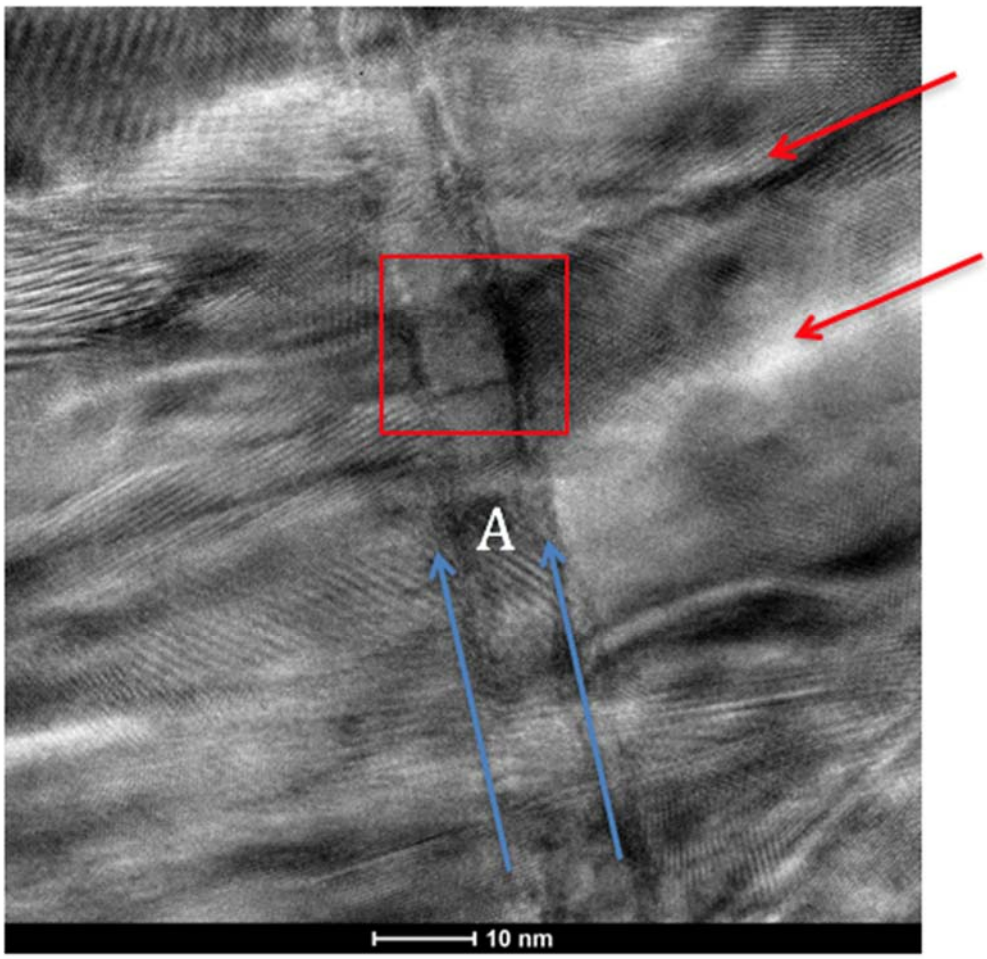

Figure 103: Example high resolution cross-section from the upper NiFe/FeCo/Ru interface. Point A indicates the area around where FFTs were taken.

186. Similar to the analysis for the example high resolution cross-section from point A above, FFTs were taken, from left to right, at the FeCo, NiFe, FeCo, Ru, and FeCo layers. Again, the area sampled for each FFT was confined to an area of the size indicated by the red square. The set of FFTs are shown in Figure 103 below.

CONTAINS CONFIDENTIAL ATTORNEY EYES ONLY
INFORMATION SUBJECT TO PROTECTIVE ORDER

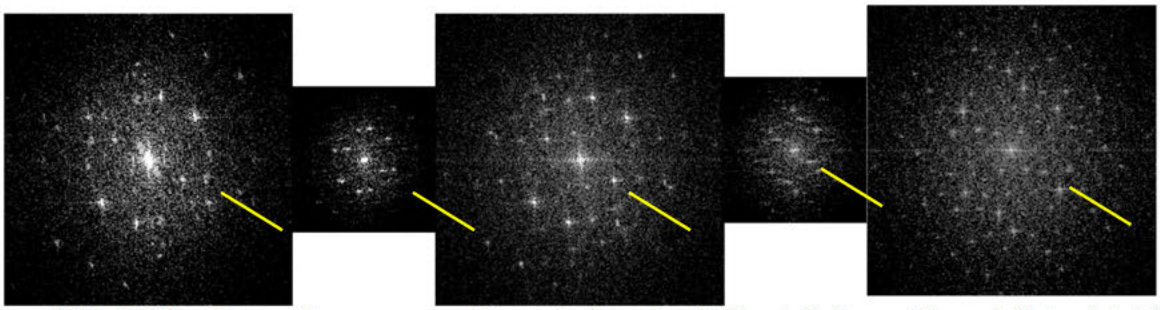

Figure 104: Diffraction patterns across the central region indicated above. From left to right they are: FeCo, NiFe, FeCo, Ru, FeCo. The continuity of the lattice fringes is reflected in common directions in all five patterns, indicated by the yellow lines.

187. While the FFTs as specific directions in the layers are not all readily ascertainable, the three Fe Co layers all exhibit a common pattern, and all five patterns share a common direction, indicated by the yellow lines, that runs from the lower FeCo layer to the upper, through the Ru, NiFe, and center FeCo layers. Given that the FeCo crystallites in the lower part of the write head have been identified earlier as BCC, the common form of the three FeCo patterns here indicates that they are all BCC. Likewise, from the high resolution cross-sections above, because we can see that the lattice fringes are continuous, this is indicative of the crystal structure of the extent of the NiFe and FeCo layers.

188. Common directions in all three layers show the persistence of the epitaxial relationship between $<111>_{BCC}$ and $<110>_{FCC}$, as was found at the NiFe/FeCo interface of region A. Again, this is indicative of the upper NiFe layer exhibiting (111) texture, and the FeCo layers exhibiting (110) texture. This also indicates the Kurdjumov-Sachs orientation relationship between the upper NiFe and upper FeCo layers.

189. Again, the parallel directions in the FCC and BCC layers normal to the interface show repeatedly <110> direction in the BCC layers and <111> direction in the FCC layers. Therefore, this analysis shows that the upper NiFe layer has a predominant (111) texture, and the upper FeCo layer has a predominant (110) texture.

CONTAINS CONFIDENTIAL ATTORNEY EYES ONLY
INFORMATION SUBJECT TO PROTECTIVE ORDER

190. Further, the FFT patterns show that there are two parallel directions, one in the upper NiFe layer and one each of the adjacent FeCo layers, pointing out of the page. When analyzing the pattern from the spot spacing and distribution, it can be seen that a $<111>_{FCC}$ direction in the NiFe is parallel to a $<110>_{BCC}$ in the FeCo, and lie in the plane of the page; both of these directions are indicated by the yellow lines marked on the FFT. The directions are also perpendicular to the upper NiFe/FeCo interfaces, and so confirm the epitaxial growth in that direction and is evidence of the epitaxial growth of the lower FeCo layer on the lower NiFe layer, which functions as an atomic template. These two mutual orientation relationships are also sufficient to determine the relative orientation of the lower NiFe layer and the lower FeCo layer above it. Therefore, the lower NiFe layer exhibits (111) texture, and the lower FeCo layer exhibits (110) texture.

191. The parallel directions in the FCC and BCC layers normal to the interface show repeatedly <110> direction in the BCC layers and <111> direction in the FCC layers. Therefore, this analysis shows that the lower NiFe layer has a predominant (111) texture, and the lower FeCo layer has a predominant (110) texture.

192. As discussed in Section F.2.a.4 below, the microbeam diffraction analysis confirms the presence of Kurdjumov–Sachs orientational variants in the lower FeCo layer. I would not expect such variants but for the lower FeCo layer to be grown upon a predominately (111) FCC NiFe template later.

193. I also note that the FFTs taken from various points along the NiFe layers, while they maintain a common direction with the FeCo layers normal to the interface, change significantly with position along the interface. These changes in the FFT indicate differences in orientation along the template, and thus the grain size in the template. The grain size in the NiFe

CONTAINS CONFIDENTIAL ATTORNEY EYES ONLY
INFORMATION SUBJECT TO PROTECTIVE ORDER

template layers is comparable to the width of the FeCo grains, so that the grain sizes in the two are similar. Thus, there is ordinarily only one or two FeCo grains per NiFe template grain.

(4) **TEM—microbeam diffraction on plan view samples**

194. Microbeam diffraction, as described in Section E.2.d above, was performed on a region of the lower FeCo layer of the write pole as shown by the red square in Figure 105 below. A plan view sample was prepared such that the upper layers were removed, leaving the lower FeCo layer of the write pole exposed for microbeam diffraction. From the area indicated by the red square, 1,600 diffraction patterns were obtained by scanning the electron beam incrementally across the area in the box. A typical diffraction pattern is shown on the right. Note that all diffraction patterns below were annotated using Keynote, software available from Apple.

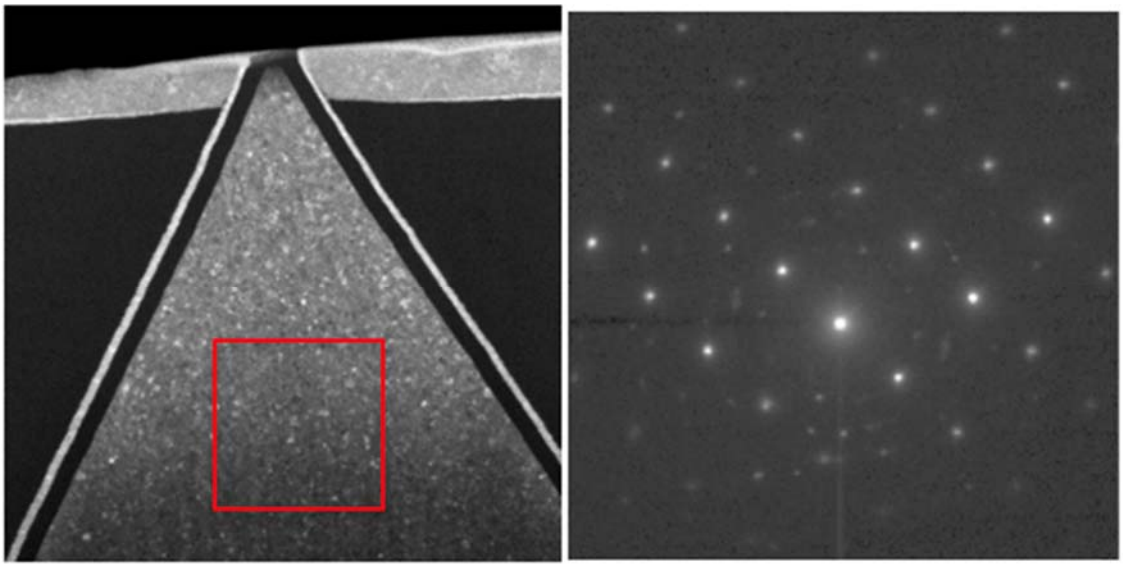

Figure 105: Plan view STEM image of SBRD8K near the pole tip of the write head (left). 1,600 diffraction patterns were taken from the area outlined in red. A typical diffraction pattern is shown on the right.

195. By defocusing the diffraction pattern image slightly, as shown on the right of Figure 106 below, we obtain an enlarged central spot that contains an image of a portion of the sample. This shows that the image of the plan view sample on the left and the diffraction pattern

CONTAINS CONFIDENTIAL ATTORNEY EYES ONLY
INFORMATION SUBJECT TO PROTECTIVE ORDER

on the right are in near perfect alignment, to ±10˚. Thus, directions associated with the sample can be related to directions in the diffraction pattern, and those directions may be indexed.

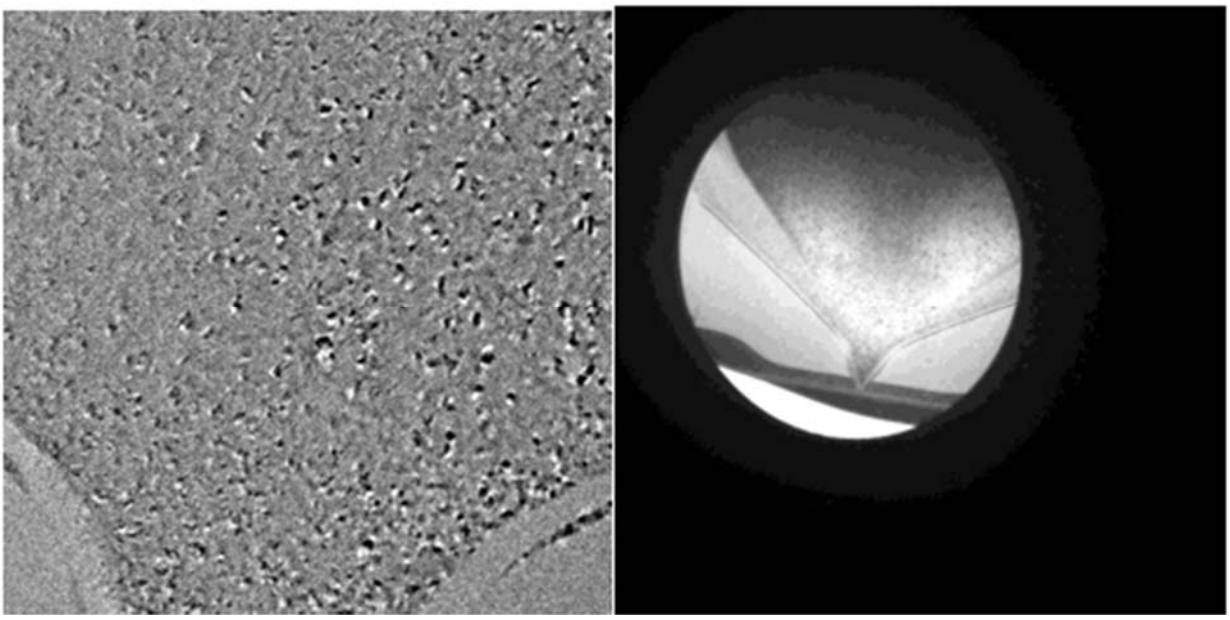

Figure 106: Plan view STEM image of SBRD8K (left), with a de-magnified image of the central spot of its diffraction pattern (as shown in Figure 105 above) in which the image of the head can be seen. This fixes the relative orientation of the image (left) and any diffraction patterns.

196. Individual frames from this set of 1,600 may contain diffraction patterns from one, two, or sometimes more separate FeCo crystallites. Typical single crystal patterns obtained for this analysis are shown in Figure 107 below. These patterns are readily identified and indexed as patterns in the $(110)_{BCC}$ orientation. This is confirmed by measurement of the ratio of the sides of the rectangles, found to be 5.4:3.8 = 1:√2, as required. Further, this is the epitaxial growth direction for the lower FeCo layer on the lower NiFe layer (the atomic template) as expected. These patterns are further confirmation that the FeCo layer is BCC with (110) texture.

CONTAINS CONFIDENTIAL ATTORNEY EYES ONLY
INFORMATION SUBJECT TO PROTECTIVE ORDER

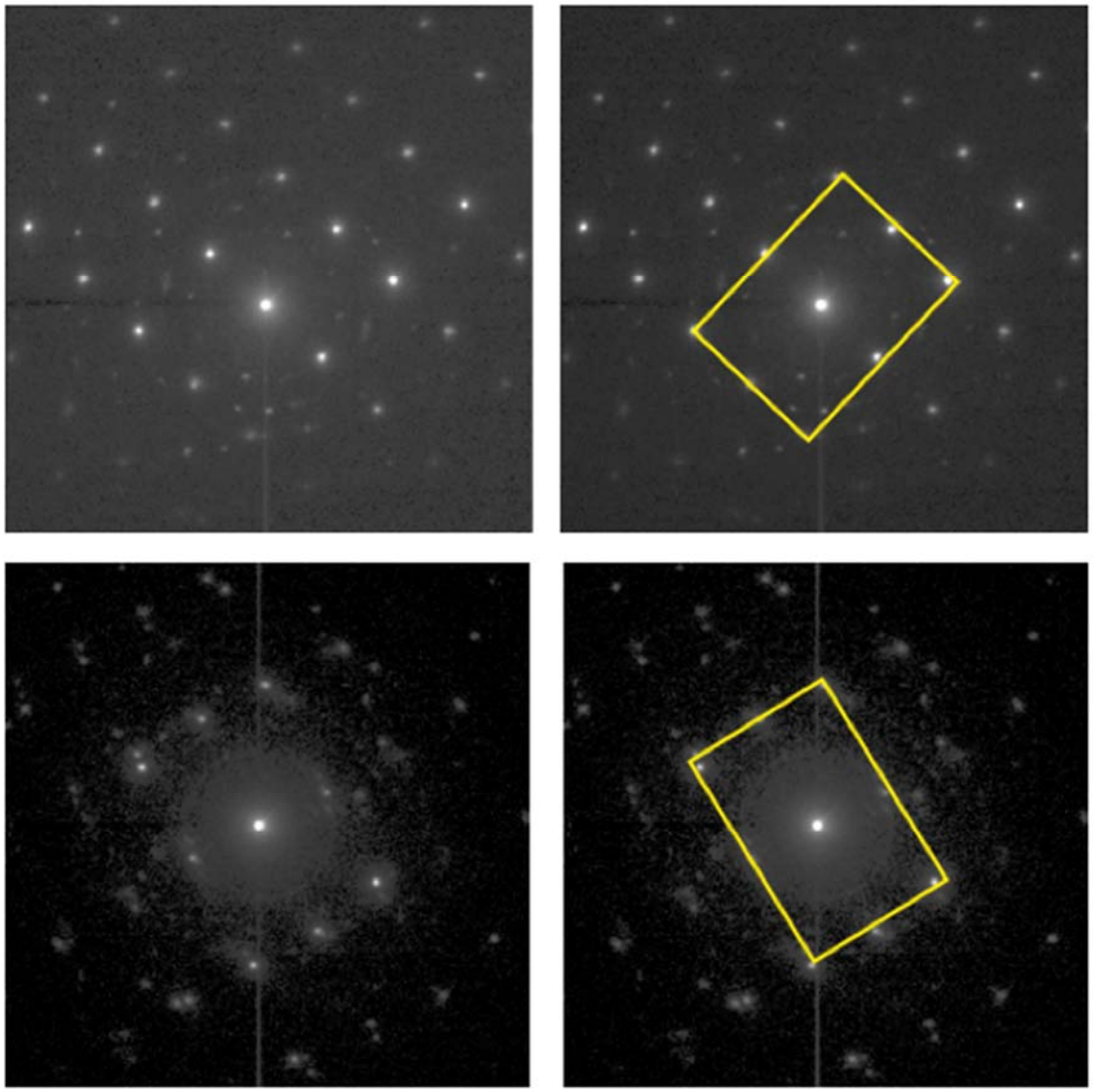

Figure 107: Single crystallite diffraction patterns, frames 1329 (upper) and 242 (lower), in the (110) orientation. These patterns visually identify as standard $(110)_{BCC}$ patterns.

197. Figure 108 below shows an example diffraction pattern with two crystallites, both in the $(110)_{BCC}$ orientation, but rotated by ~55˚ about their common $[110]_{BCC}$ direction. This is the separation of two variants in the Kurdjumov-Sachs orientation. The measured ratio of the sides of the motif are 1:√2 as required. Angles were measured directly in Keynote.

CONTAINS CONFIDENTIAL ATTORNEY EYES ONLY
INFORMATION SUBJECT TO PROTECTIVE ORDER

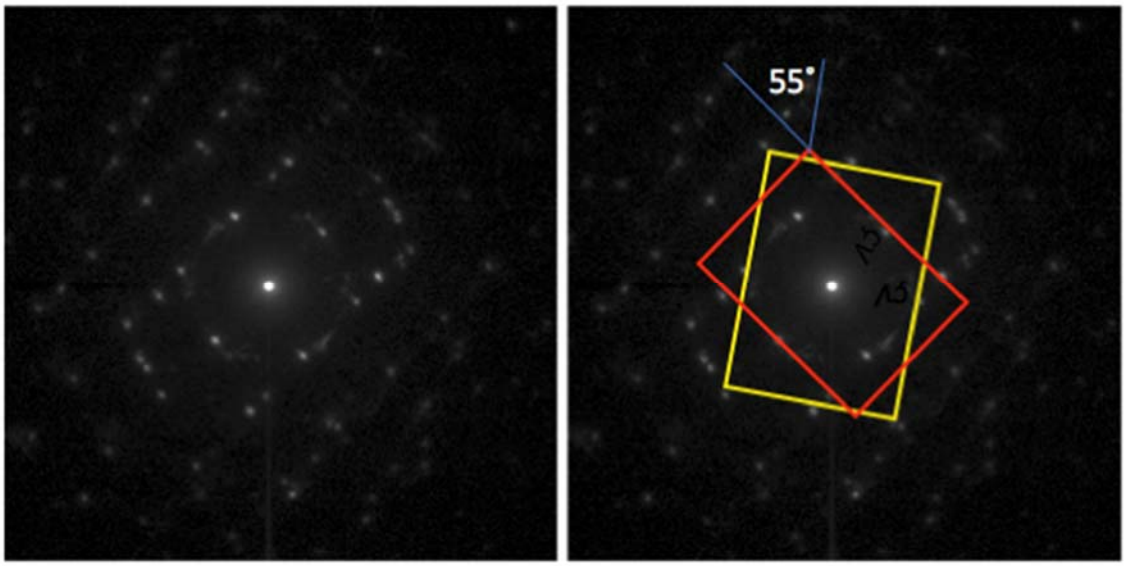

Figure 108: Two crystallites, both in the $(110)_{BCC}$ orientation, frame 1313, rotated by ~55˚ about their common $[110]_{BCC}$ direction.

198. Figure 109 below shows a diffraction pattern showing two crystallites both in the $(110)_{BCC}$ orientation, rotated about their common $[110]_{BCC}$ direction by ~70.53˚. This is also the separation of two variants in the Kurdjmov-Sachs orientation. This also means that the crystallites are in the "twin" orientation, which is alternatively described as a 180˚ rotation about their common <211> direction (circled in red below), or a mirror reflection in the <211> plane (dashed line).

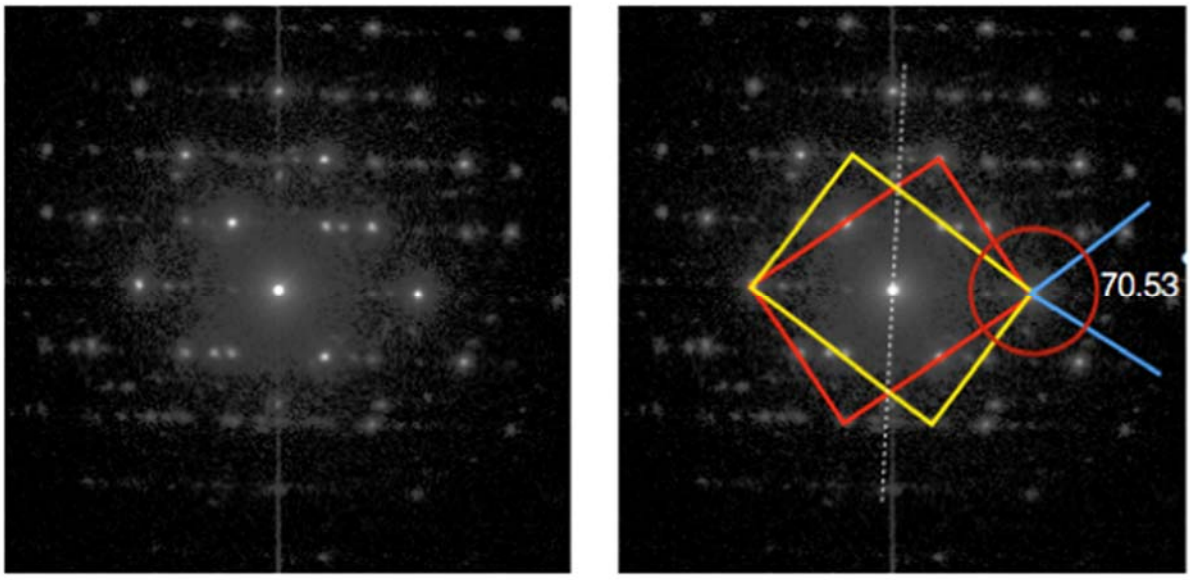

CONTAINS CONFIDENTIAL ATTORNEY EYES ONLY
INFORMATION SUBJECT TO PROTECTIVE ORDER

Figure 109: Frame 328, showing two crystallites both in the $(110)_{BCC}$ twin orientation, rotated by ~70.53˚ about their common $[110]_{BCC}$ direction

199. Figure 110 below also shows the "twin" orientation, but with two pairs twinned.

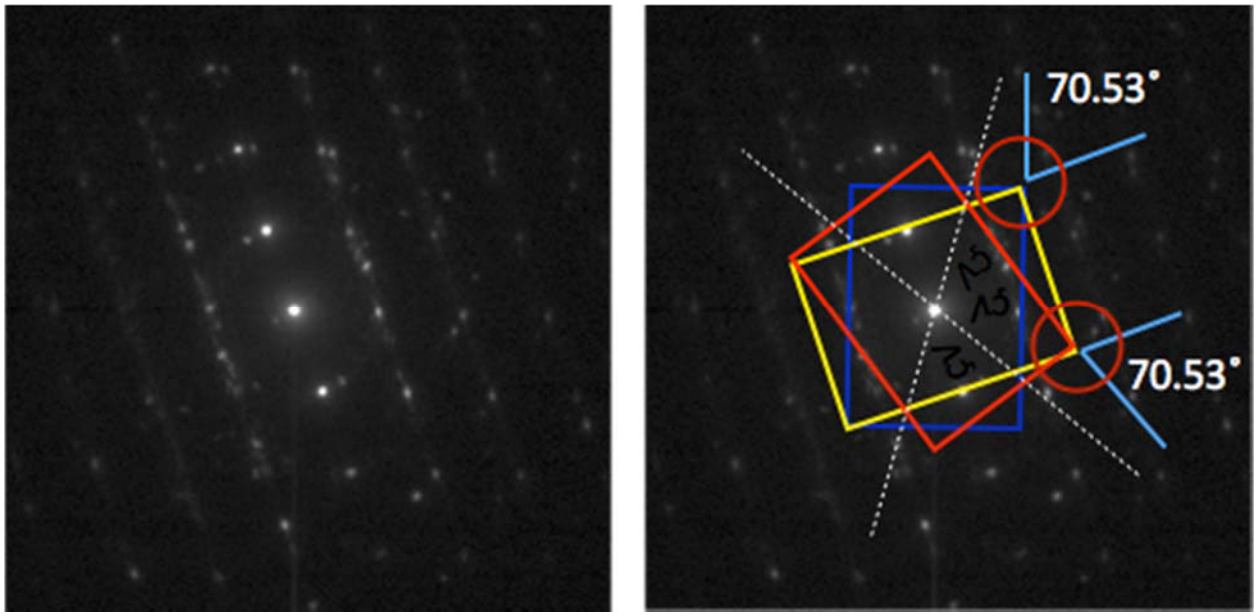

Figure 110: Three crystallites, frame 1437, showing two pairs twinned in $(110)_{BCC}$ orientations, rotated by ~70.53˚ about their common $[110]_{BCC}$ direction. The first twin pair are indicated by the blue and yellow motif, while the other pair are the outlined by the red and yellow rectangles. The two twin planes are shown by the white dashed lines.

200. In addition to the analysis of individual patterns, 100 out of the 1600 diffraction patterns were selected using a random number generator. These 100 were categorized as either a) showing no recognizable pattern, b) showing a single {110} patterns, c) showing multiple {110} patterns, d) showing {110} twins, or e) showing a pattern other than {110}. The results show the following numbers in each category – a) 71, b) 5, c) 0 d) 0 e) 24.[28]

201. Thus, microbeam diffraction imaging results confirm that the lower FeCo layer is BCC and contains variants with the expected orientation relationship for the Kurdjumov-Sachs

[28] These numbers are influenced by the initial orientation of the sample in the microscope, such that if the sample is precisely aligned so that the predominant $<110>_{BCC}$ direction is not anti-parallel to the electron beam, fewer $\{110\}_{BCC}$ patterns will be observed. This does not indicate, however, that there are in fact fewer $\{110\}_{BCC}$ crystals in the sample, and as discussed herein, I conclude that the FeCo layer is predominately $(110)_{BCC}$.

CONTAINS CONFIDENTIAL ATTORNEY EYES ONLY
INFORMATION SUBJECT TO PROTECTIVE ORDER

six variant system. Typical FeCo diffraction patterns exhibit the $(110)_{BCC}$ orientation, consistent with the epitaxial growth relationship of $(110)_{FeCo}$ on $(111)_{NiFe}$.

(5) **Dark field image analysis**

202. The principles behind dark field imaging and analysis are discussed in Section E.2.f above. Figure 111 below shows the area from the write head of SBRD8K where the diffraction data was taken on the left (this plan view sample is the same as that analyzed regarding microbeam diffraction above, exposing the FeCo layer), and a defocused diffraction ring pattern on the right which reveals an image of the sample in the central spot, similar to that discussed in Section F.2.a.4 above. This provides the orientation of the write head with respect to the diffraction pattern, as seen in Figure 111 below. From this image, it is clear that the diffraction pattern and the tip of the sample are almost exactly parallel, with less than 10˚ rotation from one to the other.

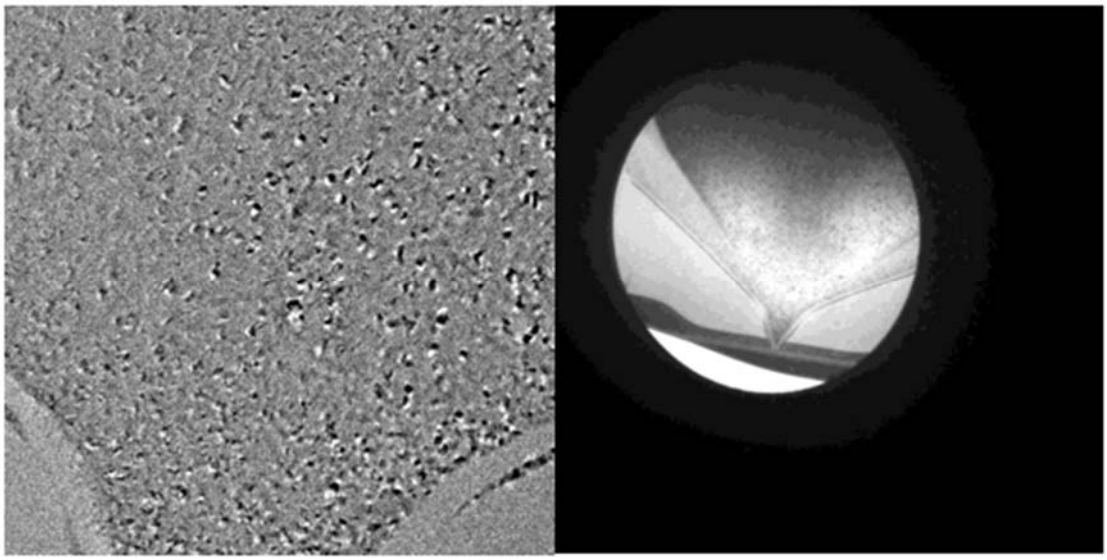

Figure 111: Defocused diffraction pattern (right) reveals alignment with sample (left) to be almost exactly parallel.

203. First, a small objective aperture is inserted to enclose a segment of the {200} diffraction ring, as shown on the right in Figure 112 below. Next, a dark field image of an area of

CONTAINS CONFIDENTIAL ATTORNEY EYES ONLY
INFORMATION SUBJECT TO PROTECTIVE ORDER

the lower FeCo layer is obtained, as shown on the left in Figure 112 below. Where crystallites show up bright in the dark field image, it indicates that their {200} planes are oriented so as to diffract into the direction enclosed by the objective aperture. The yellow arrow in the annotated image points in the direction of the objective aperture from the center of the diffraction pattern. This means that the bright crystallites have their <200> directions aligned parallel to the arrow, i.e., perpendicular to the long axis of the write head. Also note that the sample is oriented such that the $<110>_{BCC}$ directions are antiparallel to the electron beam.

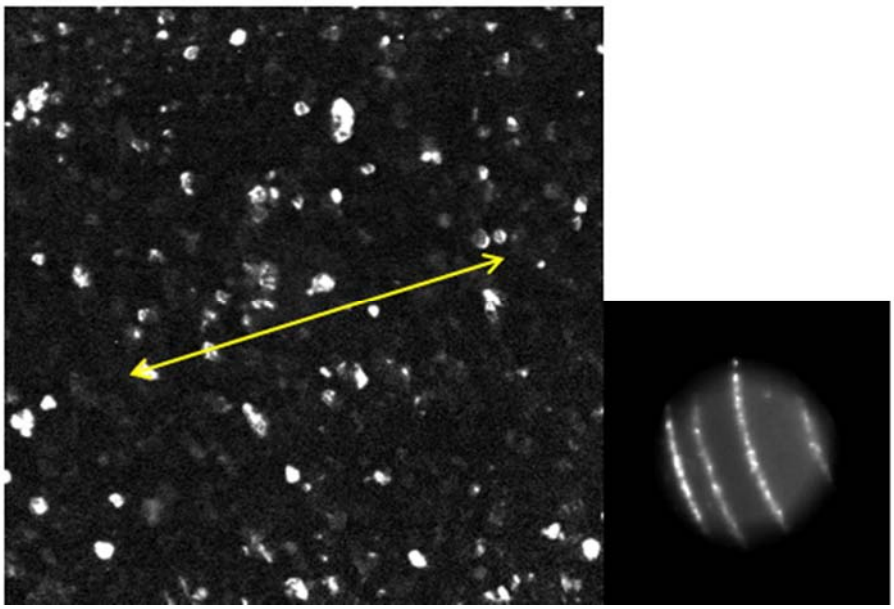

Figure 112: Dark field image showing crystallites with <200> directions aligned parallel to the yellow arrow (left). Enclosed segment of {200} diffraction ring (right).

204. In contrast to Figure 112 above, an image taken with the objective aperture at roughly 90˚ to the position above, as shown on the right in Figure 113 below, produces an image in which significantly fewer of the crystallites are illuminated as shown on the left in Figure 113, indicating that a smaller fraction of crystallites have their <200> directions aligned parallel to the long axis of the head.

CONTAINS CONFIDENTIAL ATTORNEY EYES ONLY
INFORMATION SUBJECT TO PROTECTIVE ORDER

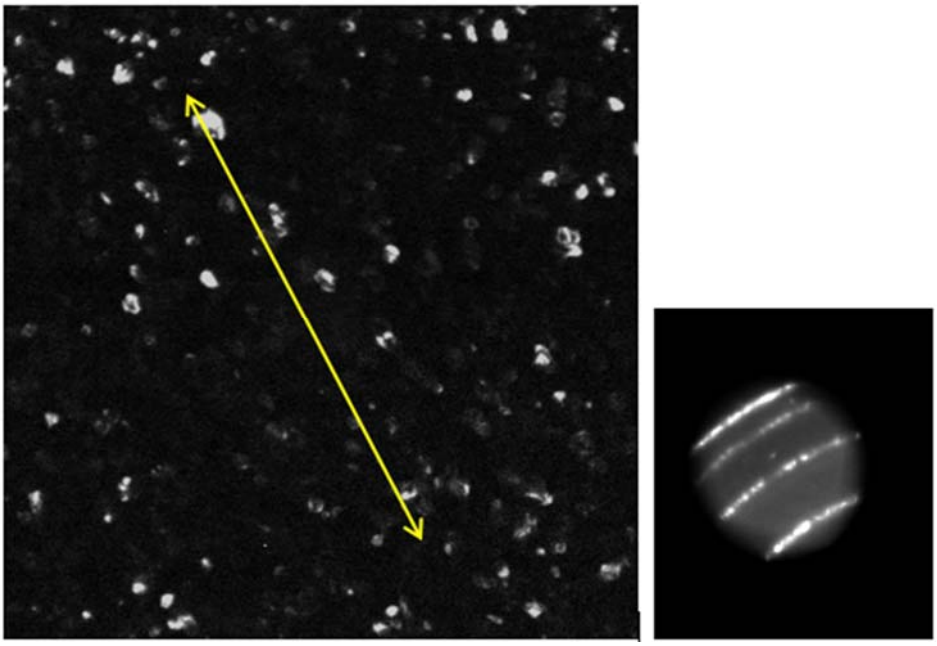

Figure 113: Dark field image showing crystallites with <200> directions aligned parallel to the yellow arrow (left). Enclosed segment of {200} diffraction ring (right).

205. This procedure is repeated at 10˚ intervals around the diffraction ring in at least a 180˚ rotation, producing dark field images similar to shows in Figures 112-113 above. To analyze these images, first, a large area of the dark field image is separated. The size and location of this area for sample SBRD8K is shown in the red box of Figure 114 below.

CONTAINS CONFIDENTIAL ATTORNEY EYES ONLY INFORMATION SUBJECT TO PROTECTIVE ORDER

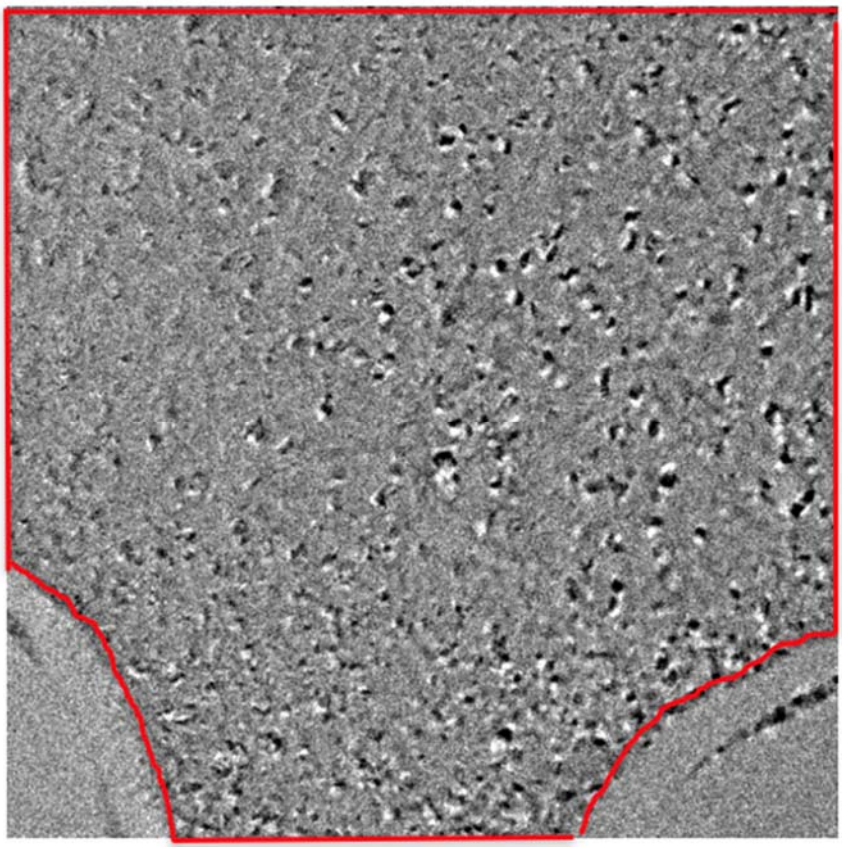

Figure 114: Dark field image with area under analysis shown enclosed by the red box (left) and extracted image (right).

206. Next, to analyze these images, a standard stereological computer program is used. I used ImageJ in my analysis. For each image, a threshold is applied to the isolated area as described by Figure 114 in order to produce a binary black and white image shown in Figure 115 below.

CONTAINS CONFIDENTIAL ATTORNEY EYES ONLY INFORMATION SUBJECT TO PROTECTIVE ORDER

Figure 115: Binary black and white image of the area described by the red box of Figure 114 above.

207. This image is operated on by ImageJ to measure the area fraction of crystallites that are white – that is, the area fraction of crystallites that scatter into the objective aperture at that particular position – and that area fraction for that particular position is tabulated. The image created by ImageJ enumerating the white crystallites is shown in Figure 116 below. The area fraction for each enumerated crystallite is shown in Appendix C.

CONTAINS CONFIDENTIAL ATTORNEY EYES ONLY INFORMATION SUBJECT TO PROTECTIVE ORDER

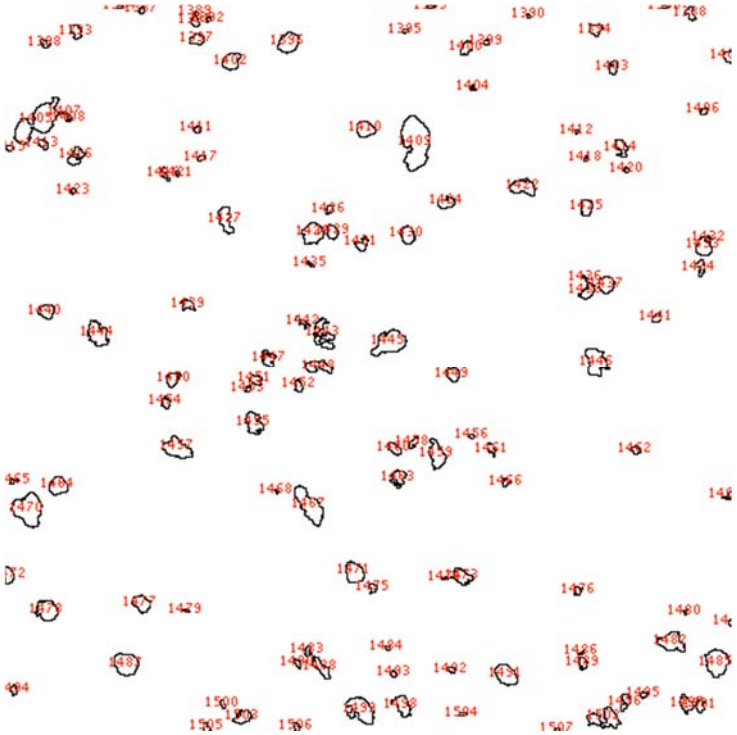

Figure 116: Image enumerating the white crystallites from Figure 115 above. Note that ImageJ enumerates each crystallite individually, and then calculates the relative area occupied by each crystallite.

208. Finally, the area fractions are added for each 10˚ increment to arrive at the total area of white crystallites for that particular increment, and the results for all positions are then tabulated. The results for SBRD8K are shown in Table 3 and graphed in Figure 117 below. The full results of this dark field analysis are attached in Appendix C.

Angle	%Area
0	1.994
10	1.769
20	2.08
30	2.089
40	2.018
50	1.624
60	2.308
70	2.238
80	2.134
90	3.271
100	2.758

CONTAINS CONFIDENTIAL ATTORNEY EYES ONLY
INFORMATION SUBJECT TO PROTECTIVE ORDER

110	2.18
120	1.769
130	1.947
140	1.905
150	1.341
160	1.27
170	1.264
180	0.807

Table 3: Number and area fractions of white crystallites at each angle in 180 degrees of rotation.

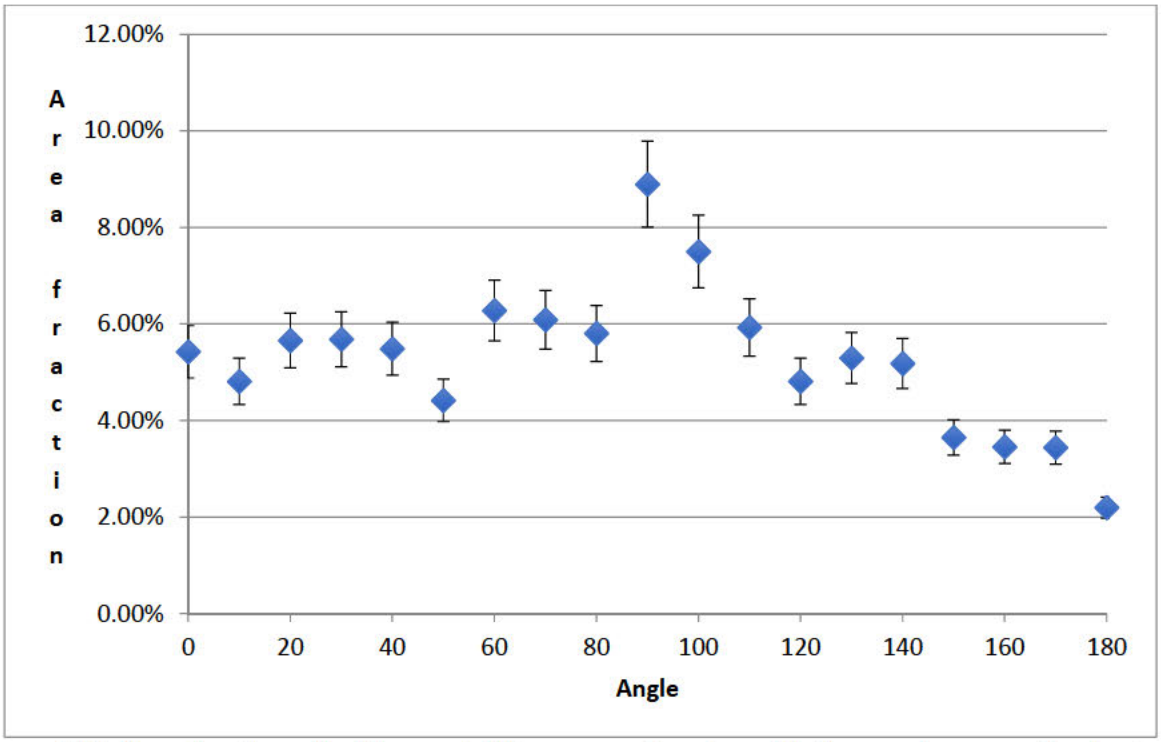

Figure 117: Area fraction of white crystallites vs. angle, where 90 degrees is perpendicular to the long axis of the write head. Error bars also shown.

209. These results indicate that there is a maximum area at 90 degrees, indicating that more crystallites are oriented with their <200> (easy) directions perpendicular to the long axis of the write head.

210. Further, as I explained in Section F.2.a.2, the sizes of the grains in the NiFe template layers and FeCo layers are similar, such that there is only one or two FeCo grains per NiFe template grain for the great majority of NiFe template grains. Further, this dark field

analysis, in conjunction with the microbeam diffraction analysis discussed above, shows that the various FeCo grains on top of the various NiFe template layer grains have members of the six-variant system preferentially aligned such that there is an unequal amount of the six variants in the FeCo layer. Given the relative grain sizes in the FeCo layer and NiFe template layer, there are no NiFe template grains that have six different overlying grains in the FeCo layer, let alone that each of the six different overlying grains would have equal area and each represent a different variant from the six-variant system present in the FeCo layer.

G. Reservation of Rights

211. I may modify or supplement my opinions and/or the basis for my opinions based on the nature and content of the documentation, data, proof, and other evidence or testimony that Seagate or its experts may present or based on any additional discovery or other information provided to me or found by me in this matter.

CONTAINS CONFIDENTIAL ATTORNEY EYES ONLY INFORMATION SUBJECT TO PROTECTIVE ORDER

Dated: May 2, 2018

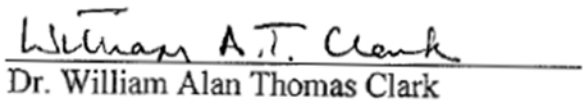

Dr. William Alan Thomas Clark

CONTAINS CONFIDENTIAL ATTORNEY EYES ONLY INFORMATION SUBJECT TO PROTECTIVE ORDER

CERTIFICATE OF SERVICE

I hereby certify that a true and correct copy of the within PLAINTIFF LAMBETH MAGNETIC STRUCTURES, LLC'S INITIAL EXPERT REPORT OF DR. WILLLIAM ALAN THOMAS CLARK is being served by e-mail upon all counsel of record on May 2, 2018.

RADULESCU LLP

/s/ *Mindy Tsoi*
Senior Paralegal